Evaluation of an Interference Filter Photometer for the Measurement of Atmospheric Ozone and Aerosol Scattering

A thesis
presented for the degree of
Doctor of Philosophy in Physics
in the University of Canterbury,
Christchurch, New Zealand.
by
Stephen Wyatt Wood
1989

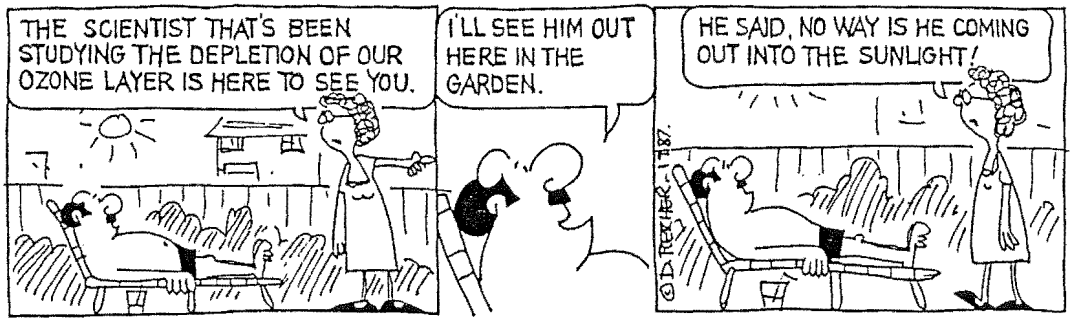
THE SCIENTIST THAT'S BEEN STUDYING THE DEPLETION OF OUR OZONE LAYER IS HERE TO SEE YOU.
I'LL SEE HIM OUT HERE IN THE GARDEN.
HE SAID, NO WAY IS HE COMING OUT INTO THE SUNLIGHT!
©D TREICHLER '87.

Abstract

A multi-wavelength, narrow-band, interference filter spectrophotometer has been designed by the New Zealand Meteorological Service. Its intended function is to provide measurements of atmospheric transmission at ultraviolet, visible, and infrared wavelengths, and from these measurements be able to characterise the aerosol scattering optical depth as a function of wavelength and determine the total amount of ozone in a vertical column of the atmosphere. The design was prompted by the similarity of conventional sun photometers to the photometers built at the University of Canterbury, New Zealand, solely for the measurement of total ozone. The instrument has been built to this design by the Physics Department, University of Canterbury, and has been tested and evaluated by the author.

The photometer has eleven filters with bandpasses in the range from 310 nm to 940 nm. The bandwidths are 5 nm in the ultraviolet and 10 nm elsewhere. The three shortest wavelength filters lie in the Huggins absorption band of ozone and are to provide an estimate of the quantity of atmospheric ozone. The remaining filters are principally at wavelengths intended for the measurement of aerosol optical depth. The filter at 940 nm is for the determination of the quantity of water vapour in the atmosphere. Two detectors are used to cover the range of wavelengths. The photometer tracks the sun by means of a heliostat.

A description of the photometer and the measurements made with it in New Zealand and the Antarctic are presented. These show that this is a design that comes close to meeting its objective. Despite the set back of one of the important ultraviolet filters changing in transmission characteristic, the instrument can still provide approximate values for ozone. The systematic errors in these values are discussed. The values it gives for aerosol optical depth show the varying wavelength dependence of aerosol scattering.

The specific problems that limit both the accuracy of the measurements and the range over which they can be made are identified and possible solutions are suggested.

To everyone *that has been a part of my life during the course of this project.*

Contents

List of Figures

List of Tables

Chapter 1

Introduction

The middle atmosphere, the region between ten and a hundred kilometres in altitude, is currently generating a great deal of interest. The cartoon included on the title page is an illustration of this. It is only in the past few decades that this region has been made more accessible by the development of various remote sensing techniques, which have led to an appreciation of the importance of the region in determining global climate. In that same time we have realised that it is a region that is subject to change, from both anthropogenic and natural causes, that can influence climate on a global scale. Concentrations of many trace atmospheric constituents, such as carbon dioxide and chlorofluorocarbons, are increasing and the effects of these increases are likely to be significant.

It is a region where the thermodynamics and dynamics cannot be separated from the photochemistry and chemistry, so that many fields of study must come together to achieve an understanding of the processes involved. The importance of that understanding lies in being able to forecast the changes that will occur in the future so that informed measures can be taken to minimise any anthropogenic changes to the region. At present the understanding is not complete, nor is it likely to be for some time. Computer models of the middle atmosphere are able to make forecasts, but they are limited by not being able to fully represent all the atmospheric processes and interactions that occur. Their first goal must be simulating the present state of the atmosphere. Measurements of atmospheric parameters are crucial in both refining and testing the models and monitoring change.

This project is concerned with the measurement of two atmospheric characteristics; namely aerosol[1] scattering and the quantity of atmospheric ozone. Both of these have become more important in recent years with the growing realisation that man is capable of altering the radiation balance and climate of the earth. The increased use of nitrogen fertilisers and increasing emissions of gases that are radiatively or chemically active, or both, must be having a forcing effect on the

[1]The word aerosol means a suspension of solid or liquid particles in a gas. It is used here to refer to those particles suspended in the atmosphere. In common use, an aerosol is also a general term for the pressurised containers in which a propellant is used to produce a fine spray, that is, an aerosol. To avoid confusion between the two uses in this work the word aerosol is used only in the former sense and the term spray-can is used for the latter.

atmosphere and climate.

Recent events such as the formation of the "ozone hole"and the eruption of El Chichón, described on pages 10 and 14 respectively, have demonstrated that perturbations are possible and potentially serious. The ozone hole is an example of a relatively sudden atmospheric change which appears to be caused by the "switching on" of some new process. Such non-linear changes are extremely difficult to predict.

The possibility of a large scale nuclear exchange is an awesome possibility, whose effects on the atmosphere and climate are sure to be extensive. The smoke from extensive fires and the dust raised by blasts would modify the atmosphere in a manner similar to a large volcanic eruption. There have been many models that provide possible scenarios: including Turco et al. (1983); Covey et al. (1984); a report by the National Research Council (1984) and more recently Malone et al. (1986) Schneider (1987) provides a general discussion on this and on the more general climate modelling problem.

Recently there have been reports (Bowman, 1987; Heath, 1988; Reinsel et al., 1988) of significant reductions in ozone on a global scale. While these are not as severe as the depletion found in the Antarctic ozone hole they are nevertheless of concern, especially the possibility of depletion in Arctic regions. An international panel to look at the ozone trends has been assembled. Its full report is due to be published soon but a shorter report has already been published (NASA, 1988). The trends from ground-based Dobson measurements in Northern mid-latitudes were established by the panel (Table 1.1). The global trend from the satellite records, after removing the drift by correlating with Dobson measurements, is smaller than earlier estimates at around 2.5% for the period 1978–1985, with significant variation with latitude. Some of this, from 0.7 to 2%, could be due to the natural variation associated with the 11-year solar cycle of ultraviolet activity which reached its minimum in 1985. These findings have strengthened calls to limit the production of chlorofluorocarbons. The Montreal Protocol, set up in 1987 and coming into force when countries representing 66% of world chlorofluorocarbon production have ratified it, calls for a 50% reduction in production by 1999. The protocol is due for review in 1991, by which time measurements will have more accurately determined to what extent chlorofluorocarbons are responsible for depleting ozone, as that is the time of the next solar maximum. The problem of ozone depletion is a long term one as the lifetime of chlorofluorocarbons in the lower atmosphere is of the order of 70-100 years and only a small fraction of the total reaches higher up, where the damage is done, each year.

The problems of modification of the ozone distribution and modification of climate can no longer be treated separately. While the main climatic concern used to be the greenhouse effect of increasing carbon dioxide, illustrated in Figure 1.1, there is now the added concern that many trace constituents are also increasing and their cumulative greenhouse effect is as large as that of carbon dioxide. Many of these gases, such as methane, hydrocarbons and halocarbons, are active in the chemistry that controls ozone. In addition ozone itself is a greenhouse gas, as it absorbs in the near infrared, and variations in its quantity or distribution directly alters the long-wave or terrestrial radiation balance as well as that of the shorter

	53–64°N	40–52°N	30–39°N
Annual average	-2.3 ± 0.7	-3.0 ± 0.8	-1.7 ± 0.7
Winter average	-6.2 ± 1.5	-4.7 ± 1.5	-2.3 ± 1.3
Summer average	$+0.4 \pm 0.8$	-2.1 ± 0.7	-1.9 ± 0.8

Table 1.1: Trends in total ozone from Dobson spectrophotometer measurements. The figures are percentage changes for the period 1969-86.

solar wavelengths.

Measurements of climatic parameters such as surface temperature are extremely important for the detection of long term trends. Natural variability in the parameters measured, on several timescales from minutes to decades, complicate the detection. As a general global warming would be accompanied by regional temperature changes of varying sizes, both smaller and larger than the global average, care is needed in the interpretation of measurements. The model predictions of present greenhouse warming are still too small to be statistically different from the natural temperature fluctuations so none of them has yet received positive verification.

Models that aim to predict future climatic change cannot be confined to the middle atmosphere as the climate is an interaction between the large masses of the atmosphere, ocean and land. The amount of heat, momentum and matter exchanged between these three systems depends on parameters such as surface temperatures, vegetation cover, winds and cloudiness. These parameters are influenced by the climate and will have important feedback effects in determining the state of quasi-equilibrium that determines that climate. Many of these feedback mechanisms are not well understood and are difficult to model. How, for example, will the amount of carbon dioxide that is dissolved in the oceans respond to a change in temperature? The answer is crucial to the carbon dioxide budget of the atmosphere but as yet cannot be given. Clarifying our understanding of these questions will require a co-operative effort spanning many fields of study. In the meantime, model predictions of future climate change must be treated with caution. A review of many recent climate models with specific reference to the carbon dioxide increase is given by Schlesinger and Mitchell (1987).

The two concerns of this project, atmospheric ozone and aerosol scattering, have often been treated separately but because measurements of one are complicated by uncertainties in the other a combined approach is fruitful. A brief introduction to each follows, in the form of a history of the measurements that have been made and a discussion of their characteristics, including their importance to the climate change problem.

1.1 Atmospheric Ozone

1.1.1 History of atmospheric ozone measurement

The study of atmospheric ozone had its beginnings at the end of last century. Ozone had been identified as a constituent in the air at ground level and monitored for several years by a chemical method discovered in 1844 by Schonbein. Cornu had been investigating the sharp ultraviolet cut-off of solar radiation with photographs of the spectrum (Cornu, 1879). In 1881 Hartley made some absorption measurements for ozone and then made the connection between the two (Hartley 1881a, 1881b). Absorption bands in stellar spectra in the region 300–340 nm were noticed first by Huggins (1890) and these were later attributed to atmospheric ozone by Fowler and Rayleigh (1917). During 1912–13 Fabry and Buisson made laboratory measurements of ozone absorption from 254–334 nm (Fabry and Buisson, 1913). They calculated that to reproduce atmospheric absorption at 300 nm would require total atmospheric ozone equivalent to a 0.5 cm layer at standard temperature and pressure[2]. The first measurements they made in the summer of 1920, with a double spectrograph, found ozone amounts in the range equivalent to 0.28–0.34 atm-cm. During the 1920's spectrographic methods for measuring total ozone were refined by Götz and Dobson. Dobson's instrument used a Féry prism and photographic recording. Six instruments were made and deployed at various stations around Europe during 1925–6 and were re-deployed in 1928 to give a more global coverage. Observations made in this period were building up a picture of seasonal and latitudinal variation in total ozone (Dobson, 1930; Götz, 1931). This gave the first clues to the circulation patterns in the middle atmosphere.

In 1931 a general theory, now known as Chapman theory, was presented to explain the formation of characteristic layers in the atmosphere by looking at the absorption of incoming solar radiation as a function of height (Chapman, 1931). This could describe any process in the atmosphere that absorbs radiation, such as photoionisation or photodissociation. When applied to ozone it predicted a layer of ozone in the lower stratosphere.

A new spectrophotometer was designed by Dobson in the period 1929–31 using photoelectric cells and a double monochromator (Dobson, 1931). The relative intensity of light at two wavelengths, initially 311 nm and 326.5 nm, was measured by moving a calibrated wedge in one beam until it produced an equal photocell output to the other. This instrument, with later modifications, including the provision of more wavelength pairs, became the standard instrument for ground based ozone measurements and still is.

Götz and Dobson also looked at the use of the Umkehr or inversion effect in determining the vertical distribution of ozone, (Götz and Dobson, 1928). This effect occurs where the ratio of light scattered from the zenith sky at two different wavelengths which normally decreases as solar zenith angle increases, increases for a short interval at large zenith angles. Their aim was to try and link absorption by ozone to the temperature profiles measured by balloons and to Chapman theory.

[2]This unit is refered to as the atmosphere-centimetre (atm-cm) in this work. Its sub-multiple, the milli-atmosphere-centimetre, is known as the Dobson unit in honour of G.M.B. Dobson.

They found that the main concentration of ozone was around 20–30 km, somewhat lower than expected.

The global ozone measurements initiated by Dobson have become more extensive especially as a result of the additional efforts during the International Geophysical Year (1958) and with the advent of satellite measurements. These have helped in the study of both the photochemistry and the dynamics in the atmosphere, both of which control the distribution of ozone, the latter being more dominant in the lower stratosphere with the former having more control at higher altitudes.

The Dobson spectrophotometer, including a recent semi-automated version is still the principal instrument for ground-based determination of ozone. However there have been other instruments. For example, there have been a number of Russian ozonometers that use glass filters and a Canadian instrument that uses a diffraction grating as its dispersive element (Brewer, 1973: Brewer and Kerr, 1973) for example. Craig (1965) and Khrgian (1973) give surveys of some of these as well as in situ measurements. Instruments using interference filters have been built here at Canterbury, New Zealand, and are described briefly in Section 1.3.

Balloon soundings of the vertical profile can be made by either a chemical or an optical instrument, and satellite observations of both total ozone and part of its vertical profile are now routinely made. It might be thought that the extensive ground coverage of satellite measurements make ground based measurements obsolete, but they have a very important role to play in the calibration and detection of trends in the satellite measurements.

Accounts of the various methods of ground based, in situ and satellite ozone measurement, and intercomparisons between them can be found in the measurement sections of the proceedings of the last two ozone symposia held by the International Ozone Commission (IOC, 1980 and 1984) and in the papers describing an experimental intercomparison campaign (Chanin 1983a, 1983b, and accompanying papers).

1.1.2 Characteristics of atmospheric ozone

Ozone is a trace gas in the atmosphere that has absorption features in the ultraviolet, visible, and infrared regions of the electromagnetic spectrum. The absorption in the infrared region contributes to the greenhouse effect, illustrated in Figure 1.1. However, the contribution is not straight forward. An increase of ozone in the stratosphere, where its principal effect is the absorption of short wave (solar) radiation, will warm the stratosphere but cool the troposphere and surface because less short-wave radiation gets through. On the other hand, an increase in ozone in the troposphere will have the opposite effect: the surface is warmed because the absorption of long wave (terrestrial) radiation is ozone's dominant effect as there is less ultraviolet radiation.

Ozone is formed in the atmosphere by the combination of atomic and molecular oxygen according to

$$O + O_2 + M \rightarrow O_3 + M \tag{1.1}$$

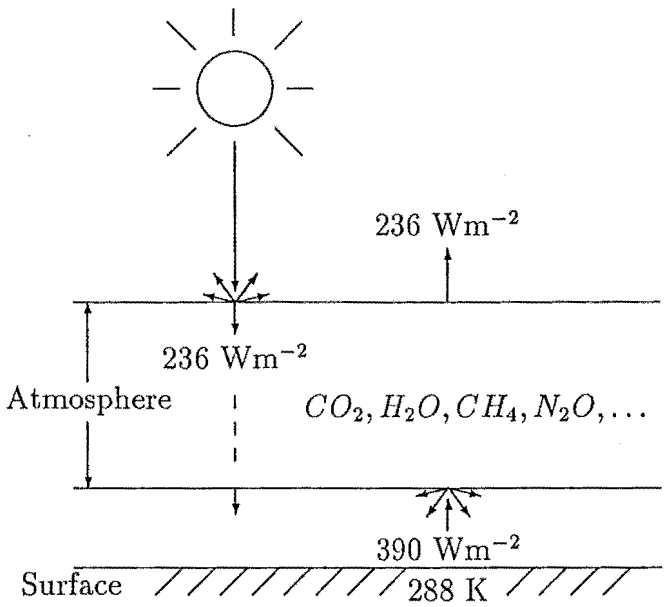

Figure 1.1: The Earth's energy balance and the greenhouse effect. The surface is warmer because of the absorption and re-emission of terrestrial radiation by gases in the atmosphere, principally carbon dioxide and water vapour. Without this, the surface would have an average temperature of just 254 K. Figures for energy fluxes are global averages.

where M is a third body, an air molecule, that removes excess kinetic energy. The atomic oxygen comes principally from the photodissociation of oxygen molecules by ultraviolet light with wavelengths less than 242 nm, although there are other sources such as the photodissociation of nitrogen dioxide.

$$O_2 + h\nu \rightarrow O + O \tag{1.2}$$

It is the height dependence of Reaction 1.2, as explained by Chapman theory, that produces a layer of ozone in the lower stratosphere. A typical profile of ozone and temperature is shown in Figure 1.2.

Despite having a maximum mixing ratio of only a few parts per million by volume in the atmosphere, ozone is an extremely important trace gas. It is the only atmospheric gas which significantly absorbs radiation at wavelengths between 240 and 360 nm. This absorption is due to the dissociation reaction

$$O_3 + h\nu \rightarrow O + O_2 \tag{1.3}$$

The presence of ozone in the atmosphere means that wavelengths from 200–300 nm are reduced to levels that are unobservable at ground level and those from 300–340 nm are greatly attenuated. This is biologically important as radiation of these wavelengths has adverse effects on both plant and animal forms of life. In humans it causes sunburn, various skin cancers, and eye cataracts. Mackie and Rycroft (1988) provide a discussion of these effects in relation to the current concern over depletion of atmospheric ozone. The ultraviolet absorption is important for a

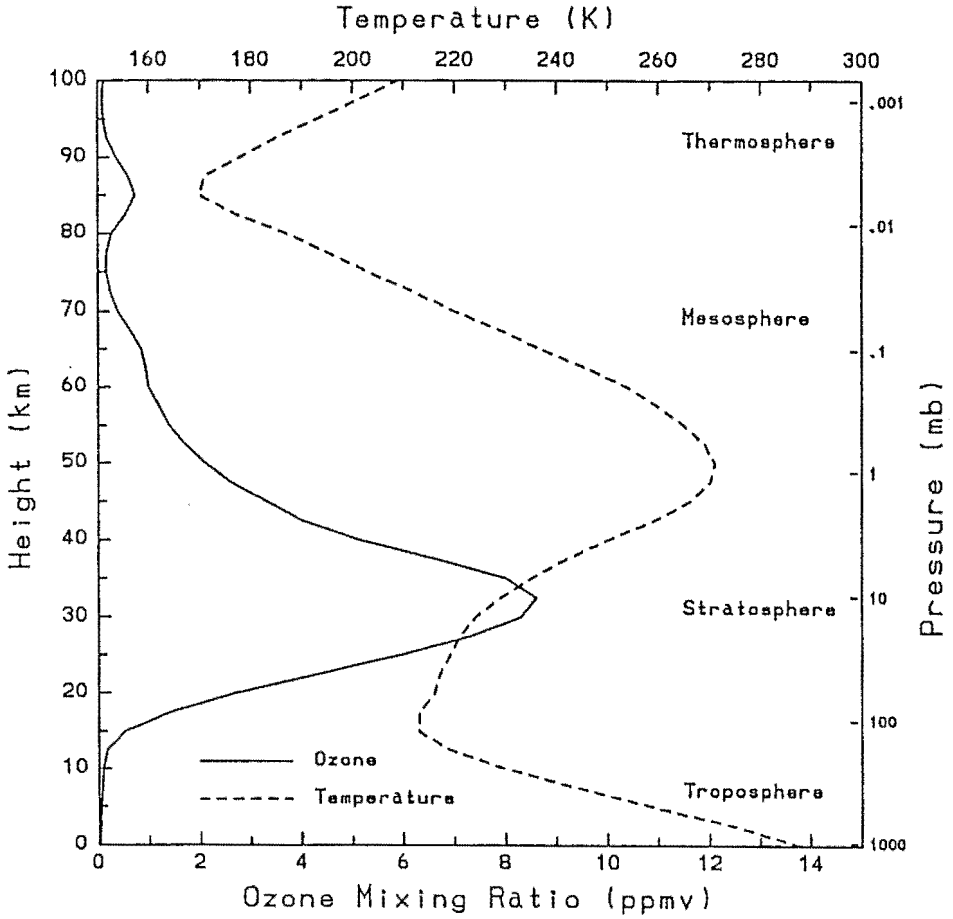

Figure 1.2: Typical profiles of ozone and temperature in the atmosphere.

second reason: it intercepts approximately 4% of the radiant energy of the sun and this provides the main source of heating in the stratosphere. Without this heating the stratosphere, the region of the atmosphere with temperature increasing with height, would not even exist. Because the heating at a given place in the stratosphere is dependent on how much ozone is there, the distribution of ozone plays a primary role in determining the temperature structure and the consequent motions within the stratosphere. That stratospheric circulation in turn affects the ozone distribution by transporting ozone. The average quantity of ozone as a function of latitude and season is shown in Figure 1.3.

There are also variations on shorter and longer timescales such as the diurnal variation, variations from day to day, and variations linked to the quasi-biennial oscillation in atmospheric motions in the tropics and the solar activity cycle. Because the circulation of the atmosphere and the distribution of ozone within it are so strongly coupled, predicting the effect of changes in either is made more difficult.

Reaction 1.3 does not usually remove ozone from the atmosphere as it is usually followed by Reaction 1.1. When this happens the quantity of ozone is unchanged and the net effect is to absorb ultraviolet radiation and heat the surrounding air.

A change in the rate of ozone formation, for example by a change in the

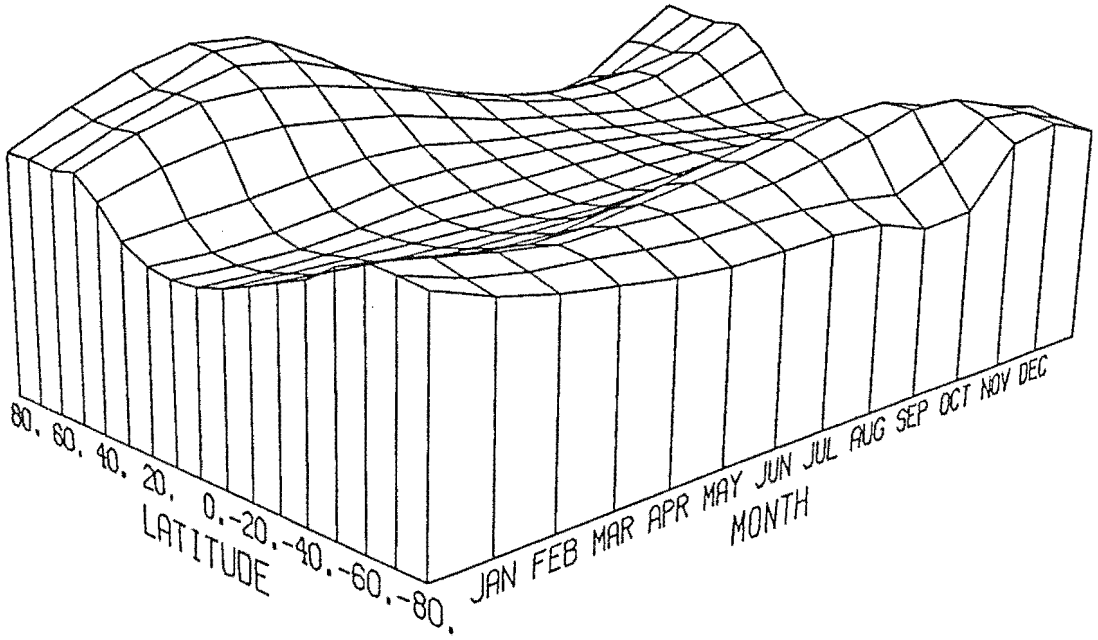

Figure 1.3: Average distribution of ozone as function of latitude and season. The level at the equator is nearly constant at approximately 0.25 atm-cm. Variations at high latitude in the North are large and reach a peak of approximately 0.40 atm-cm in Spring. The effect of the Antarctic ozone hole can be seen in the September and October values. The values are from NOAA (1988) and represent averages over the period from November 1978 to October 1986.

distribution of ultraviolet radiation caused by solar activity, will alter the quantity of ozone in the atmosphere. However, it is the processes that remove ozone that are more sensitive to possible change. The reaction

$$O + O_3 \rightarrow 2O_2 \tag{1.4}$$

that removes ozone can occur directly but more often occurs as a catalytic process, involving a radical X, of the form

$$\begin{aligned} X + O_3 &\rightarrow XO + O_2 \\ XO + O &\rightarrow X + O_2 \end{aligned} \tag{1.5}$$

giving the same net effect. H or HO, NO, Cl and Br all act in this way. A review such as that by Murgatroyd (1982) provides further details.

For each radical the effect on ozone is determined by its concentration which is in turn determined by the its rate of production, destruction and transport. Different catalytic reactions vary in importance at different heights as shown in Table 1.2. The radicals can be grouped in to catalytic families that may consist of a number of radicals along with gases that act as sources, sinks, and temporary reservoir species for those radicals. Figure 1.4 represents the three most important catalytic families. Interactions between catalytic families are rife; one may interfere with another by forming a common reservoir or a mixed ozone destruction cycle of the form

$$X + O_3 \rightarrow XO + O_2$$

Altitude (km)	$k(O)(O_3)$ (%)	$k(NO_2)(O)$ (%)	$k(ClO)(O)$ (%)	$k(HO_2)(O)$ (%)	$k(HO_2)(O_3)$ (%)
50	25	7	4	52	-
45	29	24	10	31	-
40	18	53	16	10	-
35	11	68	13	4	1
30	10	69	8	2	3
25	12	78	5	1	8
20	11	70	1	1	26

Table 1.2: Calculations of the relative importance of different odd oxygen destruction reactions at different heights. Values are expressed as a percentage of the production at that height. Source, WMO 1982a.

$$\begin{aligned} Y + O_3 &\rightarrow YO + O_2 \\ XO + YO &\rightarrow X + Y + O_2 \end{aligned} \tag{1.6}$$

where X and Y are radicals and which has the net effect of

$$2O_3 \rightarrow 3O_2 \tag{1.7}$$

The last line of Reaction 1.6 may not be a single reaction but consist of several steps. Cycles like this are more important at lower altitudes than those of the form of Reaction 1.5 as they are not dependent on the photolytic production of atomic oxygen. Concentrations of the active catalysts in the parts per trillion range can affect the destruction of ozone significantly. There has been concern whenever a major anthropogenic source of these radicals has been introduced that modification to the chemical balance will occur. For example in the seventies there was considerable concern about injection of nitrogen oxides into the stratosphere by a proposed fleet of supersonic aircraft and there is current concern about chlorine radicals that are produced when chlorine bearing halocarbons are photodissociated in the stratosphere.

To successfully model the chemistry of destruction processes a large number of species and reactions must be taken into account[3]. A system of differential equations, in which the dependant variables are the concentrations of each species, can be set up to form a chemical model. Each equation is a continuity equation for a particular species, with terms for production, removal, and transport included. The rate of each reaction will be a function of the temperature and possibly the pressures and radiation flux. If these rates are known, from laboratory measurements, then the system may be solved. The coupling between radiation and the chemistry is well handled by such a model. The coupling or feedback with the dynamics is more difficult to account for. Such a simple model will include the effect

[3]Brasseur and Solomon (1986) list 125 reactions involving approximately 60 neutral species and a similar number of reactions involving ions

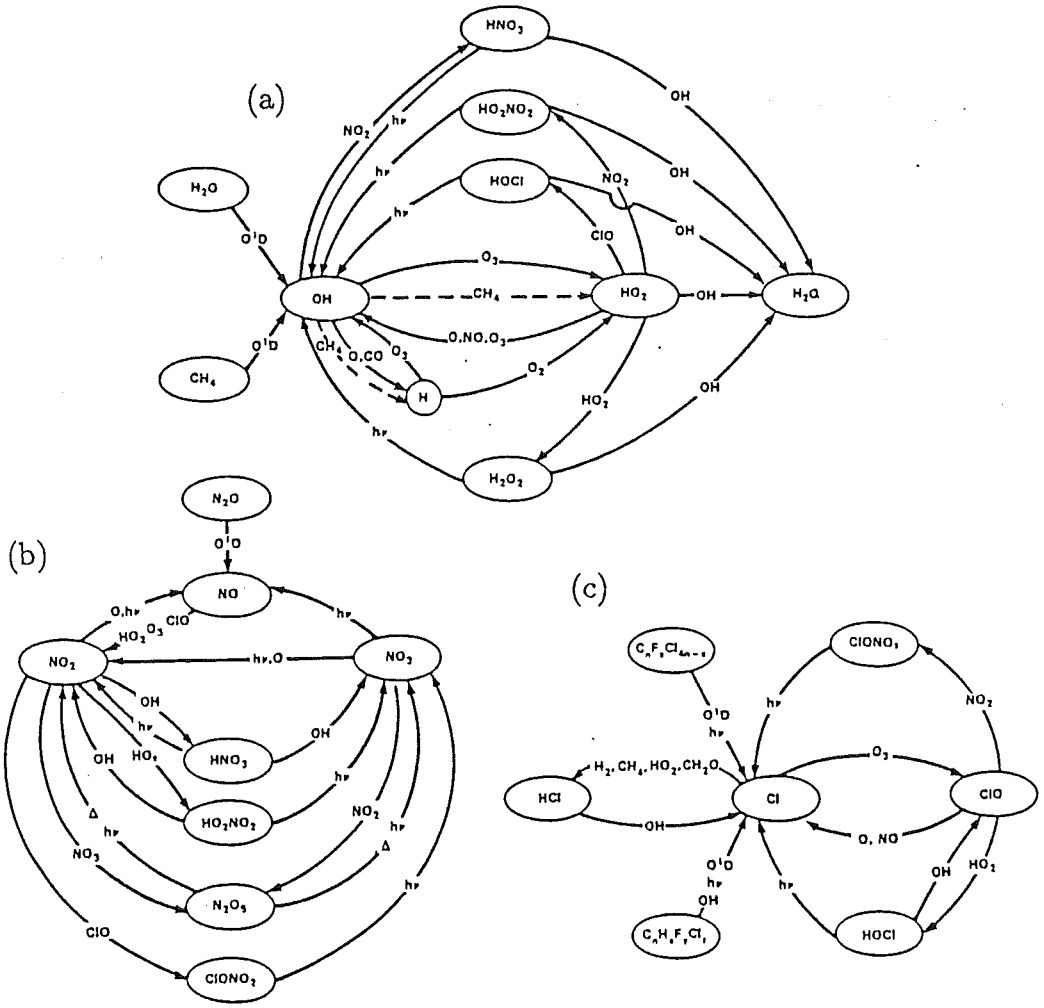

Figure 1.4: The three most important catalytic families involved in the removal of ozone: (a) Odd-hydrogen; (b) Odd-nitrogen; (c) Odd-chlorine. From NASA (1986).

of the existing transport only by a simple parameterisation and consequently will not have any dynamic feedback at all. The complexity of the chemistry makes anything more that a one-dimensional time dependent model difficult so variations with latitude and longitude are often ignored. The uncertainty in predicting the future level of emissions of various source gases adds to the difficulty in assessing the possible chemical changes. Brasseur and De Rudder (1988) discuss the results of their chemical-radiative model as well as providing references to other recent models.

Measurements of as many species as possible are important in verifying these chemical models and in establishing if there are any chemical reactions missing from them. Extensive reviews of the current understanding of the processes that control atmospheric ozone can be found in the assessment reports by the World Meteorological Organisation (WMO, 1982a and 1986) and the National Aeronautics and Space Administration (NASA, 1986), on which much of the preceding discussion is based.

The Antarctic ozone "hole", first reported by Farman et al. (1985), is an excellent example of an atmospheric change that was almost impossible to foresee. It consists of a drastic reduction in ozone over most of Antarctica in the early springtime, at the time when sunlight has returned after the polar night. An analysis of TOMS and SBUV[4] satellite data has shown it to have developed over the last decade with its severity generally, but not always, increasing from year to year (Stolarski et al., 1986). It has spawned intensive research with several possible explanations, both chemical (for example Solomon et al., 1986; McElroy et al., 1986; Crutzen and Arnold, 1986) and radiative (Tung et al., 1986; Mahlman and Fels, 1986), being put forward. There was a special issue of Geophysical Research Letters (Vol 13, No.12, November 1986) containing forty five papers on the topic and an overview (Schoeberl and Krueger, 1986, and accompanying papers).

It was not until measurements of key trace gases and of detailed ozone profiles made as part of a special expedition to the Antarctic in 1986 were made that these hypotheses could be tested. Profiles showed that the depletion was occurring at heights from 10-20 km (Hoffman et al., 1987) and that the chemistry was significantly different from that observed at other latitudes and times. Low levels of odd-nitrogen, which normally limits the quantity of free odd-chlorine by the formation of a common chlorine-nitrogen reservoir, $ClONO_2$, allows very high levels of odd-chlorine to exist (Farmer et al., 1987; P.M. Solomon et al., 1987; S. Solomon et al., 1987; Mount et al., 1987). Findings from a second expedition in 1987 and a concurrent campaign of in situ measurements from aircraft have added to the knowledge (Pyle, 1988) The mechanism that is depleting the odd-nitrogen in the lower stratosphere is related to the presence of polar stratospheric clouds, which are formed at temperatures of 195 K or lower and are more common in the South than the North because of the lower stratospheric temperatures there (McCormick et al., 1982). The most likely mechanism is the condensation of ice containing HCl and HNO_3 onto the cloud particles. This ties up the odd-nitrogen until the particle either evaporates or is removed by precipitation. The release of active chlorine from reservoir species may be enhanced by heterogeneous reactions between chemicals in the solid phase and the active nitrogen and chlorine gases on the surfaces of these particles (Wofsy et al. 1988). It is interesting to note that the reduced levels of nitrogen dioxide were reported before the ozone hole itself by McKenzie and Johnson (1984).

However the hole is not caused solely by perturbed chemistry; the circulation of the south polar region, which keeps it largely isolated from lower latitudes by a pattern known as the polar vortex, provides the conditions (lower stratospheric temperatures and hence a higher incidence of polar stratospheric clouds) for the hole to form. The shape of the depleted area at any time is governed by the shape of the vortex and can be seen to rotate, driven by planetary scale waves (Krueger et al., 1987). The break up of the hole is related to the break up of the vortex in late spring and observations of ozone deficient air have been made at mid-southern latitudes at this time. The review by Solomon (1988) and the

[4]The Total Ozone Mapping Spectrometer and the Solar Backscattered UltraViolet experiments on the Nimbus 7 satellite.

special section on polar ozone in Geophysical Research Letters recently published (Solomon and Schoeberl, 1988, and accompanying papers) provide accounts of the present state of knowledge.

1.2 Aerosol Scattering

The second field of study with which this project is concerned is scattering and absorption of light in the atmosphere by suspended particles or aerosols.

1.2.1 History of aerosol scattering and turbidity measurements

The first determination of the diminution of light by the atmosphere was made by Pierre Bouger in November 1725 by comparing the apparent intensity of the moon at two different elevations (Middleton, 1961). This diminution varies as the number of scattering particles in the atmosphere varies due to such things as weather patterns, volcanic eruptions, forest fires and anthropogenic sources.

It was the eruption of Krakatoa in 1883 that first prompted broad band measurements of transmitted solar flux. Since the turn of the century, with improved instruments such as the Ångström compensating pyroheliometer (Ångström, 1932) being readily available, many measurements of turbidity, or the dirtiness of the atmosphere, have been made (Volz, 1968).

The measurement was usually reduced to some standard parameter such as the Linke turbidity factor which is the number of clean, dry atmospheres that would produce the same attenuation as that observed (Linke, 1922). A clean dry atmosphere is defined as one in which the only scattering process is that due to air molecules. This measure is still in use as it was during the International Geophysical Year, (Ohman, 1958) although other wavelength averaged measures such as an average attenuation coefficient were and are also used.

However, scattering by atmospheric particles does not have the same wavelength dependence as molecular (Rayleigh) scattering [5]. This can be seen by comparing the washed out skylight of a hazy day with the deep blue of an exceptionally clear day. Scattering by aerosols is generally a more slowly varying function of wavelength than Rayleigh scattering so the sky is closer to a uniform white. This limits the usefulness of wavelength averaged measures of turbidity, such as the Linke factor, because they are a function of the wavelength sensitivity of the detector used and the solar elevations over which the determination is made. Thomason et al. (1982) provide a discussion of these difficulties. One way of overcoming this (Ångström, 1929) was to account for the varying wavelength dependence of aerosol scattering by relating it to wavelength with a simple power law

$$\tau_A \propto \lambda^{-\alpha} \tag{1.8}$$

[5]The dependence of Rayleigh scattering on wavelength, λ, is approximately λ^{-4}. It is described in Chapter 3 on page 34.

Wavelength (nm)	368* 384 500* 778* 862
Bandwidth (nm)	5–10

Table 1.3: Wavelength bands recommended by World Meteorological Organisation for measurement of turbidity. * indicates a "primary" standard.

Where τ_A is the optical depth due to aerosol scattering and the wavelength is expressed in microns (μm). The exponent of wavelength dependence, α could vary from 0 for large particles (the geometric limit) to 4 for very small particles (the Rayleigh limit) and was thus a crude measure of the typical particle size. A typical value for α being in the range 1–2. Measurements using coloured glass filters to determine the coefficient were possible but suffered from large and unreliable errors (Ångström, 1961; Armstrong and Richards, 1982).

More accurate measurements can be made with instruments that have narrow wavelength bands. The first such instrument, designed by Volz (1959), had channels at 380 nm and 500 nm. These channels could be treated as monochromatic and so did not suffer from the difficulties of broad band measurements. A value for the wavelength coefficient could be obtained with much less difficulty. Modern sunphotometers have evolved from this instrument (Shaw, 1983). The World Meteorological Organisation now has standards for the measurement of turbidity at preferred wavelengths (WMO, 1978). These are shown in Table 1.3

The particle sizes that contribute to optical turbidity lie in the range 0.1 to 10 μm . Measurements of the wavelength dependence of turbidity contain information about this size range. As computing power and techniques have improved, more and more information about the size distribution has been extracted. In some cases it is possible to infer a size distribution from a knowledge of the wavelength dependence of the scattering. While this is an ill-posed problem in that many differing size distributions can give the same scattering, successful inversions are possible if the solution process is subjected to suitable constraints. The mathematical techniques are described in Twomey (1963, 1965) and King (1982) and there have been a number of accounts of successful inversions (for example, Yamamoto and Tanaka, 1969; Quenzel,1970; King et al., 1978, Tanré et al., 1988).

There are other ways by which information of the size distribution of particles that scatter visible light can be obtained. Because the angular dependence of aerosol scattering is a strong function of size, methods sensitive to the direction of scattering can be quite successful. Measurements of the solar aurora fall into this category, as do active measurements with LIDAR[6] systems. Accounts of these sorts of methods are to be found in Twomey (1977) and Deepak (1980). Aerosols can also be studied by various forms of in situ measurements, which may involve collecting the particles or measuring the optical properties of the sample.

[6]LIDAR is an acronym for **LI**ght **D**irection and **R**anging

1.2.2 Characteristics of Aerosol Scattering

Aerosols in the troposphere consist of particles of mineral dust, sea salt, soot and ash from various combustion processes, organic condensates and products of gaseous condensation. The size range can be anything from 10^{-3} to $10^{3}\mu$m and different sources will produce different characteristic size distributions. The particles can act as condensation nuclei for the formation of raindrops which is one of the processes by which they are removed from the atmosphere; other processes are washout by falling raindrops and gravitational settling out. The lifetime of aerosols is short, a matter of a few days or weeks so their distribution varies a great deal as production and transport varies. There is however a background aerosol in the upper troposphere representing particles that have got through the cloud filter.

There is also a stratospheric aerosol, known as the Junge layer which consists mainly of condensates of various sulphate compounds. This layer normally contributes only a small fraction of the total aerosol scattering but has a much longer lifetime. More complete accounts of the nature of atmospheric aerosols and the processes that control them can be found in the books by Junge (1963), Twomey (1977) and Monin (1986).

The importance of atmospheric scattering by aerosols lies in their ability to modify the radiation balance in the atmosphere by scattering. Any process or event that changes the quantity or nature of atmospheric aerosols will change the radiation balance. Increased emission of particulate matter from combustion in transport and industry have this potential.

Large volcanic eruptions provide opportunities to study examples of such climate modification. They inject large quantities of dust and gas into the atmosphere. The dust usually falls out within a few weeks or months and so provide only a short term modification to the radiation scheme. However the gases, mainly sulphur dioxide, form droplets of sulphuric acid which can persist in the stratosphere for a year or more.

The possible link between volcanic eruptions and climate modification was first suggested by Benjamin Franklin when Europe had a severe winter, apparently as a consequence of the eruption of Laki in Iceland in 1783 which produced a dense haze over most of the region (Mitchell, 1982). With increased scattering in the atmosphere, more short-wave radiation is intercepted in the atmosphere and less reaches the ground, causing a surface cooling along with an atmospheric warming. Radiative transfer models can quantify the effect.

The eruption of El Chichón in April 1982 has been the most studied volcanic eruption ever; it was the first eruption with significant climatic effects that has been monitored from satellites. There has been a special issue of Geophysical Research Letters (Volume 10, November 1984) on the eruption and Hoffmann (1987) provides a more recent review paper detailing the chemical and dynamic effects of the eruption.

Apart from the radiation balance, aerosols are important for the role they play in thermodynamic and chemical processes. They act as condensation nuclei for cloud droplets and provide surfaces on which chemical reactions can occur.

When condensates are formed, species are removed from the gas phase. They are therefore important in the chemical budget of the atmosphere and in the climate as a whole.

1.3 Aims of this Project

Some years ago Dr G. J. Fraser of the Physics Department, University of Canterbury, instigated the construction of a photometer that used interference filters to isolate wavelength bands in the ultraviolet and whose purpose was to provide an alternative to the Dobson spectrophotometer for the determination of total atmospheric ozone. This was motivated by the fact that the Dobson spectrophotometer was out of production, was heavy and difficult to move, and required a skilled operator (Dobson, 1957a). The first prototype had six filters with passbands in the ultraviolet close to the wavelengths used by the Dobson. They were mounted on a wheel which was rotated so that each interrupted the light path in turn, enabling the measurements at all wavelengths to be made very nearly simultaneously. The photodetector used was a photomultiplier tube with good ultraviolet sensitivity. It was made to track the sun by means of an equatorial mount and a constant velocity drive to counter the earth's rotation. This instrument is described by Matthews in his doctoral thesis (Matthews, 1971) and subsequently (Matthews, 1972). It was reasonably successful but suffered from some systematic errors. An investigation of these errors by Basher led to the construction of a second prototype which overcame many of them by improving filters and some of the electronic circuits. An account of this second project can be found in Basher's doctoral thesis (1975) and elsewhere (Matthews et al., 1974; Basher 1977, 1978).

In any measurement of ozone by differential absorption one of the unknown errors is the effect of aerosol scattering. The assumption made in a measurement of ozone using only two bands, such as a single pair measurement with the Dobson spectrophotometer, is that aerosols do not affect the ratio of intensities. This is the same as assuming that aerosol scattering is independent of wavelength and that any relative variation in the two signals is due to ozone. A measurement with more bands allows a more sophisticated assumption about the wavelength dependence of the aerosol scattering. For example, the Dobson double pair method assumes that two pairs of wavelengths with similar separation are affected similarly by aerosol scattering. This is equivalent to the assumption that the aerosol scattering is a linear function of wavelength. The more information available on aerosol scattering the better it can be characterised and compensated for in the measurement of ozone. The converse is also true, measurements of irradiation in the visible to determine aerosol scattering are less accurate because ozone has a broad absorption band, the Chappuis band, in the visible. A typical value for the ozone amount, according to the latitude and season is often assumed, for example by Shaw et al. (1973) but because there are significant short term variations of as much as 20% from one day to the next an error is introduced.

The ozone photometers built at the University of Canterbury were very similar to the instruments used in many places for the measurement of atmospheric

attenuation or turbidity at visible wavelengths. For example an instrument at the University of Arizona (Shaw, 1973) had eight filters with passbands from 0.4-0.8 μm mounted on a similar wheel. This similarity led to the idea of an instrument that was designed with a large enough range of wavelength bands to be able to characterise both ozone and aerosol attenuation. The basic design of this instrument was put forward by Dr Reid E. Basher who is now with the New Zealand Meteorological Service. There was some delay between the instrument's conception and its completion as the project was shelved until a willing graduate student, the author, arrived to take it on. At that point the filters had already been bought and the design was at the stage of rough sketches. There were still some minor design decisions to be made and the author and members of the Physics Department's mechanical workshop contributed to these. The electronics design was handled by the electronic workshop of the Department, some of it based on the designs used for the earlier instruments and some of it new (principally the computer interfacing). A full description of the photometer is given in Chapter 2. There are of course disadvantages in a multi-function design and these are discussed in the Chapters 5 and 6.

The aim of this project was to build, commission, test and use this new photometer and to evaluate the measurements it could make. One of the hopes was that if successful it could provide information on the way in which variations in aerosol scattering interfere with the determination of ozone.

Chapter 2

Description of the Photometer

The photometer built for this project, in common with the previous photometers built at the University of Canterbury, uses interference filters to isolate wavelength bands of radiation for measurement. These earlier instruments were designed for the sole purpose of measuring atmospheric ozone by differential ultraviolet absorption of direct solar radiation, in the same way that the Dobson spectrophotometer does. The small number of channels and the limited range of wavelengths serve this single purpose well.

The current photometer was designed to combine the functions of measuring turbidity and the total ozone content of the atmosphere. A number of features reflect this. Firstly, the number of channels is larger. There are twelve in all, one of which is blocked to monitor the dark response of the instrument. They cover a range of wavelengths from the near ultraviolet, through the visible, to the near infrared. The provision of such a large number allows the passbands to be chosen to provide different kinds of information. Filters with passbands at wavelengths with little or no gaseous absorption provide information on aerosol scattering whilst others can provide information on particular absorbing species.

Secondly, to cover the wide range of wavelengths envisaged, there are two detectors. One is the same type of photomultiplier as used in the previous photometers and the other is a silicon photodiode which, despite an enhanced ultraviolet sensitivity compared with other diodes, is most sensitive in the visible and infrared. Although having two detectors complicates the instrument, there is the advantage that comparisons between the two can be made in channels where they both have useful response. Another major departure from previous designs is in the method of tracking. Because this instrument is bulkier it is more difficult to use an equatorial mount as is would involve turning the whole apparatus. For this reason, and because it gives added flexibility for other kinds of measurement, a heliostat was used to direct the radiation to the filters and detectors, which were held fixed. The heliostat could be moved to any position and was not limited to the sole function of tracking the sun.

A sketch of the photometer is shown in Figure 2.1. A detailed description of the various mechanical parts is given in Section 2.1. That is followed by a description in Section 2.2 of the electronic circuits needed to control those parts and to convert the signals from the detectors to a usable form. Because the instrument was more

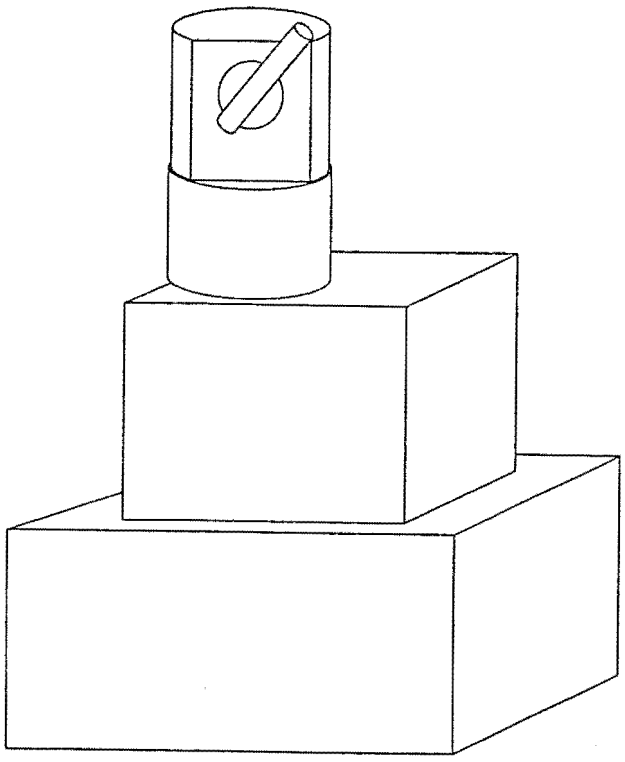

Figure 2.1: Sketch of the photometer. The motors, tubes and mirrors of the heliostat are housed in the cylindrical part at the top. Beneath that is the chamber containing the filter wheel and the detectors. At the bottom is the box housing the electronic circuits and power supplies.

complex than before, and because the heliostat required input of elevation and bearing, a microcomputer was used to control it and to record the data collected. This made the taking of measurements almost completely automatic. Details of the computer and how it was interfaced and programmed are given in Section 2.3.

2.1 Mechanical details

2.1.1 The heliostat

The heliostat consists of closed tubes, mounted on bearings so that the objective can be pointed in any direction and contains mirrors directing light from the objective vertically downward. Baffles are provided to limit the amount of off axis light reaching the filters and detectors further down. The field of view is determined by apertures at the objective end of the heliostat and near the detectors. The semi-angle of the field of view is 0.9° (54 minutes of arc). This was kept large enough to be sure that the whole of the solar disk was included and small enough to minimise the errors due to light scattered into the field of view.

The alignment of the two mirrors within the tubes was important. They were mounted on holders that ensured they were at 45° to the axis of the tube. Each then had two degrees of freedom, a lateral movement along the tube and a rotation.

The accuracy to which they could be aligned was approximately 0.2 mm and 5 minutes of arc respectively. This was sufficient to ensure that the whole of the rear aperture was illuminated by the direct solar radiation.

In order to set the instrument up to correctly track the sun, it had to be level. That is it had to be positioned so that the vertical axis of rotation of the heliostat corresponded to the local vertical. A small spirit level of approximately 1.5 cm diameter was mounted on a horizontal surface of the photometer. This little device is able to level the photometer to an accuracy of a surprising 4 minutes of arc. Levelling feet were installed beneath the photometer that between them could accommodate up to 2° adjustment. Then the instrument could then be set up on any stable and approximately level surface.

Two electric stepper motors move the heliostat, one for azimuthal movement (or bearing) and one for changing the zenith angle (or elevation). Each drives the heliostat through a worm drive gear that has an 80:1 reduction ratio. Worm gears were used because they provided a large reduction with only one compact pair of gears. The step size of the motors is 1.8° which makes the angular precision to which the heliostat can be positioned 1.35 minutes of arc. This is far smaller than needed, given the field of view and the precision to which the heliostat is set up. The gear ratio would have been better at a smaller value. This would have had another advantage in that the scan speed of the heliostat would have been greater. The value chosen was a compromise between these factors and mechanical considerations. The worm wheel had to encompass the tubes of the heliostat and a lower ratio could have been achieved with either a double worm or a much coarser pitch, neither of which is desirable from a mechanical point of view. The gears themselves were machined in the Physics Department. The drive for the elevation also has a pair of 1:1 bevel gears that help avoid mounting difficulties by allowing a more convenient orientation of the motor.

The position of the motors at any time is known only by counting the steps since each motor was at its zero position as identified by a limit switch. The difficulty of setting up positive position sensing with sufficient precision made this the more attractive option. The zero position of the zenith motor was carefully checked to be perpendicular to the surface on which the level was mounted to a precision of two minutes of arc. The photometer was usually positioned so the zero position for the azimuth drive corresponded to the photometer pointing approximately southwards. This means that, with the exception of Antarctic measurements, the photometer did not have to cross the zero position during any readings.

In any gear system, one must be aware of the problem of backlash and handle it adequately. The backlash in the two gear trains is approximately twenty minutes of arc at the objective. There is a delicate balance between setting the gears close enough to minimise backlash and getting them so tight that they may bind. The effect of backlash is largely eliminated by the way the computer did the positioning as described in Section 2.3.2.

2.1.2 Filters

Directly below the heliostat is an enclosed chamber containing the filters. They are mounted around a horizontal wheel of 300 mm diameter which is rotated about its vertical axis at a constant speed of one revolution per second so that the filters interrupt the light path in turn. Attached to the wheel is a disk with timing notches around its edge. There are thirteen notches, twelve evenly spaced to mark the filter positions and an extra to mark a reference position on the wheel, by which the filters could be identified by the computer.

The transmission of an interference filter at a particular wavelength depends on the interference, destructive or constructive, of radiation reflected at the surfaces of carefully deposited dielectric layers. Anti-reflective coatings on photographic lenses that strive to maximise transmitted light at all visible wavelengths by having reflections destructively interfere work on the same principle. Interference filters have the much more difficult task of transmitting only a small range of wavelengths and blocking as much as possible of the others. Several deposited layers are required and broad band blocking filters may be added to limit transmission at wavelengths far removed from the main passband.

Specifications for the filter set were sent to a number of possible suppliers[1]. They indicated the type of instrument the filters would be used in, and set values for the principal characteristics of each. These characteristics are listed in Table 2.1.

The bandwidths have to be a compromise between the need to be wide enough to blur out the Fraunhofer structure in the solar spectrum but not so wide that the effect of atmospheric transmission varies too widely over the passband. The bandwidths in the ultraviolet are wider than those of filters used in previous photometers which were 1–2 nm. This means that they cannot be considered as monochromatic. The implications of this are discussed in Chapter 3. The very restrictive specifications on rejection ratio were made to counter problems of leakage of side bands that were experienced with earlier Canterbury instruments. This meant that the filters would not require additional blocking.

The filters had to be mounted in holders of a specified size so that any stress in the mountings was borne by the holders rather than the filters. They were also required to be hermetically sealed in their holders to minimise the absorption of water vapour by the dielectric layers of the filters. Details of this and other aging processes are discussed in Chapter 5.

Rather than assuming that the filters matched the specifications exactly the transmission of each was carefully measured using a Cary 14 spectrophotometer. Details of this instrument and how the measurements were made with it are given in Appendix A. In some respects the filters did not meet the specifications precisely. The departures were considered acceptable, in fact the specifications allowed for such departures if they brought considerable cost savings.

The measured parameters of the passbands are shown in Table 2.2. Figures 2.2 to 2.4 show their shapes in both linear and logarithmic plots. Table 2.3 shows the

[1]The filter set was supplied by Barr Associates Inc.

Wavelength (nm)	Bandwidth (nm)	Transmission (greater than)	Rejection (better than)
311.5 ± 1	5 ± 2	20%	10^{-5}
317 ± 1	5 ± 2	20%	10^{-5}
332.5 ± 1	5 ± 2	20%	10^{-5}
368*± 1	10 ± 3	30%	10^{-4}
420 ± 1	10 ± 3	30%	10^{-4}
500*± 1	10 ± 3	30%	10^{-4}
600 ± 1	10 ± 3	30%	10^{-4}
675 ± 1	10 ± 3	30%	10^{-4}
778*± 1	10 ± 3	30%	10^{-4}
862*± 1	10 ± 3	30%	10^{-4}
940 ± 1	10 ± 3	30%	10^{-4}

Table 2.1: Specifications of the Filter Set. The three shortest wavelength filters are for the measurement of ozone. The filters marked with an asterisk are in areas free of gaseous absorption and have been chosen to conform to the World Meteorological Organisation standards for measuring turbidity as shown in Table 1.3. The filter at 420 nm may provide information on NO_2 as that gas has some absorption in that region. wavelength. The filters at 600 and 675 nm are in the weak Chappuis absorption band of ozone and so are not usually used in turbidity measurements. The filter at 940 nm is centred on an absorption band of H_2O.

parameters those sidebands which did not meet the specifications for each filter. The effect of these sidebands is discussed in Chapter 5.

The filter transmission characteristics are also temperature dependent. Because this temperature effect was a problem with earlier machines the filter chamber in this one is insulated and maintained at a nearly constant temperature with a thermostatically controlled heater. The filter wheel has fan blades to help keep even temperatures throughout the chamber. To avoid temperature effects at the start of each days readings the instrument was left powered up for some time before measurements were begun, usually overnight.

2.1.3 Detectors

Beneath the filter wheel and in the light path is a half-silvered mirror at 45° to the vertical. It splits the light so that some goes to each of the two detectors, one of which is directly below the mirror and the other is to the side. The mirror was positioned so that the active areas of the two detectors are imaged at the same place in order that they both saw the same field of view. It was positioned with a precision similar to that of the two fully silvered mirrors described in Section 2.1.1.

The first detector is a silicon photodiode manufactured by E & EG, type number UV–215B. It was selected for its enhanced ultraviolet sensitivity. Its spectral sensitivity is broad enough to cover the whole of the wavelength range of the filters and is shown in Figure 2.5. Its usefulness in the ultraviolet, however, is

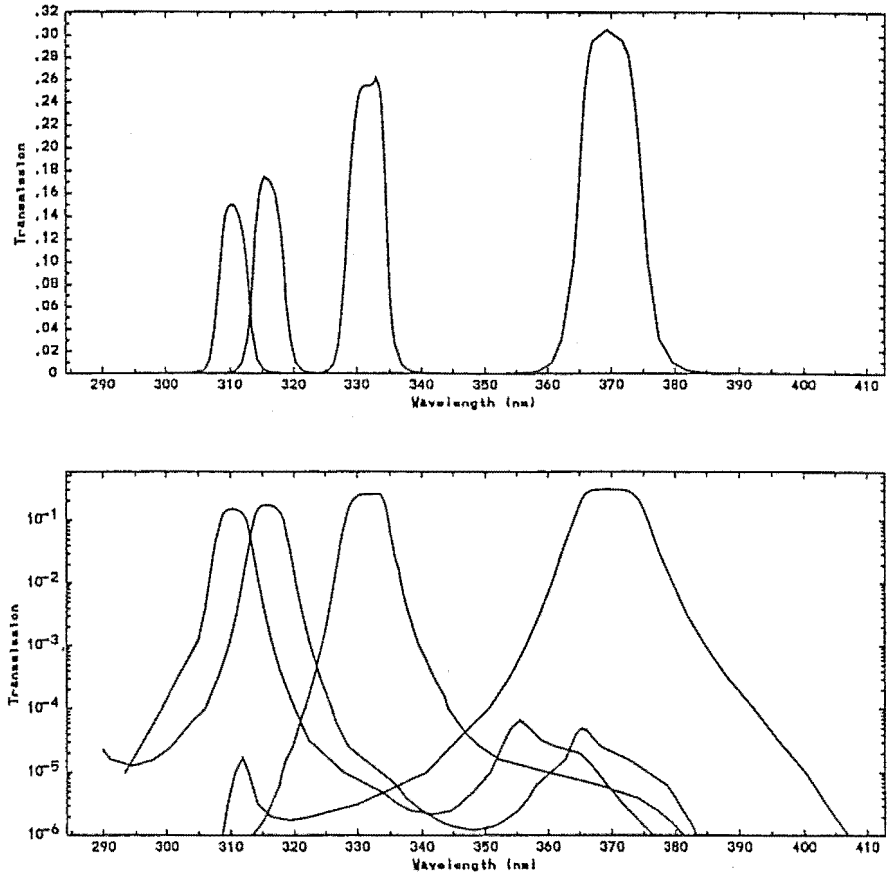

Figure 2.2: Measured transmission functions for the ultraviolet filters. The two shortest wavelength filters have significant leakages at wavelengths longer than their passband. The two plots show the same curves but with linear and logarithmic scales for transmission respectively.

Filter Number	Centre Wavelength (nm)	Peak Transmittance (%)	Bandwidths (nm)		
			$\frac{1}{2}$ Trans.	$\frac{1}{10}$ Trans.	$\frac{1}{100}$ Trans.
1	310.5	15	4.8	7.2	11.0
2	316.0	17	5.0	7.6	9.5
3	331.5	26	6.1	8.8	12.9
4	369.8	30	10.0	15.0	23.0
5	419.6	45	8.9	12.6	18.8
6	501.1	72	10.6	14.9	22.4
7	600.9	65	10.7	14.9	24.0
8	676.8	79	9.6	15.6	21.2
9	779.0	78	10.3	14.3	21.6
10	862.1	78	10.5	15.4	23.8
11	941.3	65	9.9	13.3	20.0

Table 2.2: Measured Passbands of the Filter Set

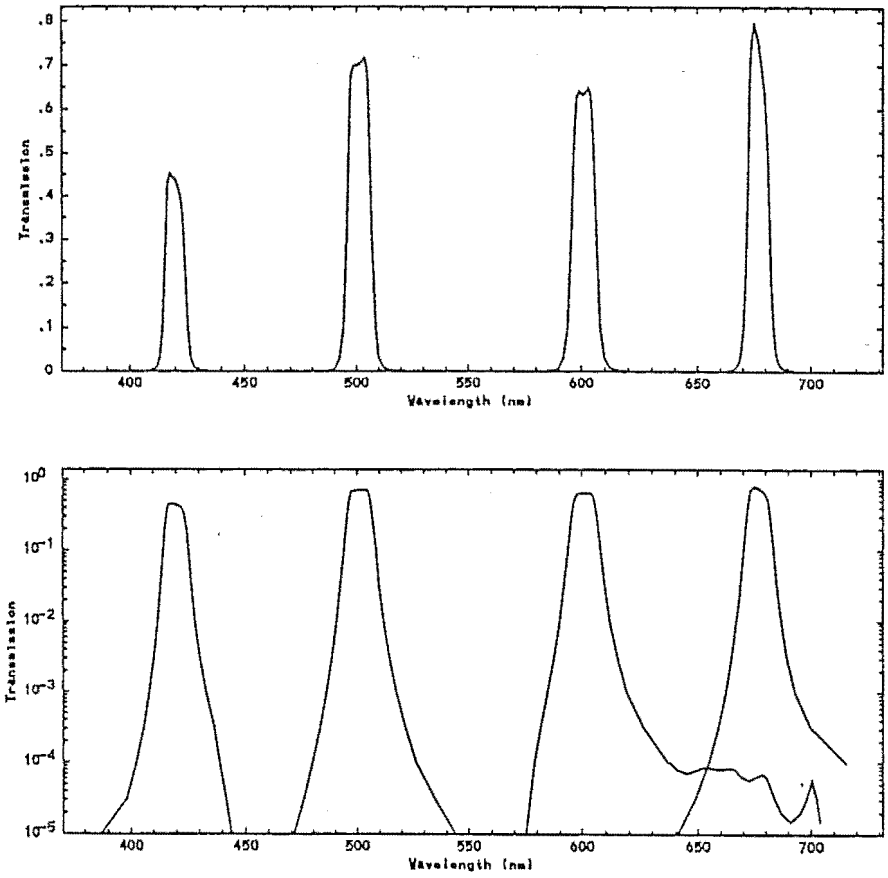

Figure 2.3: Measured transmission functions for the visible filters. Transmission scales as for Figure 2.2.

Filter Number	Centre Wavelength (nm)	Peak Transmittance (%)	Width (nm)	Transmission Ratio
1	355	0.007	5.8	4.4×10^{-4}
2	365	0.005	4.8	5.0×10^{-4}
4	310	0.0017	2.7	5.6×10^{-5}
6	>1200	*0.0004	—	$*6\times10^{-4}$
7	700	0.006	5.2	9.0×10^{-5}
7	1175	0.009	24	1.5×10^{-4}
8	1150	1.9	4.5	0.02

Table 2.3: Measured Sidebands of the Filter Set. Filter No. 6 has a passband at wavelengths larger than 1200 nm but the parameters are given at that wavelength. The side band for Filter No. 8 is the most serious.

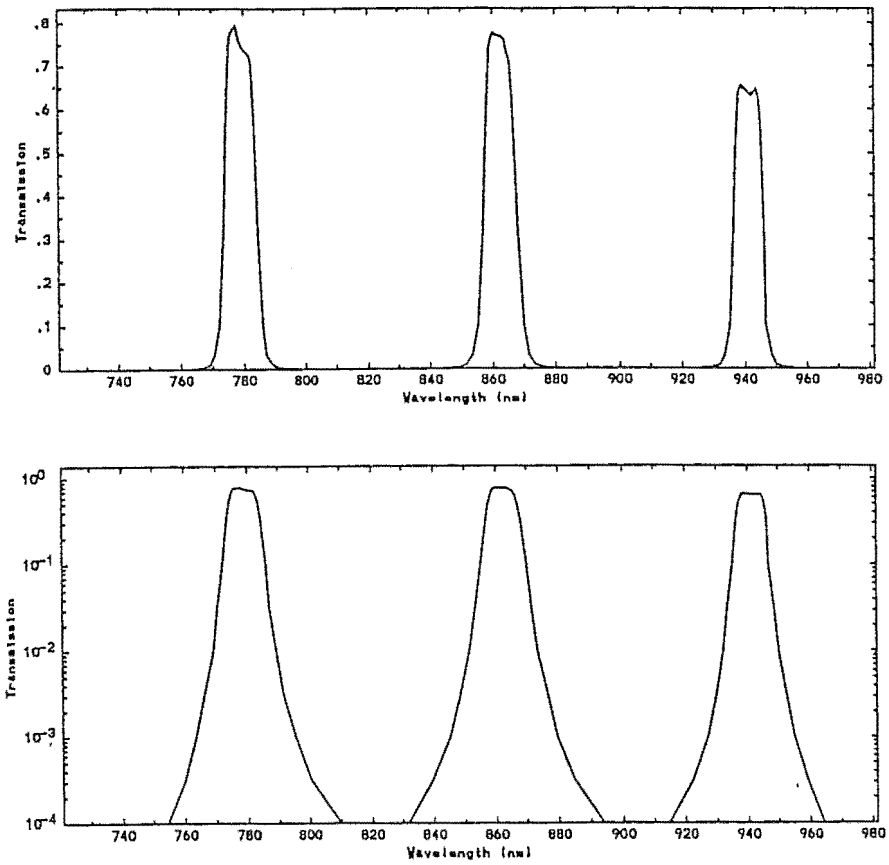

Figure 2.4: Measured transmission functions for the infrared filters. Transmission scales as for Figure 2.2.

limited by the fact that the signals in that region are smaller due to a combination of narrower filter bandwidths, lower filter transmissions and a smaller spectral solar irradiance. To minimise the effect of the diode's temperature dependence it is mounted in the same chamber as the filter wheel which is temperature controlled as described in Section 2.1.2.

The other detector is an 1P28 photomultiplier tube manufactured by RCA. This is a nine stage side-window device using caesium-antimony dynodes and a caesium-bismuth photocathode. Details of its power supply are given in the following section. The spectral sensitivity is classified as S-5 which peaks at 340 ± 50 nm and is shown in Figure 2.5. Its long wavelength cutoff is approximately 640 nm. An aperture of 5 mm diameter was placed directly in front of the photocathode to ensure that the same part of the cathode was illuminated at all times. This was important to avoid errors due to non-uniformities in the sensitivity of the cathode surface and to ensure that the active areas of the two detectors were the same size in order that they have a field of view of the same size. Photomultipliers are complex devices and their performance has as much to do with how they are used as with any inherent features. A full discussion of the errors in the readings of this photomultiplier tube is given in Chapter 5.

The photomultiplier tube is mounted in a chamber directly below that con-

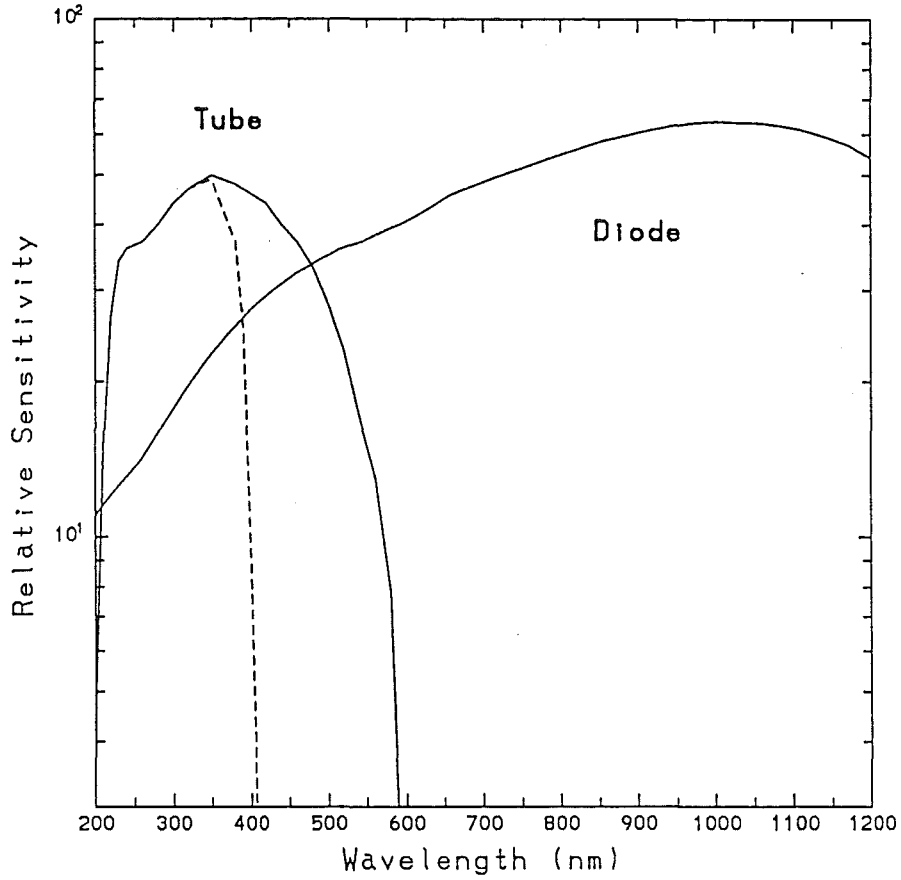

Figure 2.5: Spectral sensitivity of the photodiode and the photomultiplier tube. The dotted line shows the effective sensitivity of the latter due to a blocking filter that was added later and is described in Section 4.2.1.

taining the filter wheel and photodiode as the elevated temperature of the filter chamber would degrade its performance. Both the chambers had to be made as light tight as possible. Joints were designed so to minimise straight line paths for light to enter the instrument.

2.2 Electronic details

The electronic circuits in the photometer consist of the following elements:–

Drivers for the two stepper motors: These consist of constant current supplies to maintain holding currents in the motors' windings with the facility to switch off and reverse each one in order to step the motor.

Sensors for the zero positions of the heliostat: The zenith zero position is detected with an optical switch[2] on the edge of a disk that turned with the objective and had one hole drilled in it to activate the switch. Its setting was critical

[2]This consists of a light emitting diode on one side and a photosensitive transistor on the other.

for the alignment of the heliostat: the direction indicated by the switch had to be the same as the vertical axis of rotation of the heliostat. This was achieved to a precision of 5 minutes of arc. The switch for the azimuth movement is a mechanical microswitch. In addition to providing a reference point it allows the photometer to be programmed not to wrap its cables by more than one revolution [3].

A driver for the filter wheel motor: This is set to run the motor at a constant speed. Using an identical stepper motor simplified the provision of spare parts, and allowed the flexibility of being easily able to change the speed at which the wheel was rotated. In fact the initial speed of one wheel revolution per second was never changed as there was no need.

A heater and thermostat for the filter chamber: The heater consisted of a number of resistors glued to heat dissipating fins, capable of dissipating 50 W, and a temperature sensing circuit wired to switch it on and off. The temperature was stable at $38 \pm 1°C$

A sensor for the filter wheel position: This is an optical switch, identical to that used for the zenith zero position, mounted around the edge of the timing disk on the filter wheel to sense the timing notches on it, and circuits to separate its output into two signals, one to give the filter wheel reference once per wheel revolution and one to give a pulse for each filter position. The latter is used to indicate when the filter is in a suitable position for taking a measurement.

A high voltage supply for the photomultiplier tube: This could be adjusted manually from 600 to 1100 Volts in order to vary the gain. The voltage at each individual electrode of the tube was determined by a resistive voltage divider as shown in Figure 2.6. The power supply was stabilised to ensure it did not cause unacceptable variations in the photomultiplier's signal.

Photomultiplier protection: This was a solenoid operated shutter directly above the photomultiplier tube to protect it from light when the filter chamber is opened up. This means that the top chamber could be opened up without the precaution of disconnecting the high voltage supply from the photomultiplier tube.

Temperature sensors: These consist of a semiconductor device, an LM335, that has a temperature dependent breakdown voltage which is amplified to produce a usable voltage signal. They are used to monitor ambient and filter compartment temperature.

A voltage to frequency converter for the photodiode output: This is based on the LM331 high-precision voltage to frequency converter. Its output consists of a sequence of pulses whose frequency is proportional to it input voltage. To

[3]See the section on Antarctic measurements in Chapter 4

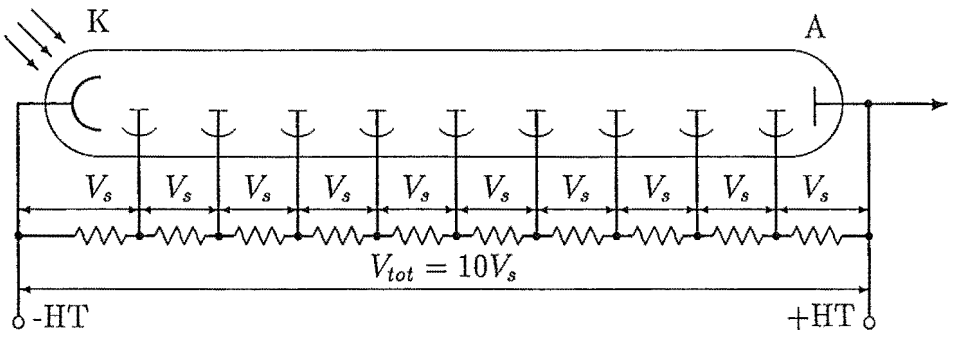

Figure 2.6: The voltage divider for the photomultiplier tube. The resistors are all 100 kΩ

provide a suitable input for the converter there is a pre-amplifier, the gain and offset of which can be adjusted.

A current to frequency converter for the photomultiplier tube output: This is similar in operation to the circuit used in the last prototype photometer. It consists of a small capacitor that is charged by the photomultiplier's output current and discharged when it reaches a given voltage by a transistor that is switched by CMOS logic gates.

Most of these circuits, and their power supplies, are housed in a separate box below the photometer's detector chambers.

2.3 Interfacing and Programming details

2.3.1 Interfacing with the Microcomputer

The photometer is interfaced with a Commodore PET microcomputer. This is an eight bit machine that has a 6502 processor. It has been well surpassed by more modern microcomputers but is adequate for the job of controlling the photometer. The electronic workshop of the Physics Department and the author had previous experience with interfacing and programming these machines.

Connected to the microcomputer, and housed in a box beneath it, is an SS-30 interface board with five slots which are addressable from the computer. In each slot an interface chip, generally a 6522 peripheral interface adapter (PIA), is connected to part of the photometer's circuitry. The connections are all made through a single 50 conductor cable so that the interface and computer can be some distance from the photometer itself. The various connections are:–

A timer and counter for each detector: At the appropriate time the timer is initiated to send the frequency output from the detector circuits to a 12 bit counter for a duration of 20 ms, during which the filter has moved about

one quarter of its diameter. At the end of the timed period the value held by the counters is proportional to the detector outputs.

The analogue to digital converter: This is a chip, ADC0809, with eight analogue inputs and lines that enable any one of the inputs to be selected and converted to digital form (8 bits). Only three of the inputs are currently used. One, the most important, is connected to a simple voltage divider on the photomultiplier tube power supply. This signal could be scaled by the computer to give the voltage of the supply. The other two are connected to the temperature sensors in the filter chamber and on the outside of the photometer. A pulse to initiate the conversion for each input is sent whenever a reading is required.

A real time clock: While a real time clock has now become standard on microcomputers the PET did not have a usable clock system so an external one was added. This is a single chip, type MSM5832, controlled by a 32 768 Hz crystal. The output of the crystal is divided to produce signals for the chip's internal registers that keep track of the date and the time to the nearest second. The clock is connected to a standard PIA and is powered by a battery so that the time is not lost if the instrument is switched off. Its accuracy was about ± 1 seconds per day which was sufficient for the purpose of sun tracking but was checked and corrected once every few days.

The motor controllers: These are purpose built integrated circuits that switch the appropriate windings of the zenith and azimuth motors given the desired direction to be stepped.

Various other inputs and outputs to the computer were also necessary. They included:

- an input for the filter wheel timing pulse
- an input for the filter timing pulse
- inputs for the limit switches of the motors
- an output to control the shutter protecting the photomultiplier tube.

2.3.2 Programming the Microcomputer

The microcomputer's operating system is Commodore's version of the BASIC language. Its main drawback is speed; BASIC is slow because it is interpreted as it executes rather than being compiled before run time. Since most of the time the photometer is waiting to take a reading this does not cause many problems. There are however a number of operations that must be done at a rate faster than the BASIC could handle. Consequently, the programming for the computer was written in three levels. These are:–

1. Machine code routines to perform the operations that must be done faster than BASIC can handle.

2. Modules written in BASIC to perform all of the tasks required of the photometer. Some of these perform calculations and others will call routines from the previous level.

3. The main controlling program, written in BASIC that calls modules of the previous level.

Machine code routines

The operations that had to be done with machine-code routines were:–

Read from the real time clock: Since reading the clock involves putting it on hold while its registers are read, the whole operation must be completed in somewhat less then a second if the time is not to be affected.

Drive the stepper motors: With the reduction of the worm gear system the faster the motors could be stepped the more acceptable the scan speed. A count of the steps made had to be kept as this was the only way of knowing the position of the motor and hence the direction the heliostat was pointing [4] . After each step the two motor limit switches were checked to see if they were active and appropriate action taken if they were. This meant that if the counts of steps were corrupted in any way then the machine would still not get in a tangle by over stepping the limit switches.

Take readings from the detectors: This involves sensing when a filter is in position by waiting for the appropriate pulse, gating the counter to integrate the readings from the detector and storing the count. This must be done fast enough to be ready for the next filter in 80 milliseconds time. The operation is continued for several revolutions of the filter wheel, with counts being added to previous counts from the same channel until either a specified number of revolutions have completed or one of the accumulated counts exceeds a preset value.

Routines to perform these tasks were written by the author in 6502 machine code using a simple assembler. All input and output for these routines was handled through a buffer of about 80 bytes with each byte being used for only one purpose. Calling one of the routines from a BASIC program involved placing any required input in the appropriate buffer position, calling the routine and then reading any output from the buffer. The intention was that once the machine code routines were written, the remaining programming could be done in BASIC. This was achieved and none of the routines has required modification from its final tested form. It was originally planned to have these routines written or burned into a programmable read only memory (EPROM) so that they formed part of the permanent system of the instrument. However, it was found during the programming and testing phase that it was as convenient to have the routines in

[4]This need meant that the stepping rate could not be raised past the point where missed steps were likely.

volatile memory (RAM) and no great advantage was to be gained from setting the machine code into a more permanent form.

Some other routines were also assembled to do things that were always going to be done together, that helped in the testing of other routines or would be quite cumbersome if done in BASIC. These included:–

Read the analogue to digital converter: The conversion of each input is started by a pulse and the digital result is read at the appearance of a flag. This was a fairly simple task that could have been done in BASIC but was much more elegant in machine code.

Write to the real time clock: This could have been done from BASIC but would have been rather slow, making accurate setting of the clock difficult.

Initialise the interface chips: Each of the PIAs had to be configured, that is, each line had to be designated as either output or input and the way in which it was controlled or what it controlled defined. Routines to do this were written in machine code to allow the other routines to be run and tested on correctly configured devices.

Dump the buffer contents: This routine showed a listing of the contents of the buffer in hexadecimal to allow checking and testing of the other routines.

The BASIC program.

The BASIC program that ran the system was kept as modular as possible within the constraints of the language. That way the main control loop in the program was kept very short, aiding readability and modifications. It had modules to perform the following functions:–

Initialise the system variables: This includes setting the latitude and longitude required for the calculation of solar position.

Handle output of data: The data was written to floppy disk after each reading was taken. This consisted of taking a copy of the buffer used to communicate with the machine code routines along with a checksum to allow for some error checking when the data was read. This was the most compact way of recording the data.

Calculate the position of the sun: This was split up into a determination of solar position in celestial coordinates (i.e. determining the solar declination and right ascension from a knowledge of the season) and a second step, the transformation from celestial to local terrestrial coordinates (this required knowledge of the local time, time zone and position on the earth, i.e. the latitude and longitude)[5]. The checks of the algorithm were two fold. The values of solar declination and right ascension it produced were checked

[5]This division was made in case moon measurements were to be considered at a later date. The second step would be common to a calculation of lunar position.

against the published values in the Astronomical Almanac [6] and was also checked against a large existing program written in FORTRAN-66 by Dr N.A. Doughty at University of Canterbury some years ago for a similar purpose.

Move the motors: The desired position of the motors is converted to the step counts and the machine code routine to move the motors is called. Provision was made to avoid the effect of backlash in the gears by always approaching the final position from the same direction, downwards in the case of zenith and clockwise in the case of azimuth, even if that meant overstepping the desired position and backtracking.

In the conversion from terrestrial coordinates to step counts, the direction corresponding to the zero position of the azimuth motor had to be known. When the photometer was being operated from a fixed platform, this direction could be assigned a value as part of the initialisation routine. However, when the photometer was operated from a new or temporary platform the direction had to be established with the routine described next.

Step the azimuth motor: This allows the azimuth motor to be moved by arbitrary amounts by keyboard command in order to align the photometer with the sun. The alignment was established by a combination of positioning the shadow of the objective and checking that the signals at the detectors were maximised. When the alignment was done the offset between the photometer's coordinates and the real terrestrial coordinates was calculated so that motor positions for the rest of the day would be correctly set. If measurements were to be made over an extended period from a fixed platform then the correct offset could be written into the code of the operating program and there would no longer be a need for this routine.

Take readings from the detectors: This task is handled at the machine code level because it needs to be done at speed, so this BASIC routine is simply a shell that consists of a call to the machine code routine with the appropriate parameters set and error checking on return.

Read the analogue signals: Only three channels of the analogue to digital converter are actually used: one each for the photomultiplier tube supply voltage, the ambient temperature and the filter temperature. The first is the most important as the magnitude of the current from the photomultiplier tube depends strongly on it[7]. The others are included as checks only.

Wait until a given time occurs: Reads the time from the real time clock until it reaches the desired time. Return with an error flag if the time has already passed.

---

[6]This publication, formerly the American Ephemeris and Nautical Almanac is prepared annually by the Nautical Almanac Office, United States Naval Observatory, and Her Majesty's Nautical Almanac Office and published jointly by the United States Government Printing Office and Her Majesty's Stationery Office.

[7]Details of how the signal currents taken with different supply voltages are related are given in Section 4.1.

Once the simple modules were written more complex ones could be built from them. For example, a routine to calculate the sun's position for a given time, move the motors to that position, wait for the specified time and take a set of readings was constructed using calls to the simpler routines. This formed one of the building blocks for the main control part of the BASIC program. That part could then be relatively short. It defines when to take readings, decides whether to save each one to disk and other general housekeeping tasks such as when to open and close disk files. Its form was changed for different locations with relative ease. Details of these changes are given in Chapter 4.

The description of the programs has been made deliberately brief. Listings of the programs, with explanatory notes, are in Appendix B.

Chapter 3

Theory of Direct-Sun Measurements

The simplest description of direct-sun measurements is one which treats each measurement as if it were made at a single wavelength. This is referred to here as the monochromatic theory. While it is an inappropriate approximation in many cases, it provides a good starting point to the discussion of more complex descriptions.

3.1 Monochromatic theory

The diminution of radiation as it passes through an absorbing or scattering medium can be described by the Bouger law which relates the fraction of the radiant flux $I(\lambda)$ in the small wavelength range λ to $\lambda + d\lambda$ that is removed in traversing a path of length ds by an attenuation coefficient k.

$$\frac{dI(\lambda)}{I(\lambda)} = -k(\lambda)ds \tag{3.1}$$

Since the attenuation is usually [1] proportional to the concentration of whatever particles are responsible, k can be written as

$$k(\lambda) = \sigma(\lambda)N \tag{3.2}$$

where N is the number density (number per unit volume) of the particles and σ is a coefficient with units of area called the effective cross-section. If there is more than one mechanism that removes the radiation then k is the sum of the individual contributions of the form of Equation 3.2.

In the atmosphere there are at least three such components. The first is that due to scattering by air molecules, called Rayleigh scattering after Lord Rayleigh who first described a theory to explain it (Rayleigh, 1899). Rayleigh produced an expression for the scattering cross-section of a molecule by treating

[1] Exceptions are discussed later on page 37.

it as an isotropic dipole that oscillated in response to the applied electric field of the incident radiation. For this the scattering cross-section is

$$\sigma_R(\lambda) = \frac{8\pi^3}{3}\frac{(\nu^2-1)^2}{\lambda^4 N^2}D \tag{3.3}$$

where ν is the refractive index, N the number density of all molecules, and D is the correction required due to the anisotropy of the molecules. D has a value slightly larger than one but there has been some recent debate over the correct value to use. This is discussed more fully in Section 5.3. The dependence of the scattering cross-section on λ^{-4} was the first correct explanation of the blue of the sky. The actual wavelength dependence is close to, but not quite λ^{-4}, the deviation being due to the wavelength dependence of the refractive index ν (and also D).

The second component of k is that due to suspended particles or aerosols. This depends in a complex way on the size, the shape and the composition (refractive index) of the particle. Mie (1908) described a theory explaining the scattering of a uniform spherical particle of arbitrary size. It gives expressions for the scattered radiation in the form of an infinite series of spherical Bessel functions. For measurements of extinction, the directions in which the radiation is scattered are not important but the total amount of radiation removed from the incident beam by scattering is. This is expressed in terms of the scattering efficiency Q, which is the ratio of its effective scattering cross-section to its actual cross-section , $\pi\times$ the square of the radius. This efficiency is a function of the size parameter, the ratio of the radius of the particle to the wavelength of the incident light, and the refractive index ν of the particle. At very small values of the size parameter, the scattering agrees with Rayleigh theory. At large values the efficiency approaches two, twice the intuitive geometric limit of a particle casting a shadow equal to its cross-section [2]. Between these extremes the behavior of the efficiency is complex and oscillatory. The net effect of a distribution of such spherical particles, in which the number density of particles in the size range r to $r + dr$ is $n(r)$, is

$$k_M = \int_{r_{min}}^{r_{max}} \pi r^2 Q(r,\lambda,\nu) n(r) dr \tag{3.4}$$

The size limits of the integral are the sizes that ensure that all aerosol particles are included. While Mie's theory is applicable only to uniform spherical particles, it is often applied to real particles because to treat them completely is extremely difficult. Results from complete solutions for other shapes of particle have different features but these tend to be smoothed out when a population of such particles of varying size and orientation is considered. Details of this sort and methods of calculating Q can be found in Twomey (1977).

The final component of the total extinction is that due to molecular absorption. Various gases will absorb at particular wavelengths and the contribution of each will generally be the product of the molecular absorption cross-section and the number density as in Equation 3.2. Ozone is the principal absorbing gas at the

[2]This is because diffraction at the edges of a relatively large particle also removes light from the direct beam.

wavelengths considered here. It has strong absorption in the ultraviolet Huggins band (300–340 nm) and a broad absorption in the visible Chappuis band (400–700 nm). Other gases with absorption in this range are nitrogen dioxide and water vapour.

The absorption coefficient k in Equation 3.1 can be written as

$$k = k_R + k_M + k_{O_3} + \ldots \tag{3.5}$$

where the ellipsis indicates that further terms to include other absorbing gases will be included as necessary.

For direct solar radiation in the atmosphere the path length ds can be written as $\sec\psi(h)\mathrm{d}h$, where ψ is the angle between the zenith and the beam (known as the zenith angle) and h is the height. The direct solar radiation reaching the ground $I(\lambda)$, can be found by integrating Equation 3.1 from $h = 0$ to h_{ET}, where h_{ET} is the height above which absorption can be ignored. Thus we have

$$\begin{aligned}\ln\left[\frac{I(\lambda)}{I_0(\lambda)}\right] &= -\int_0^{h_{ET}} \sigma_R(\lambda)N(h)\sec\psi(h)\mathrm{d}h \\ &\quad -\int_0^{h_{ET}}\int_{r_{min}}^{r_{max}} \pi r^2 Q(r,\lambda,\nu)n(r,h)\mathrm{d}r\sec\psi(h)\mathrm{d}h \\ &\quad -\int_0^{h_{ET}} \sigma_{O_3}(\lambda)N_{O_3}(h)\sec\psi(h)\mathrm{d}h \\ &\quad -\ldots\end{aligned} \tag{3.6}$$

where $I_0(\lambda)$ is the intensity of solar radiation outside the atmosphere, the extraterrestrial solar radiation. As it stands the equation is unwieldy and some simplifications can be made. Each term can be simplified by taking the cross-sections out of the integral and writing the equation as

$$\begin{aligned}\ln\left[\frac{I(\lambda)}{I_0(\lambda)}\right] &= -\sigma_R(\lambda)\int_0^{h_{ET}} N(h)\sec\psi(h)\mathrm{d}h \\ &\quad -\int_{r_{min}}^{r_{max}} \pi r^2 Q(r,\lambda,\nu)\mathcal{N}(r)\mathrm{d}r\int_0^{h_{ET}}\sec\psi(h)\mathrm{d}h \\ &\quad -\sigma_{O_3}(\lambda)\int_0^{h_{ET}} N_{O_3}(h)\sec\psi(h)\mathrm{d}h \\ &\quad -\ldots\end{aligned} \tag{3.7}$$

This involves an approximation in the case of the aerosol scattering term as the aerosol is assumed to have the same size distribution at all heights. $\mathcal{N}(r)$ is the number of particles, in a vertical column of unit area, with sizes between r and $r + \mathrm{d}r$.

A further simplification is to separate the part of each term that varies with the zenith angle. This is done with a quantity expressing the ratio of that term to its value for an overhead sun, known as the relative airmass or the column ratio, expressed as a function of the apparent zenith angle at ground level, $\psi(h = 0) = \psi_0$.

ψ_0. For example the column ratio for the Rayleigh term is the function

$$\mu_N(\psi_0) = \frac{\int_0^{h_{ET}} N(h) \sec \psi(h) \mathrm{d}h}{\int_0^{h_{ET}} N(h) \mathrm{d}h} \tag{3.8}$$

and the ratios for the other terms are defined similarly. Those for the ozone term and the aerosol term are denoted μ_{O_3} and μ_A respectively. The values of these ratios are not identical because the height distributions of the different entities are different. They are approximated as follows:

μ_N Values of the integrals in Equation 3.8 are evaluated for a standard atmosphere and an empirical fit made to the resulting values following Kasten (1966). The empirical function is

$$\mu_N = \left[\cos(\psi_0) + a(b - \psi_0)^{-c}\right]^{-1} \tag{3.9}$$

where $a = 0.15$, $b = 93.885°$ and $c = 1.253$ if ψ_0 is in degrees. The resulting function accounts for both the curvature of the earth and atmospheric refraction along the light path.

μ_{O_3} Since the bulk of the ozone is concentrated between 20–25 km the secant of the zenith angle at that height is used. This is related to the zenith angle at the ground by the expression

$$\mu_{O_3} = \sec\left[\arcsin\left(\frac{R_\oplus}{R_\oplus + h_{O_3}} \sin(\psi_0)\right)\right] \tag{3.10}$$

where $R_\oplus$=6400 km, the earth's radius, and h_{O_3} is taken as 22 km.

μ_A Since most of the aerosol scattering occurs in the lower few kilometers of the atmosphere, μ_A is taken as the secant of the apparent zenith angle at the ground, that is

$$\mu_A = \sec(\psi_0) \tag{3.11}$$

The three column ratios μ_N, μ_{O_3}, and μ_A are very nearly equal for $\mu < 3.0$, that is for $\psi < 70°$, and are known collectively as the airmass. However, at $\psi = 80°$ they differ by a few percent and for larger zenith angles they are quite different. This is shown in Figure 3.1. Care must therefore be taken to use the correct ratio for each term in Equation 3.7, which can now be written in the much simpler form

$$I(\lambda) = I_0(\lambda) \exp\left[-\mu_N \tau_R(\lambda) - \mu_A \tau_A(\lambda) - \mu_{O_3} \mathcal{N}_{O_3} \sigma_{O_3}(\lambda)\right] \tag{3.12}$$

neglecting the possibility of further gaseous absorption terms and where τ_R and τ_A are the Rayleigh and aerosol optical depths respectively, and $\mathcal{N}_{O_3}$ is the column density of ozone which is the number of ozone molecules in a vertical column of unit area. The product $\mathcal{N}_{O_3}\sigma_{O_3}$ is the optical depth due to ozone and is usually converted to more convenient units using

$$\mathcal{N}_{O_3}\sigma_{O_3}(\lambda) = X_{O_3}\alpha_{O_3}(\lambda) \tag{3.13}$$

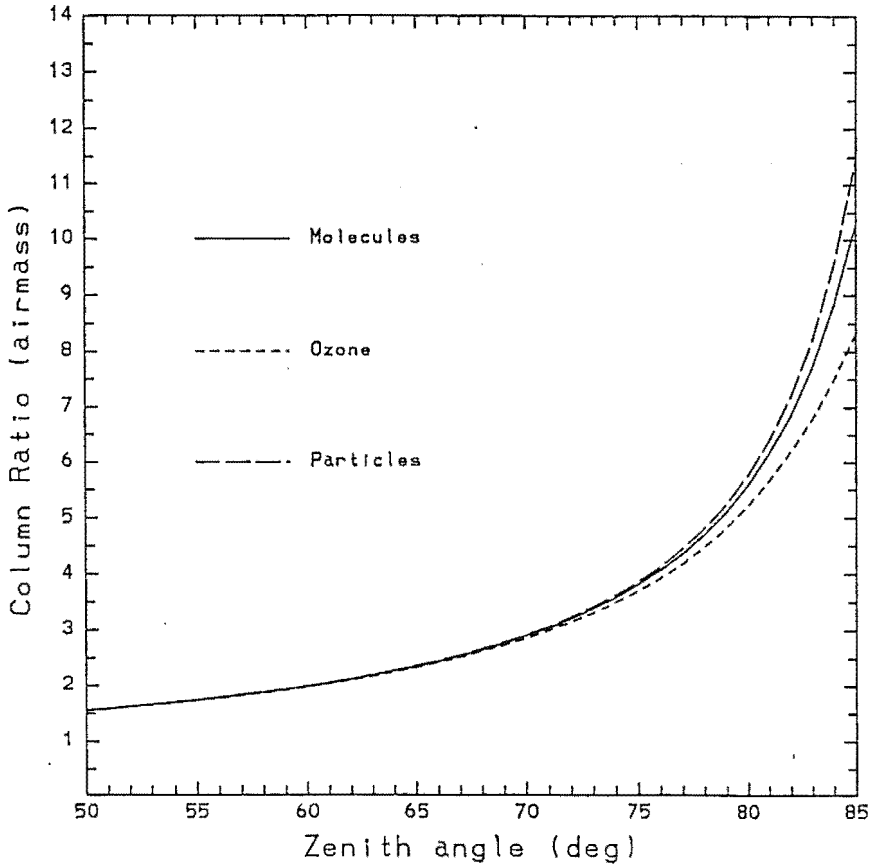

Figure 3.1: The airmass functions or column ratios for molecular scattering, ozone absorption, and aerosol scattering. The functions are almost identical for zenith angles smaller than those shown.

where X_{O_3} is the column amount of ozone in centimetres at standard temperature and pressure, known as atmosphere-centimetres, and $\alpha_{O_3}(\lambda)$ is the absorption coefficient in cm^{-1}.

A knowledge of $I(\lambda)$ at different wavelengths can yield information about the variables in the right hand side of Equation 3.12. For example, the standard single pair method used with the Dobson spectrophotometer measures the ratio of I at two different wavelengths. The wavelengths are chosen to make the ratio strongly dependent on X_{O_3}, the total ozone.

Up to this point the discussion has assumed that the Bouger law does in fact describe the reduction in radiation as it passes through the atmosphere. However, a real spectrophotometer cannot be made to respond only to a single wavelength, so a real measurement of radiation cannot be truly monochromatic. It always has a finite bandwidth, or range of wavelengths, whether that range is defined by a physical aperture in a dispersive system or by the properties of a particular element of the system. This can have a significant effect even on narrow band direct-sun radiation measurements, which are supposed to be as close to monochromatic as possible. Using a monochromatic assumption is adequate if the absorption within the band is due to numerous evenly spaced unsaturated absorption features or to

to an absorption continuum much broader than the bandwidth. If however, the bandwidth of the filter is on the wing of some absorption feature then there will be wavelengths that are less strongly absorbed by the atmosphere and those wavelengths will contribute proportionally more to the measured signal as the path length increases. In extreme cases it is possible for the most significant contribution to the measured signal to be from wavelengths some distance from the central wavelength of the band. A similar effect can occur if the filters have sidebands, are not sufficiently blocked over the range of wavelengths to which the detector is sensitive, or if the main passband has not got steep enough sides. A modification to the monochromatic theory that copes with these effects is described in the following section.

A more serious complication occurs if any of the absorption lines in or near the bandwidth are very strong. In that case the absorption within the bandwidth is no longer proportional to the quantity of the absorber because processes that broaden the line (and hence vary the total absorption) become important. These processes are dependent on the pressure and temperature along the path. Houghton (1986) provides a brief introduction on how such cases can be treated. One such case occurs in the filter set of this instrument and this is discussed in Chapter 4 on page 61.

3.2 Bandwidth theory

The result of a measurement with a real photometer P, is an integral, over a certain range of wavelengths, of the spectral response function $R(\lambda)$, as

$$P = \int_{\lambda_1}^{\lambda_2} R(\lambda) \mathrm{d}\lambda \tag{3.14}$$

The spectral response function at a given wavelength λ, can be expressed as

$$R(\lambda) = \mathcal{R} I(\lambda) F(\lambda) D(\lambda) \tag{3.15}$$

where $\mathcal{R}$ is a proportionality constant that accounts for non-spectral effects such as aperture sizes and detector gain, and the three other factors are $I(\lambda)$ the incident spectral radiation intensity, $F(\lambda)$ the transmission of the filter, and $D(\lambda)$ the relative spectral sensitivity of the detector.

In practice the wavelength limits will be determined by $F(\lambda)$ or $D(\lambda)$. If the range $\lambda_1 - \lambda_2$ is small enough that the radiation intensity does not vary much over the this range, then the measurement can be treated as monochromatic. If that is not the case, then a more thorough treatment of the measurements must be made.

For direct-sun measurements considered here the radiation intensity being measured is given in Equation 3.12. Substituting this into Equation 3.15 gives

$$R(\lambda) = R_0(\lambda) \exp\left[-\mu_N \tau_R(\lambda) - \mu_A \tau_A(\lambda) - \mu_{O_3} X_{O_3} \alpha_{O_3}(\lambda)\right] \tag{3.16}$$

where $R_0(\lambda)$ is the extraterrestrial spectral response function and $R(\lambda)$ is the spectral response function at the ground. A measurement can thus be represented

as

$$P = \int_{\lambda_1}^{\lambda_2} R_0(\lambda) \exp\left[-\mu_N \tau_R(\lambda) - \mu_A \tau_A(\lambda) - \mu_{O_3} X_{O_3} \alpha_{O_3}(\lambda)\right] d\lambda \tag{3.17}$$

At this point an equivalent ozone absorption coefficient $\overline{\alpha}_{O_3}$, is introduced. If Equation 3.17 is written as

$$P = \exp[-\mu_{O_3} X_{O_3} \overline{\alpha}_{O_3}] \int_{\lambda_1}^{\lambda_2} R_0(\lambda) \exp\left[-\mu_N \tau_R(\lambda) - \mu_A \tau_A(\lambda)\right] d\lambda \tag{3.18}$$

then $\overline{\alpha}_{O_3}$ is defined as

$$\overline{\alpha}_{O_3} = \frac{-1}{\mu_{O_3} X_{O_3}} \ln \left[\frac{\int_{\lambda_1}^{\lambda_2} R_0(\lambda) \exp\left[-\mu_N \tau_R(\lambda) - \mu_A \tau_A(\lambda) - \mu_{O_3} X_{O_3} \alpha_{O_3}(\lambda)\right] d\lambda}{\int_{\lambda_1}^{\lambda_2} R_0(\lambda) \exp\left[-\mu_N \tau_R(\lambda) - \mu_A \tau_A(\lambda)\right] d\lambda} \right] \tag{3.19}$$

Similarly an equivalent aerosol optical depth $\overline{\tau}_A$, can be defined as

$$\overline{\tau}_A = \frac{-1}{\mu_A} \ln \left[\frac{\int_{\lambda_1}^{\lambda_2} R_0(\lambda) \exp\left[-\mu_N \tau_R(\lambda) - \mu_A \tau_A(\lambda)\right] d\lambda}{\int_{\lambda_1}^{\lambda_2} R_0(\lambda) \exp\left[-\mu_N \tau_R(\lambda)\right] d\lambda} \right] \tag{3.20}$$

and an equivalent Rayleigh optical depth $\overline{\tau}_R$, as

$$\overline{\tau}_R = \frac{-1}{\mu_N} \ln \left[\frac{\int_{\lambda_1}^{\lambda_2} R_0(\lambda) \exp\left[-\mu_N \tau_R(\lambda)\right] d\lambda}{\int_{\lambda_1}^{\lambda_2} R_0(\lambda) d\lambda} \right] \tag{3.21}$$

With these substitutions Equation 3.18 becomes

$$P = P_0 \exp[-\mu_N \overline{\tau}_R - \mu_A \overline{\tau}_A - \mu_{O_3} X_{O_3} \overline{\alpha}_{O_3}] \tag{3.22}$$

where P_0 is the extraterrestrial total response

$$P_0 = \int_{\lambda_1}^{\lambda_2} R_0(\lambda) d\lambda \tag{3.23}$$

Equation 3.22 is analogous to Equation 3.12, developed in Section 3.1, for measurements treated monochromaticly. The definitions of the quantities $\overline{\alpha}_{O_3}$, $\overline{\tau}_R$, and $\overline{\tau}_M$ are dependent on the order in which they are "extracted" from Equation 3.17. A different order could have been used, giving different definitions[3]. They will in general be functions of airmass, total ozone, pressure, and aerosol content of the atmosphere. If their behaviour as these parameters vary is known then the effects of finite bandwidth and any sidebands in each filter can be accounted for. This is one of the objectives of the undertaking described in Section 3.3.

[3]The order chosen was to ensure that the most rapidly varying function of wavelength, the ozone absorption coefficient $\alpha_{O_3}(\lambda)$, appears in just one definition.

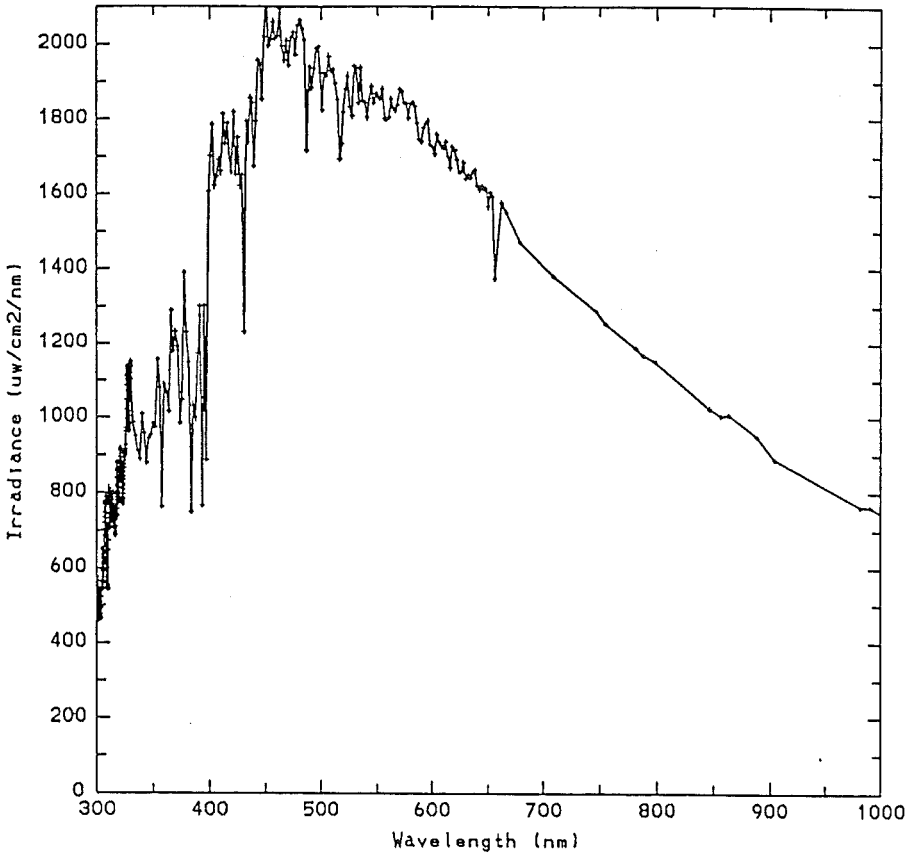

Figure 3.2: The spectral solar irradiance used in the model. The data is a composite from Neckel and Labs (1981) and Thekaekara (1974).

3.3 Spectral model of the measurements

A computer model was written to simulate the measurements made with the photometer. Spectra for the various functions required for it were either measured or taken from appropriate references. A brief description of each follows.

3.3.1 Solar irradiance

The spectrum for solar irradiance used was based on the data of Neckel and Labs (1981) which provides values of spectral irradiance for 2.0 nm bandwidths. The centre wavelengths of the bands are unevenly spaced at approximately 2 nm intervals. It covers the range 330–1240 nm. Points for shorter wavelengths were taken from the spectrum by Thekaekara (1974) which gives solar irradiance at 0.1 nm intervals. The combined spectrum is shown in Figure 3.2. The accuracy of these values is approximately ±10–15% at wavelengths less than 330 nm and ±5% at longer wavelengths (WMO, 1986).

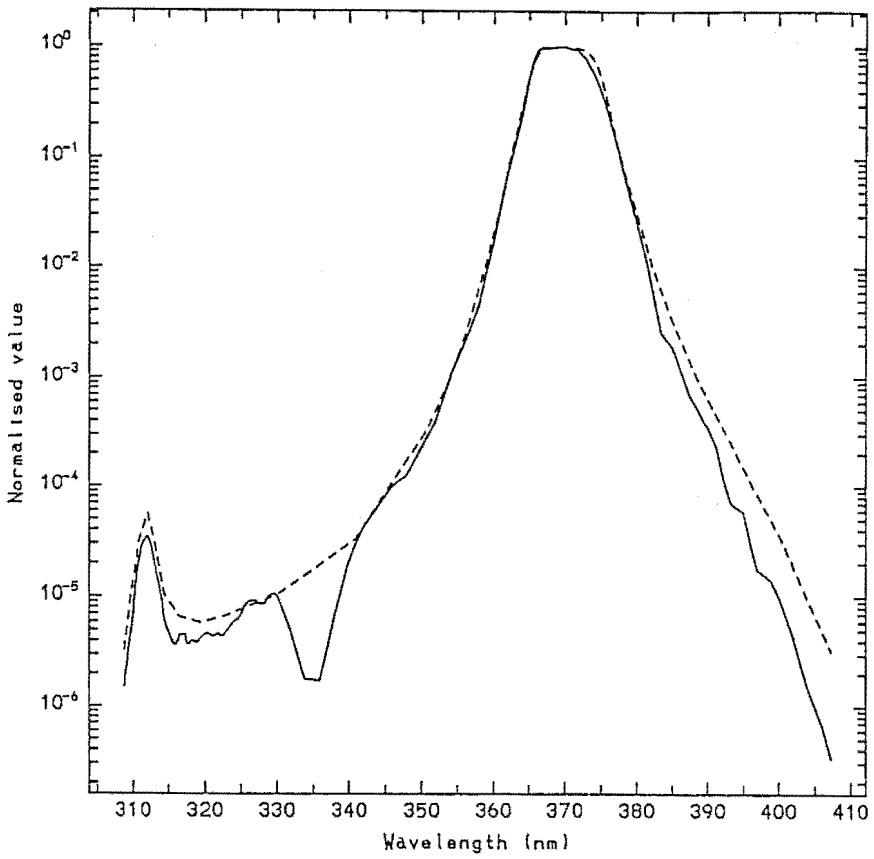

Figure 3.3: The extraterrestrial response, R_0, and the filter transmission, F (dashed line), for filter number 4. Both functions have been normalised with a peak value of 1 to aid comparison.

3.3.2 Instrumental factors

The spectral sensitivity of the detectors was assumed to be according to the manufacturers' specifications as shown in Figure 2.5. There may be some variation from these curves but, since they do not show rapid variations with wavelength in the regions in which they are used, the errors involved should be small.

The filter transmission functions were as measured by the author and described in Section 2.1.2 and Appendix A. Diagrams of the functions are shown in Figures 2.2 to 2.4.

From the functions described so far, the extraterrestrial response functions R_0, defined by Equations 3.15 and 3.16, can be computed for each channel[4]. These represent the wavelengths at which the photometer would respond without any atmospheric absorption. Some of them are are shown in Figure 3.6. In most instances these do not differ greatly from the filter transmission functions except in magnitude (see Figure 3.3), since the latter are more strongly varying functions of wavelength than the detector sensitivities. To model an actual measurement the properties of the atmosphere must also be modelled.

[4]This is not quite true, as the non-spectral part of the function, $\mathcal{R}$, is not known. The calculated functions are proportional to R_0.

Wavelength (nm)	Cross-section cm^2	Wavelength (nm)	Cross-section cm^2
270	8.956×10^{-26}	400	1.673×10^{-26}
280	7.635×10^{-26}	450	1.027×10^{-26}
290	6.553×10^{-26}	500	6.663×10^{-27}
300	5.656×10^{-26}	550	4.513×10^{-27}
310	4.910×10^{-26}	600	3.167×10^{-27}
320	4.285×10^{-26}	650	2.288×10^{-27}
330	3.758×10^{-26}	700	1.695×10^{-27}
340	3.311×10^{-26}	750	1.282×10^{-27}
350	2.929×10^{-26}	800	9.882×10^{-28}
360	2.601×10^{-26}	850	7.739×10^{-28}
370	2.318×10^{-26}	900	6.147×10^{-28}
380	2.073×10^{-26}	950	4.944×10^{-28}
390	1.860×10^{-26}	1000	4.022×10^{-28}

Table 3.1: Values of Rayleigh cross-sections (from Bates, 1984).

3.3.3 Atmospheric factors

The Rayleigh scattering cross-sections are taken from Bates (1984). They are shown in Table 3.1. The optical depth used was

$$\tau_R(\lambda) = \frac{p}{p_0}\mathcal{N}_R\sigma_R(\lambda) \tag{3.24}$$

where $\mathcal{N}_R = 2.15\times10^{25}$ is the number of molecules/cm^2 in a vertical column of the atmosphere at the standard pressure $p_0 = 1.01325\times10^5$ Pa .

The aerosol component was modelled by a simple power law according to Equation 1.8. Three model aerosols of this form were used, with coefficients 0.5, 1.0 and 1.5 respectively. The optical depths are shown in Figure 3.4. Some simulations were also done with no aerosol at all.

The ozone absorption coefficient $\alpha(\lambda)$, is taken from the Handbook of Geophysics (Valley, 1965). The values are based on the measurements of Vigroux (1953). While there have been more recent measurements of these coefficients, there have been only a few made at the low temperatures appropriate to stratospheric conditions. The values are plotted in Figure 3.5.

Each function used in the model was defined at as many points as were required to represent it well. A slowly varying function or part of a function was defined by only a few points whilst rapidly varying ones required more. In the case of functions taken from published data this meant that errors involved in changing the resolution to some standard value were avoided.

The process of combining functions, either multiplying or adding them, had to cope with functions defined at different points. This was done by evaluating the resulting function at all the points where either of the input functions had a point

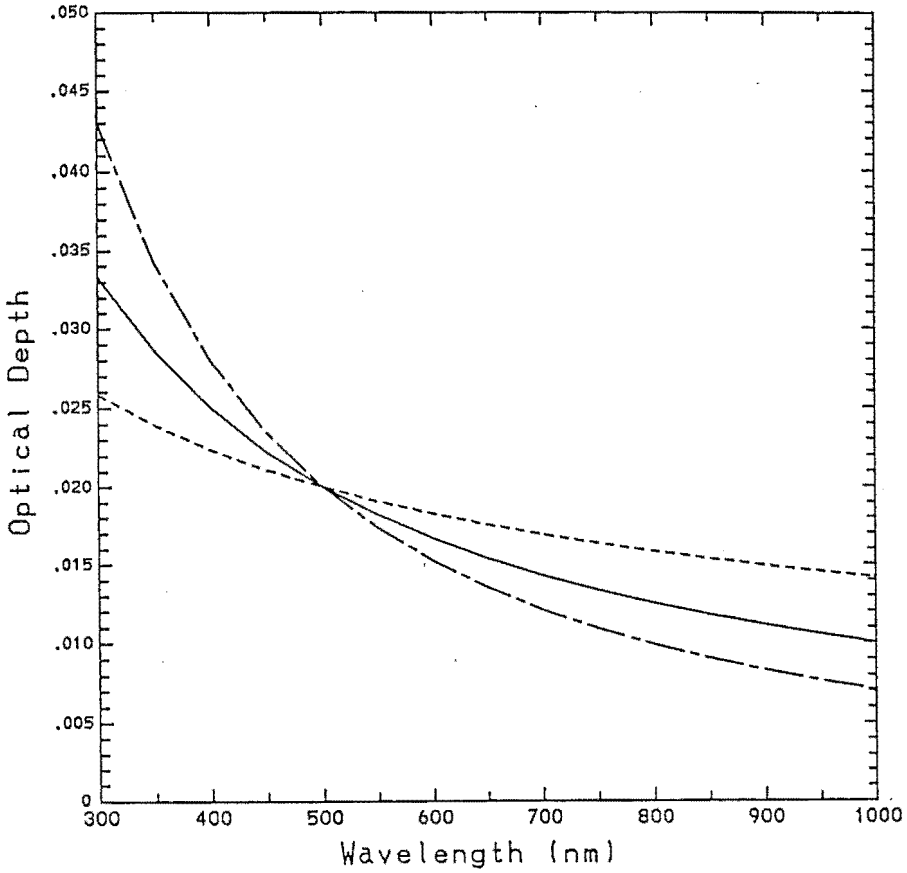

Figure 3.4: The aerosol optical depths used in model calculations. They would appear as straight lines with slopes of 0.5, 1.0 and 1.5 if plotted on logarithmic scales.

defined, using an interpolation routine at each point to obtain a value for whichever of the input functions that was not defined at that point. The interpolation routine was one that allowed the function to be defined at irregularly spaced points.

Response functions were calculated for each channel as a function of airmass. This was done for atmospheres with varying parameters of total ozone and aerosol optical depth. The absolute values of the response functions are not significant as the non-spectral factor ($\mathcal{R}$ in Equation 3.15) that determines the size of the real instrumental responses has not been accounted for in the model. However relative values are important. The calculated response functions for the channels that show a significant variation with airmass are shown in Figure 3.6. The effect of the side bands can bee seen clearly.

To simulate the measurements made with the photometer, the integrals of these response functions over wavelength were calculated. This was done with a program that could cope with an integrand defined at irregularly spaced points[5]. The numbers produced are not very useful in themselves but ratios of these numbers for different input parameters do provide important information. For example, if the calculated response for a given channel and atmosphere is divided by the response

[5]The interpolation and integration routines were taken from the library of FORTRAN routines produced by the Numerical Algorithms Group.

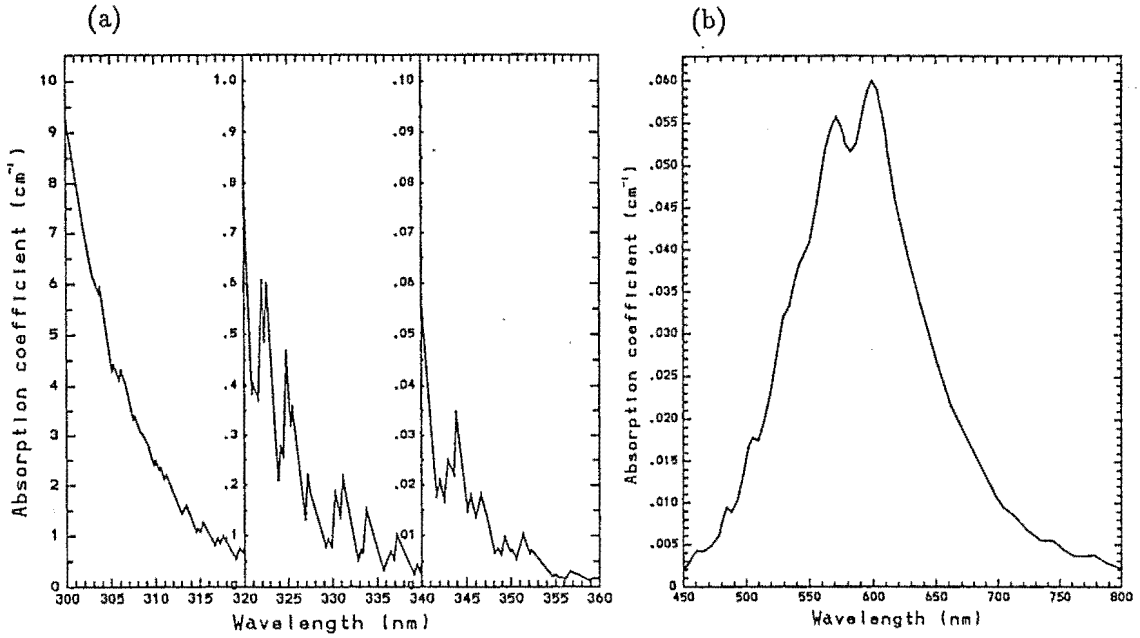

Figure 3.5: Values of the ozone absorption coefficient: (a) Huggins band; (b) Chappuis band.

calculated for that atmosphere without any ozone absorption, then this represents the ratio of integrals that defines the equivalent ozone absorption coefficient, $\overline{\alpha}_{O_3}$, in Equation 3.19. By doing this for different atmospheres the model can be used to look at the way this, and the other parameters introduced in Section 3.2, vary as functions of airmass, total ozone, and aerosol characteristics. The values calculated for $\overline{\alpha}_{O_3}$ are shown in Table 3.2 and the way in which these values vary with airmass and ozone is shown in Figure 3.7. Values for channel 1, the shortest wavelength filter, are not included for reasons explained in Section 5.1.2 on page 81. The channels in the visible band that have significant ozone absorption show much less variation in $\overline{\alpha}_{O_3}$ than do the ultraviolet channels. Channel 2 shows as much as 15% change in this parameter over the range of ozone and airmass considered. This is due to the relatively large bandwidth and to the fact that the leakage at longer wavelengths (where ozone absorbs less strongly) becomes more dominant as the airmass increases.

Values of $\overline{\tau}_A$ in each channel for one of the model aerosol functions are shown in Table 3.3. These do not significantly differ from the values of the aerosol optical depth at the centre wavelength of the filter, so the effect of finite bandwidth on this parameter is negligible. Similarly, values of the equivalent Rayleigh optical depth $\overline{\tau}_R$, which are shown in Table 3.4, are close to the values of τ_R.

The model could also be used to check for other things. The effect of sideband leakages can be determined by evaluating the integrated response for just that part of the filter transmission functions and comparing its value with the total response for the same channel. The effects of wavelength shifts in the passbands, due to temperature or aging, can be investigated in a similar way by comparing the calculated responses for unmodified and modified filter transmission functions. The results of these procedures are discussed in Section 5.1.2.

Filter Number	Equivalent Ozone Absorption Coefficient, $\overline{\alpha}_{O_3}$, $(\text{cm})^{-1}$						
	X=0.20 cm		X=0.30 cm		X=0.40 cm		
	$\mu = 2$	$\mu = 5$	$\mu = 2$	$\mu = 5$	$\mu = 2$	$\mu = 5$	
2	10.02	9.566	9.950	9.385	9.886	9.201	$\times 10^{-1}$
3	1.190	1.178	1.187	1.170	1.192	1.169	$\times 10^{-1}$
6	3.596	3.629	3.609	3.647	3.622	3.651	$\times 10^{-2}$
7	1.346	1.350	1.348	1.349	1.349	1.349	$\times 10^{-1}$
8	4.026	3.953	3.961	3.929	3.960	3.923	$\times 10^{-2}$

Table 3.2: Values of equivalent ozone absorption coefficient calculated from modelled response functions according to Equation 3.19. The channels not shown have coefficients smaller than 10^{-3}. All the values should be multiplied by the value in the right-hand column of the same row. There was very little variation in the calculated coefficients for the three different model aerosols.

Filter Number	$\tau_a(\lambda_c)$	$\overline{\tau}_A$	
		$\mu = 2$	$\mu = 5$
2	0.03154	0.03158	0.03158
3	0.03007	0.03016	0.03011
4	0.02717	0.02702	0.02706
5	0.02381	0.02384	0.02379
6	0.01999	0.01996	0.01993
7	0.01667	0.01666	0.01661
8	0.01481	0.01470	0.01476
9	0.01285	0.01278	0.01284
10	0.01160	0.01156	0.01159
11	0.01064	0.01073	0.01061

Table 3.3: Values of the equivalent aerosol optical depths $\overline{\tau}_A$, calculated from Equation 3.20 for the model aerosol that has a logarithmic slope of one, compared with its optical depths at the centre of each filters passband $\tau_A(\lambda_c)$.

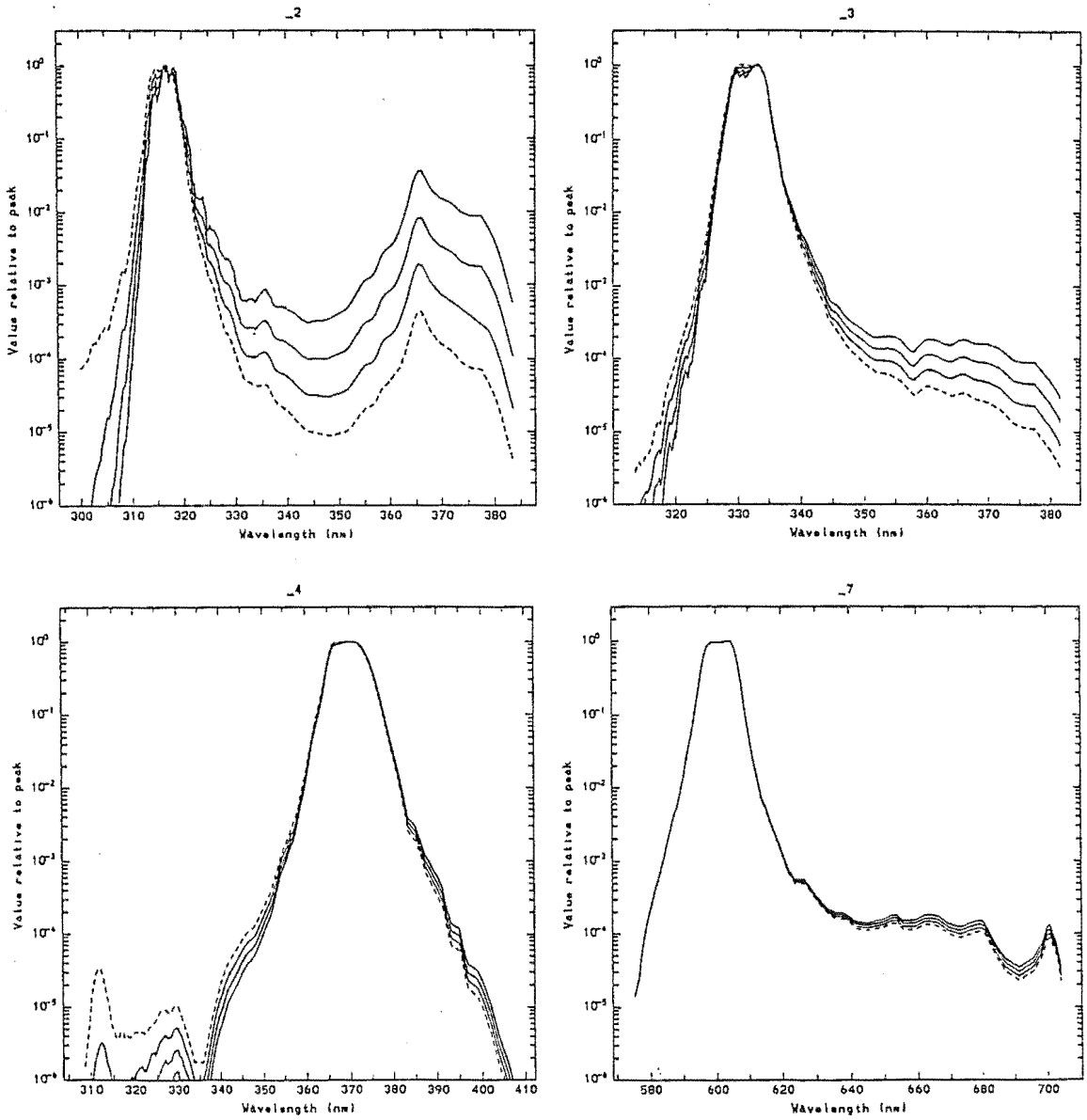

Figure 3.6: Response functions those channels that show significant variation with airmass. In each plot the dashed line represents the extraterrestrial response function $R_0(\lambda)$ and the remaining three lines are the response function $R(\lambda)$ for airmasses two, four and six respectively. All curves have been normalised with a peak value of 1 to aid comparision. The functions for the other channels showed variations of the order of the line widths in these plots.

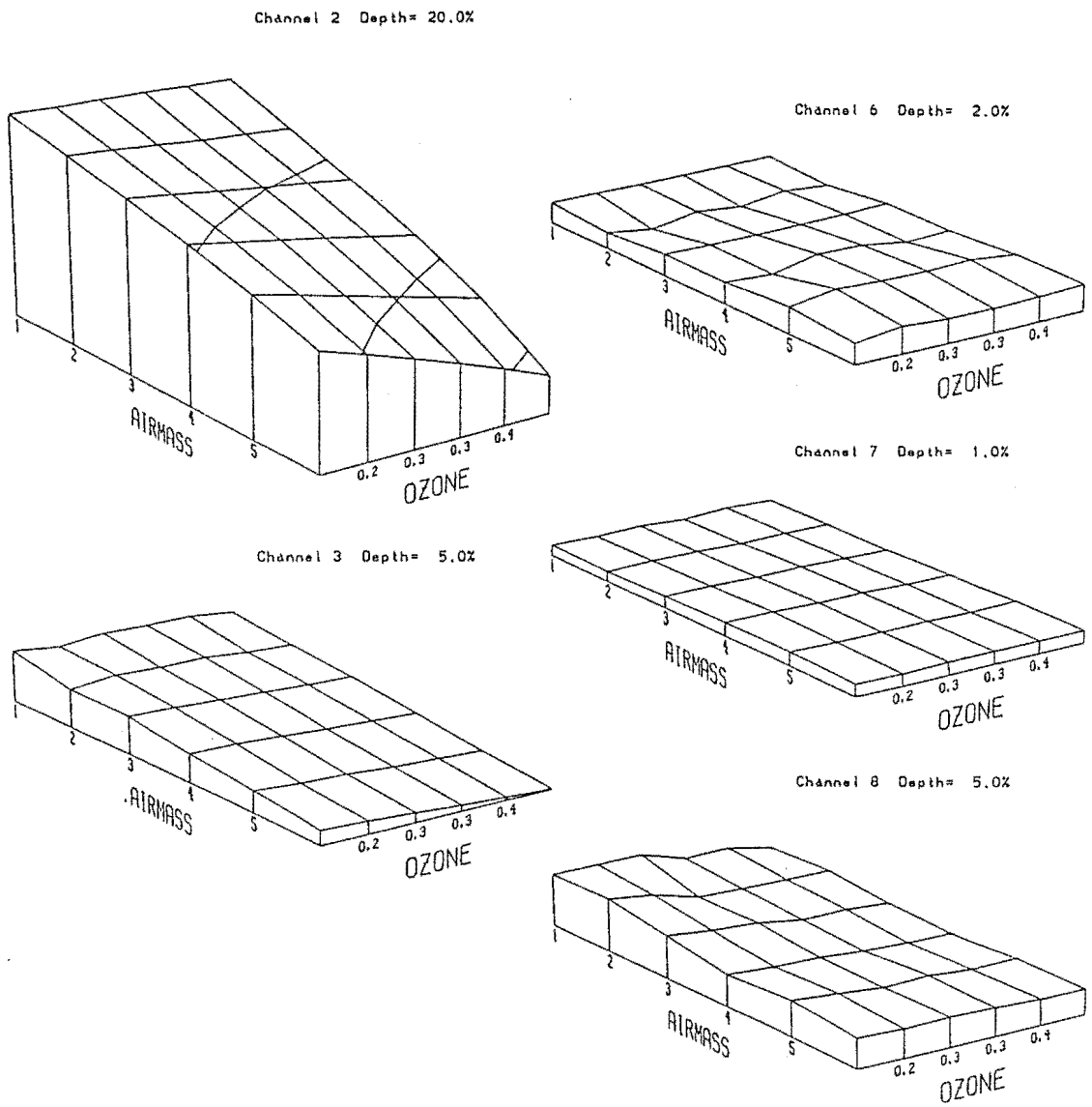

Figure 3.7: Variation in calculated equivalent ozone absorption coefficients $\overline{\alpha}_{O_3}$. with airmass and total ozone, for the channels with significant ozone absorption, presented as three dimensional blocks. The actual values of the coefficients are not shown. The depth of each block at the left hand corner, expressed as a percentage of the value at that corner, is shown.

Filter Number	$\tau_R(\lambda_c)$	$\overline{\tau}_R$	
		$\mu = 2$	$\mu = 5$
2	0.9724	0.9676	0.9662
3	0.7925	0.7914	0.7906
4	0.5099	0.5000	0.4992
5	0.2933	0.2938	0.2937
6	0.1433	0.1417	0.1417
7	0.0681	0.0675	0.0675
8	0.0422	0.0417	0.0417
9	0.0238	0.0237	0.0236
10	0.0157	0.0158	0.0157
11	0.0111	0.0106	0.0108

Table 3.4: Values of the equivalent Rayleigh optical depths $\overline{\tau}_R$, calculated from Equation 3.21, compared with the Rayleigh optical depths at the centre of each filters passband $\tau_R(\lambda_c)$.

3.4 Application to real measurements

3.4.1 Determining the extraterrestrial responses

One of the more troublesome aspects of measurements of solar radiation is calibration. The electrical signal from a photodetector is not usually related directly to standard units of radiation. One needs to know from a given signal on a particular channel at a particular time what the atmospheric attenuation at that wavelength is. This is equivalent to knowing the signal that the photometer would give on that channel at that time if there were no atmosphere. This signal is known as the extraterrestrial constant for that channel and is denoted P_0 in Equations 3.22 and 3.23. The method used to establish the extraterrestrial constant most commonly is the Langley method. This involves making the assumption that the atmosphere is not changing significantly during a day or a half day. Under this assumption the response of the photometer will depend only on the airmass, which is a known function of the solar zenith angle. If the Bouger law applies then a plot of the logarithm of the response against airmass will be a straight line with slope equal to the optical depth and intercept at zero airmass equal to the extraterrestrial constant. In practice Langley's method is difficult to use and the extraterrestrial constants derived from it vary from day to day. This is because the clear day with a static atmosphere assumed by the method just doesn't occur at most locations. The days that have variations due to small patches of optically thin high cloud are identified by dips in what is supposed to be a straight line. Even recognising these is not enough to ensure success as it is quite likely that a monotonically changing optical depth can produce a Langley plot that is perfectly linear yet gives erroneous values of the extraterrestrial constant. Shaw (1976) works through the mathematics of an example to illustrate this. Light scattered into the field of view can influence the values measured, especially at large zenith angles. This is

discussed in Section 5.1.1.

The alternative to the Langley method is an absolute calibration with standard lamps coupled with a knowledge of the solar spectrum at each wavelength band of interest. That is, if you know the response of the photometer to a known irradiance from the lamp then you can infer its response to the known irradiance of the sun. While this seems more attractive because it is independent of atmospheric conditions, it cannot give a calibration to the same precision as a good Langley plot because of the uncertainties on both the spectral output of the lamp and that of the sun. The irradiance of the sun in small wavelength bands is known only to 5% at visible wavelengths and even less precisely at ultraviolet wavelengths (WMO, 1986). The irradiance of a given standard lamp can also have an uncertainty of approximately 5% (Shaw, 1976). In addition there is also the assumption that, over the range of wavelengths that contribute to the signal in each channel, the spectral characteristics of the lamp and the sun are similar enough not to cause errors. If they are not then the results can be misleading.

In practice the extraterrestrial constant is only a constant if a correction is made for the variation throughout the year of the distance between the earth and sun. This varies by approximately 3% from extreme to extreme which means that the solar irradiance, inversely proportional to the square of the distance, varies by 6%.

3.4.2 Analysing the measurements

To extract the parameters of interest from the measurements, Equation 3.22 is rewritten as

$$\ln\left(\frac{P_0^i}{P^i}\right) = \mu_N \overline{\tau}_R^i + \mu_A \overline{\tau}_A^i + \mu_{O_3} X_{O_3} \overline{\alpha}_{O_3}^i \tag{3.25}$$

where the superscript i indicates the quantities applicable to the i^{th} channel. If P_0^i is known then the total extinction, the quantity on the left hand side of Equation 3.25, is known and one can proceed with separating the components that make it up. The Rayleigh term is known from Equations 3.24 and 3.8 and can be subtracted. The other two components are more difficult to separate and it is here that some assumption is usually made about one in order to evaluate the other as discussed in Section 1.3. If the objective is to obtain the aerosol component then measurements will have been made at wavelengths that avoid strong absorption by ozone. If wavelengths that do have some ozone absorption are included then a typical value for the total ozone is often assumed. Ideally if the quantity $\mu_A \overline{\tau}_A^i + \mu_{O_3} X_{O_3} \overline{\alpha}_{O_3}^i$ was known for all channels then the two components could be separated from the knowledge that the second term is proportional to $\overline{\alpha}_{O_3}^i$ and that the first is likely to be a fairly smoothly varying function of wavelength. This was the approach used by King and Byrne (1976) who assumed that the aerosol optical depth would take the form

$$\log \tau_A(\lambda) = a_0 + a_1 \log \lambda + a_2 (\log \lambda)^2 \tag{3.26}$$

The justification for doing this is that many measured optical depth functions follow the power law given in Equation 1.8, which make the logarithm of the

aerosol optical depth a linear function of the logarithm of wavelength. The third parameter is added to allow a degree of curvature to this relationship. A measure of how well this model fits the measured optical depths is the difference between the logarithm of the aerosol optical depth given by Equation 3.26 and that measured on each channel, assuming a value for total ozone. King and Byrne then found the values of the parameters X_{O_3}, a_0, a_1 and a_2 that minimised these differences by a weighted least-squares method. One of the options considered for analysing the readings from this photometer was to apply this method. The inclusion of the ultraviolet wavelengths with strong ozone absorption would make it more accurate than such a fit using just visible wavelengths.

If the objective is to get accurate values for total ozone then the choice of wavelengths is different. They are generally chosen in the range 310–340 nm where the Huggins absorption band of ozone varies rapidly with wavelength. At these wavelengths it is more difficult to determine extraterrestrial constants because the magnitude and variability of the total optical depth is much larger. What is done instead is to look at the ratios of channels. If Equation 3.25 is combined for two channels, then

$$\ln\left(\frac{P_0^{ij}}{P^{ij}}\right) = \mu_N \overline{\tau}_R^{ij} + \mu_A \overline{\tau}_A^{ij} + \mu_{O_3} X_{O_3} \overline{\alpha}_{O_3}^{ij} \tag{3.27}$$

where $P^{ij} = P^i/P^j$, $P_0^{ij} = P_0^i/P_0^j$, $\overline{\tau}_R^{ij} = \overline{\tau}_R^i - \overline{\tau}_R^j$, $\overline{\tau}_A^{ij} = \overline{\tau}_A^i - \overline{\tau}_A^j$ and $\overline{\alpha}_{O_3}^{ij} = \overline{\alpha}_{O_3}^i - \overline{\alpha}_{O_3}^j$.

The advantage of doing this is that the ratios of extraterrestrial responses are more easily determined than their absolute values. This is because many of the variables that interfere with an accurate determination of extraterrestrial constants for individual channels will act similarly in each channel, making the ratio more stable. This technique of taking ratios is the method used in the determination of ozone with the Dobson spectrophotometer. For a given ratio, the ozone can be determined as

$$X = \frac{\ln(\frac{P_0^{ij}}{P^{ij}}) - \mu_N \overline{\tau}_R^{ij} - \mu_A \overline{\tau}_A^{ij}}{\mu_{O_3} \overline{\alpha}_{O_3}^{ij}} \tag{3.28}$$

Since the wavelengths are so close, the simplest approximation that can be made is that the aerosol optical depth is the same in two channels. That is that $\overline{\tau}_A^{ij} = 0$. This is known as the single pair method. A better evaluation of ozone can be made by taking readings at more than two wavelengths and allowing for differing aerosol optical depths in each channel. If the aerosol optical depth is assumed to vary linearly with wavelength

$$\frac{\mathrm{d}\tau_A}{\mathrm{d}\lambda} = A \tag{3.29}$$

then Equation 3.27 becomes

$$\ln\left(\frac{P_0^{ij}}{P^{ij}}\right) = \mu_N \overline{\tau}_R^{ij} + \mu_A A \lambda^{ij} + \mu_{O_3} X_{O_3} \overline{\alpha}_{O_3}^{ij} \tag{3.30}$$

where $\lambda^{ij} = \lambda^i - \lambda^j$. Under this assumption measurements of two ratios can be used to provide a more reliable estimate of ozone according to

$$X = \frac{\ln(\frac{P_0^{ij}}{P^{ij}}) - \ln(\frac{P_0^{kl}}{P^{kl}}) - \mu_N(\overline{\tau}_R^{ij} - \overline{\tau}_R^{kl}) - \mu_A A(\lambda^{ij} - \lambda^{kl})}{\mu_{O_3}(\overline{\alpha}_{O_3}^{ij} - \overline{\alpha}_{O_3}^{kl})} \tag{3.31}$$

where ij and kl are pairs of wavelengths that may or may not have a common member. The assumption of an aerosol optical depth that varies linearly with wavelength is a reasonable one over a short spectral range and works well in practice. For the Dobson spectrophotometer pairs of wavelengths are chosen so that the difference in wavelength is similar and the aerosol term becomes zero. The double pair method is preferred for measurements of total ozone as is it more reliable (Dobson, 1957a, 1957b).

The shortest three wavelength channels for this photometer have wavelengths at suitable points in the region 310–340 nm to provide such an estimate.

Chapter 4

Measurements made with the photometer

In this chapter the measurements that the author made with the photometer are discussed.

4.1 Voltage dependence of the photomultiplier gain

The magnitude of the output current of the photomultiplier tube depends strongly on the potential differences applied to its various stages. The simplest method is to use a voltage divider to supply these potentials, as shown in Figure 2.6. With such a divider, the overall gain G, of the tube is (Philips, 1970)

$$G = \delta^N = (\kappa V_s)^N \tag{4.1}$$

where δ is the mean gain for a single stage, also known as the mean secondary emission factor, and N is the number of stages. To a good approximation, it is directly proportional to the voltage per stage V_s, as shown.

In order to be able to relate measurements taken with the photomultiplier tube at different supply voltages, a series of measurements was made over the full range (600–1100 Volts) with a constant irradiance provided by a tungsten lamp. These measurements are shown in Figure 4.1a. The data was found to lie close to the expected behaviour of Equation 4.1, as shown in Figure 4.1b. A fit based on the data for just one channel was made so that all counts taken could be related, no matter what the supply voltage was when the reading was taken. The fact that the voltage was recorded by the computer for each measurement made the correction much simpler than if it had to be recorded manually.

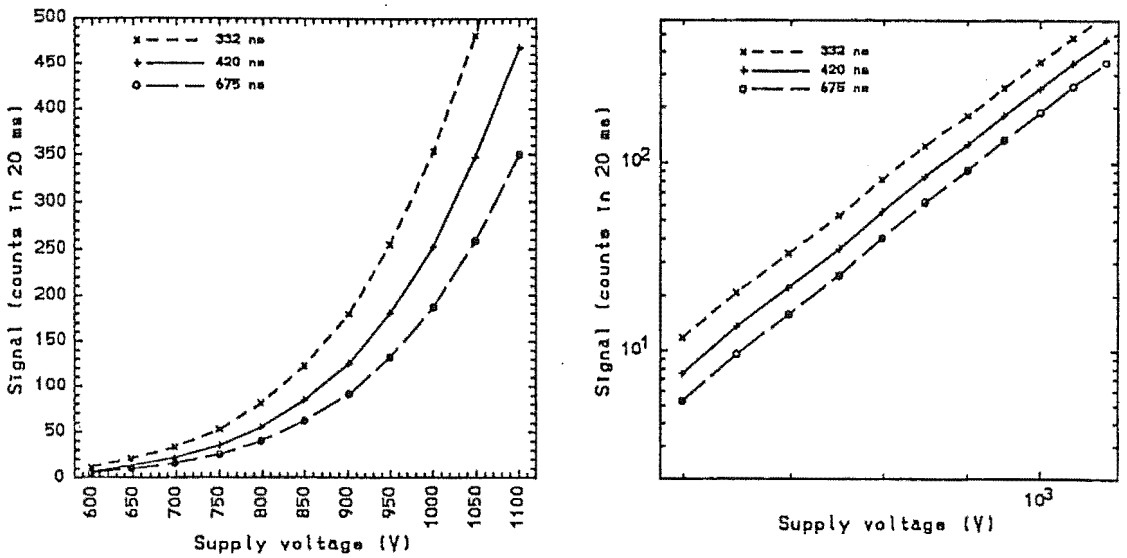

Figure 4.1: Dependence of the photomultiplier tube signal on supply voltage for three channels plotted on linear scales and then logarithmic scales.

4.2 Measurements at Christchurch, New Zealand.

The photometer was operated for most of the measurements at the University of Canterbury, Christchurch, New Zealand (43°31′S, 172°35′E). While this was not an ideal station geographically for such measurements, being at low altitude and in a city that has a significant smog problem, it had the advantage of being close to the technical support needed when problems were encountered. In addition it was easy to operate the photometer for extended periods as the author could get on with other work and yet be close to the photometer if needed. As the instrument is not completely weather proof one has to keep a weather eye out whenever it is operating. The previous University of Canterbury photometers had been successfully operated from the same position.

4.2.1 Initial Problems

As soon as the photometer was taken from the test bench and used to take direct sun measurements, a number of problems showed up. For early tests the instrument was placed on a movable platform so that it could be brought back to the workbench with ease. The first few weeks of operating and testing the instrument in the open air were involved with locating and eliminating light leaks in the detector chambers. Despite the best of intentions, these had occurred at some of the joined edges and corners and at the entry points for the electronic wiring. At each point in this procedure, it was only the largest leak that was identifiable. The final test of the effectiveness of the light proofing was to block the objective aperture of the heliostat and observe the signal of the detectors for varying ambient light conditions. Eventually no variation was found between the signals over the range

of full sunlight to darkness.

The next problem that became apparent was that there was an extremely large variation in the photomultiplier tube signals between channels. The signals in the visible channels exceeded those in the ultraviolet by more than three orders of magnitude. The ultraviolet signals are smaller due to a combination of lower solar irradiance, lower atmospheric transmission, lower filter transmission, and narrower filter passbands. Each of these factors becomes more effective as the wavelength becomes shorter so the problem is worst at the shortest wavelength filter. This made it difficult for the digital recording of the signals, because the digital electronics had a limited range (and precision) defined by the number of bits in the digital counters. Because the photomultiplier tube is intended as the detector for the ultraviolet wavelengths, the good signals in the visible region are not useful. In an attempt to reduce the difficulty, neutral density filters, made of stainless steel gauze, were placed next to the interference filters with visible passbands. This approach was not successful as very large attenuations were needed to solve the problem for the photomultiplier tube and these caused exactly the same problem for the photodiode. The solution was to place a filter that strongly attenuated the visible wavelengths in the light path between the beam splitter and the photomultiplier tube to limit the magnitude of the signal from the visible channels. This filter was a piece of visible blocking glass. The transmission of this blocking glass as measured by the author with the Cary spectrometer is shown in Figure 4.2, and the modified sensitivity of the photomultiplier tube is shown in Figure 2.5. While this reduced the problem to the extent that the digital counters could record a usable signal on all channels there was still a range of two orders of magnitude at an airmass of two. To reduce this further, a neutral density filter with a transmission of approximately 30% was retained in channel 4 (368 nm) as this was then the largest signal for the photomultiplier tube. The range required of the photomultiplier tube detector circuits is still large and this has affected the performance of the instrument.

4.2.2 Details of the measurements made

Once the initial problems described in the previous section were sorted out a more permanent mounting was constructed and a weatherproof cover made so that the instrument remained outside and that alignment at the start of each day was not required. The photometer was run on as many days as possible for the period from late March to mid September 1986 and from February to April 1987.

Initially the photometer was programmed to take readings at equally spaced time intervals of either 15 minutes or 10 minutes. It was found desirable to have the photometer perform some sort of check on whether the data was worth recording to limit the amount of disk space taken up with unusable data. This was simply a test on the size of the largest count taken: if it was below a certain limit then the reading was not recorded. The cut-off value was low enough so that there was no possibility of discarding a reading that could possibly be useful. There are still many of the recorded readings that are too low to make use of.

The idea of taking readings equally spaced in time seemed the best policy

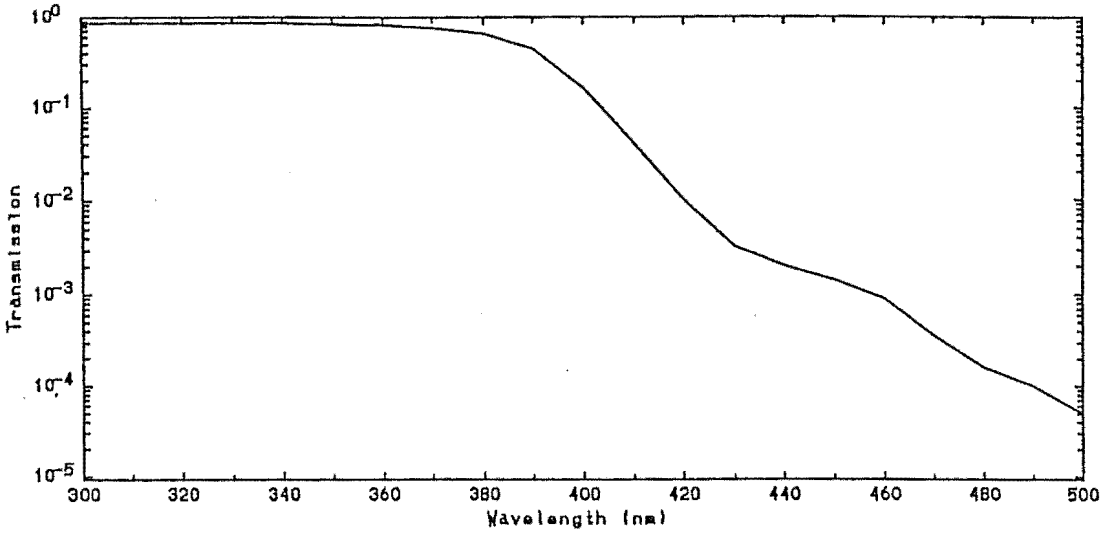

Figure 4.2: Transmission of the visible blocking filter that was added to limit the signal recorded by the photomultiplier tube in the visible channels.

at first. However it was found that this left Langley plots with very few points at high airmass. This is illustrated in Figure 4.3a which shows a plot for a day when readings were taken every fifteen minutes. To overcome this, the program was modified to take a reading if either a certain time had passed or the airmass had changed by a certain amount since the last recorded reading. So during the middle of the day, when the airmass changes slowly, the frequency of readings was determined by the time interval. As the rate of change of the airmass increased the readings became more frequent. This modification made statistical fits to Langley plots more reliable since the distribution of readings as a function of airmass was more even. A Langley plot for such a day is shown in Figure 4.3b.

A minor refinement, made at the same time, was to have the controlling program position the motors so that the objective pointed directly downwards, its most protected position, whenever the sun was below the horizon [1]. This helped keep the objective as clean as possible. The program ensured that the data file to the disk was closed at these times, since any power interruption while the file was still open would entail a time consuming process to recover the data recorded in that file. A new data file would be opened when the photometer's program was started if, and only if, the sun was in the sky. Otherwise, opening the data file was delayed until the next sunrise. At sunset the file was closed. With these modifications the instrument could be left uncovered on fine nights and could start taking readings at sunrise the next morning.

Although it was not implemented for the early measurements the program that ran the photometer was modified to print a log of when it was able to take measurements, details of data files opened and closed, and various other important operations. This was of assistance in tracking down what happened when things went wrong and provided a record of whether the measurements had been

[1] Prior to that the photometer would point in the direction of the sun, whether it was upwards or downwards in the local coordinate frame.

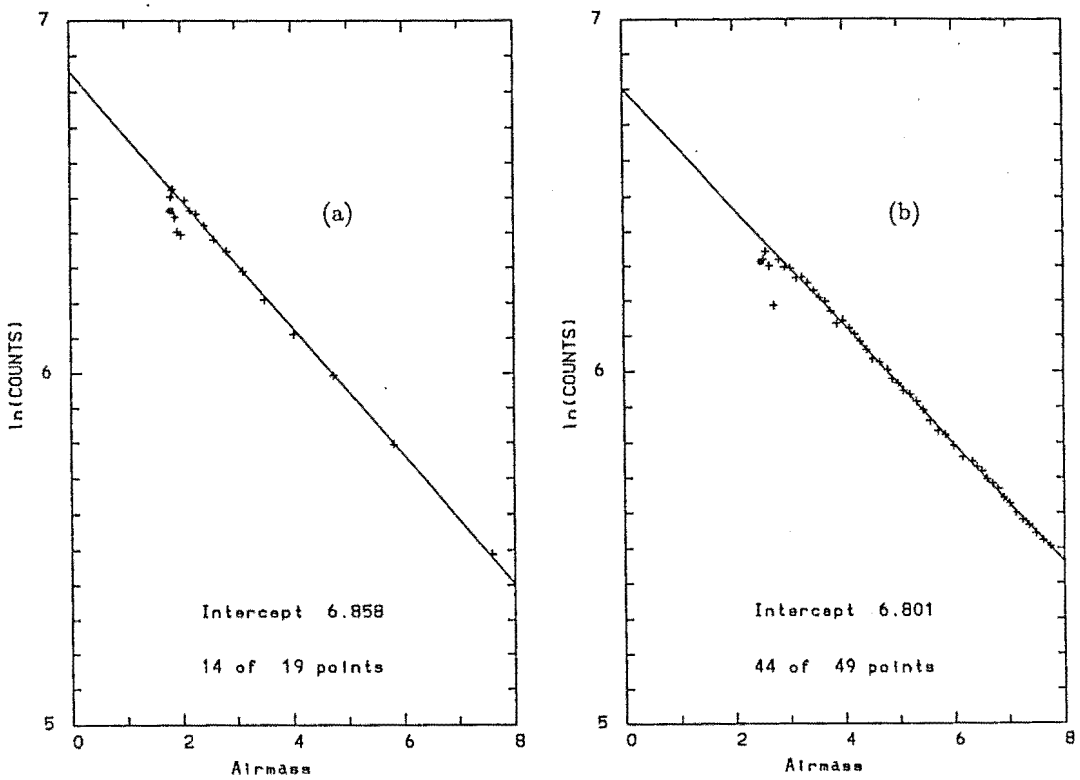

Figure 4.3: Comparison of Langley plots for different spacing readings: (a) Readings spaced evenly in time make the number of points at high airmass too small; (b) By taking readings more frequently as airmass increases, the points are more evenly spaced on the Langley plot.

discarded by the program as being too low.

4.2.3 Analysing the measurements

The first priority in analysing the readings was to establish the extraterrestrial constants P_0^i, for each channel. The Langley plots obtained for this instrument varied greatly in quality. Some of them could be immediately discarded because the plotted values did not even lie on a straight line (Figure 4.4a). After eliminating those plots that were obviously unsuited for calibration purposes, those remaining still showed considerable variation in the fitted value of the extraterrestrial constant. This is because monotonic changes in the optical depth can produce linear plots with incorrect intercepts as discussed in Section 3.4.2. Some typical plots of varying quality are shown in Figure 4.4.

By careful inspection of the fits and the kind of bias introduced in them by poor data points, especially at low airmass, values were found to be consistent to 2% for all but one of the channels in the visible and infrared. The exception was the longest wavelength filter at 940 nm. This is because there is a strong absorption feature of water vapour in that region which cannot be adequately described by the Bouger law. The Langley plots for this channel were generally curved because of this. Its extraterrestrial constant could only be found to the nearest 10%.

The only extraterrestrial constant that could be determined adequately in the ultraviolet was for filter 4 at 368 nm. This was established to 4%. The remainder could not be determined to better than 10%. Two reasons contributed to this. The first is that the optical depths are larger at these wavelengths and so the uncertainty in the intercept on the Langley plot is larger. The second is that the signals are weaker and that they are usable over a smaller range of airmass, making the Langley plots less reliable. The shortest wavelength filter provided no reliable Langley plots. This was because the signal was still so weak that it became too small to measure at an airmass of just three. This meant that Langley plots for that channel were extremely limited in their range of airmass and could not be relied upon. An example of this is shown in Figure 4.5. In addition to these problems, the passband of this filter was found to have shifted sometime during the course of the measurements. This is discussed in Section 5.1.2 on page 81.

The difficulty experienced in establishing good values for these constants was due to the poor suitability of the site for such work. It has made the analysis of results somewhat more difficult than it should have been. The difficulty in the ultraviolet especially complicates the extraction of information on ozone.

To get values for total ozone from the readings, the intention was to use the three channels (at 311, 317, and 332 nm respectively) in the Huggins absorption band of ozone to define two ratios of photometer responses and evaluate the column amount of ozone using Equation 3.31. However, since the information from the shortest wavelength filter was not usable the only option left was to use Equation 3.28 with the readings from the remaining two useful channels. Some experimentation in using the next channel at 368 nm with these two, to provide enough information to use Equation 3.31 was attempted. However this was not successful because the assumption of a linear aerosol was not a good one over the wider range of wavelengths. The ratio of channels 2 and 3 was well defined and produced Langley plots with an extraterrestrial value P_0^{23}, consistent to 3%, considerably better than values for the channels taken individually. The principal cause for the uncertainty was the fact that as airmass increases the signal on channel 2 eventually drops to a point where the detector circuit is unable to record a useful reading. The airmass at which this occurs is dependent on the total optical depth but generally occurs somewhere in the region of an airmass of four.

Using the experimentally determined value for P_0^{23}, a simple calculation using Equation 3.28, neglecting the aerosol term, produces an estimate of the total ozone. These estimates of ozone were constant, or nearly constant, through those of the days that were stable in total optical depth. At airmasses greater than four the estimate dropped considerably due to the loss of a significant signal on the shorter wavelength channel. On winter days this means that the period of time over which the estimates are reliable is relatively short. However, for much of these days this simple measure of total ozone proved stable. Figure 4.6 shows a selection of such days. The variation from one reading to the next on these days is typically 0.01 atm-cm. Although no independent measure of ozone was available it is likely that the values are significantly lower than the true value of total ozone by as much as 20–30%. This error is not surprising given the uncertainty in the value of P_0^{23} of 3% and the fact that the calculation involves the difference of the measured drop

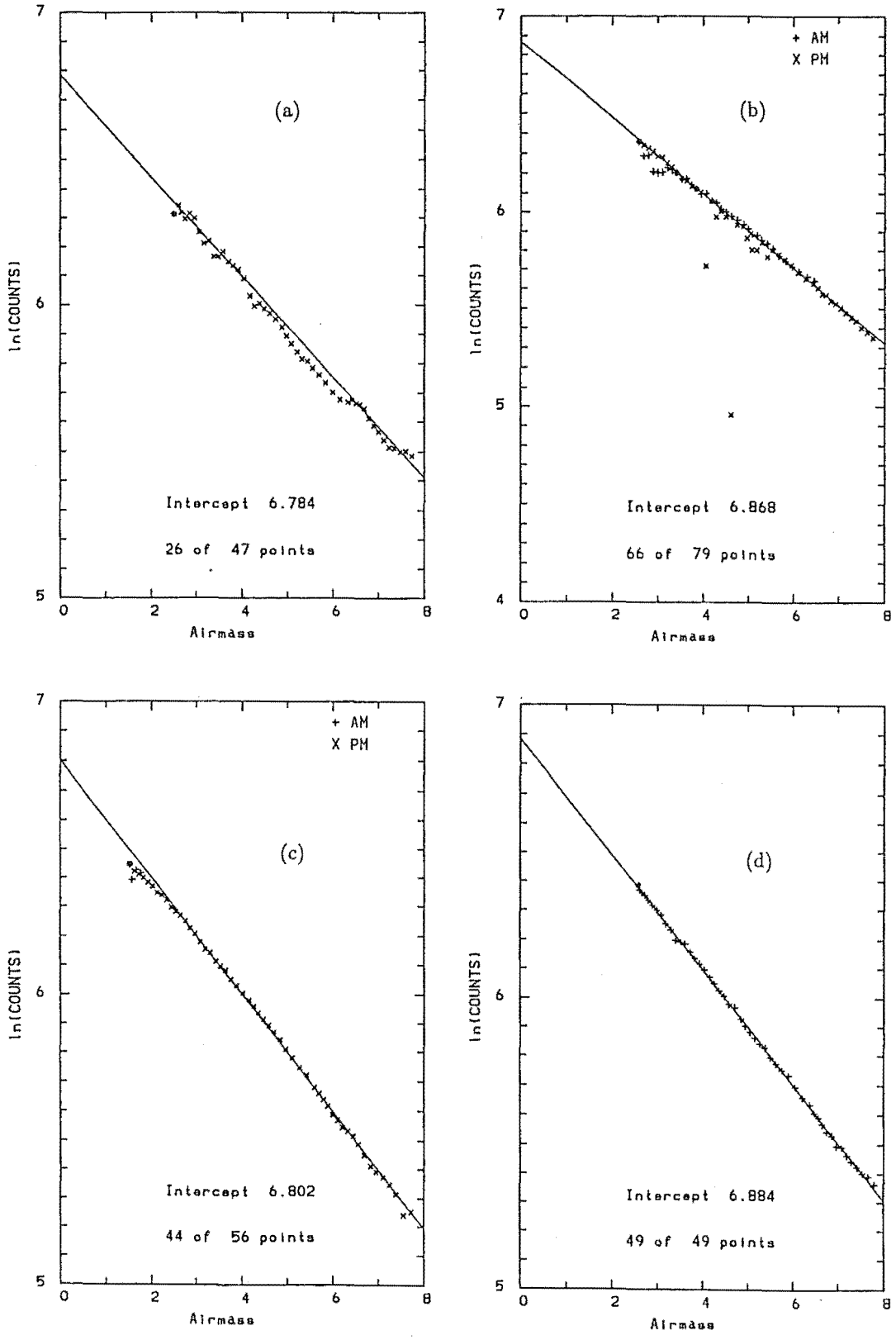

Figure 4.4: A selection of Langley plots of varying quality: (a) A plot obviously unsuited for calibration; (b) A plot affected by a number of bad points during the day; (c) A plot that looks good but is suspect because of the increase in optical depth at low airmass; (d) An excellent plot.

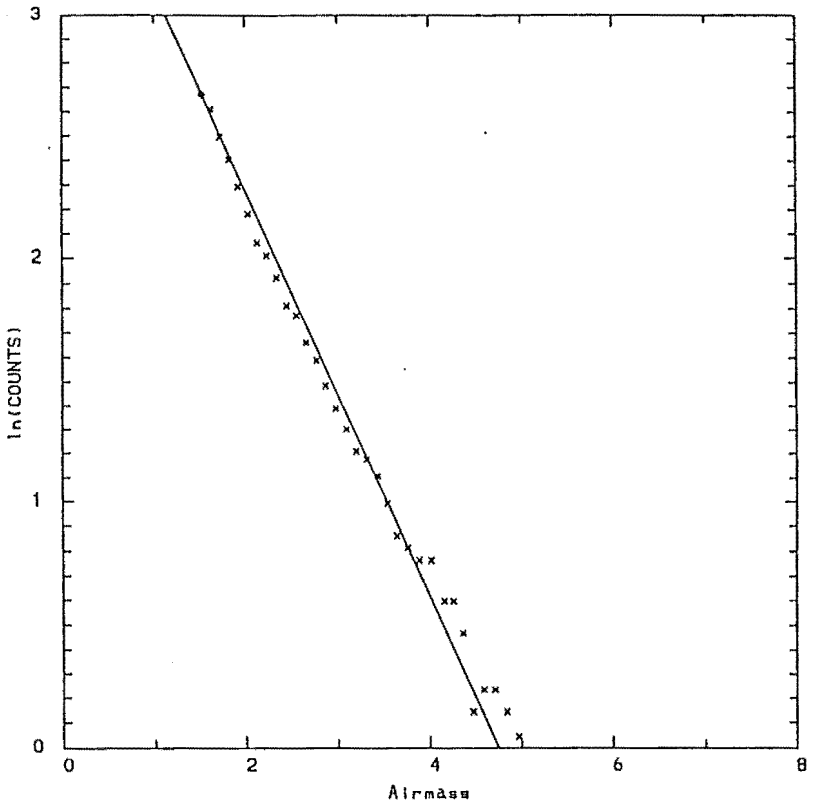

Figure 4.5: A typical Langley plot for channel 1. The point at which the signal becomes too small to accurately measure is at an airmass of approximately three.

in the ratio P^{23}, and the assumed drop due to Rayleigh scattering. Taking this difference magnifies the error. The consistently low values could however point to uncertainties in the values of the effective ozone absorption coefficients that have been calculated for these channels. Some days showed an increase in this measure of ozone at low airmass whilst others showed the opposite pattern (Figure 4.6). There are several possible reasons for this: it could be a genuine change in the quantity of ozone but it is more likely to be some sort of systematic error in the readings due to there being a significant difference in the aerosol optical depths at the two wavelengths.

Because the method used to establish total ozone from the ultraviolet channels was far from satisfactory, an attempt was made to determine total ozone independently using the readings at visible wavelengths and the fact that some of the channels lie in the weak Chappuis absorption band of ozone. As described in Section 3.4.2, it is possible to infer an estimate for total ozone from measurements of optical depth at a number of points by allowing a model aerosol (given by Equation 3.26) and an unknown quantity of ozone to vary in such a way as to fit the measured depths. This was attempted with the readings of the photometer using channels 5–10 (420–862 nm). Channel 4 (368 nm) was not included as its extraterrestrial constant was not as well determined. Channel 11 (940 nm) was not included because of the water vapour absorption in that channel. The technique is similar to that used by King and Byrne (1976) described in Section 3.4.2

on page 49. This technique, although it was not expected to perform well because of the uncertainties that remained in the values of P_0^i, and because the ozone absorption is weak and represents only a small proportion of the total optical depths, gave remarkably stable results. Because these values are the result of an optimisation routine that is given an initial estimate of the solution, the final solution may depend on that estimate. A check of this was made by repeating the procedure with a deliberately poor initial estimate (of 0.1 atm-cm) and the same solutions were found. Figure 4.7 shows the readings that were obtained on the days that are shown in Figure 4.6.

The values are of the correct order of magnitude, consistent throughout the day. The absolute value is generally higher than the value derived from the ultraviolet readings. There is also a systematic error in this measure that gives higher values for total ozone as airmass increases. The reason for this is probably that the problem is ill conditioned, and with larger values of total extinction the tendency is to attribute more of this to ozone. Past a certain point the optimisation routine fails to find a suitable minimum at all. A fuller determination of the source of this error would be possible if better values for the extraterrestrial responses P_0^i, were available. The time variation of the optical depth in one of the visible channels is given in Figure 4.8. This gives an indication of how stable the days were and to what extent the values of the counts were reduced. The typical measured aerosol optical depths for these days is shown in Figure 4.9. The accuracy of the values are limited by the precision to which the extraterrestrial constants are known. The uncertainty in the amount of ozone increases the error in aerosol optical depth around 600 nm. Those days that have an aerosol optical depth which varies little with wavelength are dominated by larger particles. Where the wavelength dependence is stronger the particle size is generally smaller. If the depths were known more precisely then it would be possible deduce particle size distributions from them. For the six days shown, the wavelength exponent of the aerosol optical depth (defined in Equation 1.8) varies from zero to 1.3 ± 0.2

It can be seen that the performance of the two measures of ozone changes as the magnitude and wavelength dependence of the optical depth vary. The days that these measures are most stable are those with a low optical depth that doesn't vary much with wavelength. When the aerosol optical depth does have a strong wavelength variation, the ultraviolet-derived values of ozone show a positive correlation with airmass and the increase of the visible-derived value at high airmass gets much worse.

The longest wavelength band, centred on 940 nm, was included on the photometer to see if a simple estimate of water vapour could be made from it. Water vapour has a strong absorption band in this region. This has been used before with other photometers (Shaw, 1976; Tanré et al., 1988). The absorption is not linear with path length so Langley plots, in which the logarithm of the measured signal is plotted against airmass, for that channel are typically curved. Consequently the extraterrestrial constant for that channel was never determined to better that about 10%. However a good approximation for the water vapour absorption, is that it is proportional to the square root of the amount of absorber (water vapour) in the radiation path (Volz, 1974). The total extinction in that channel will have

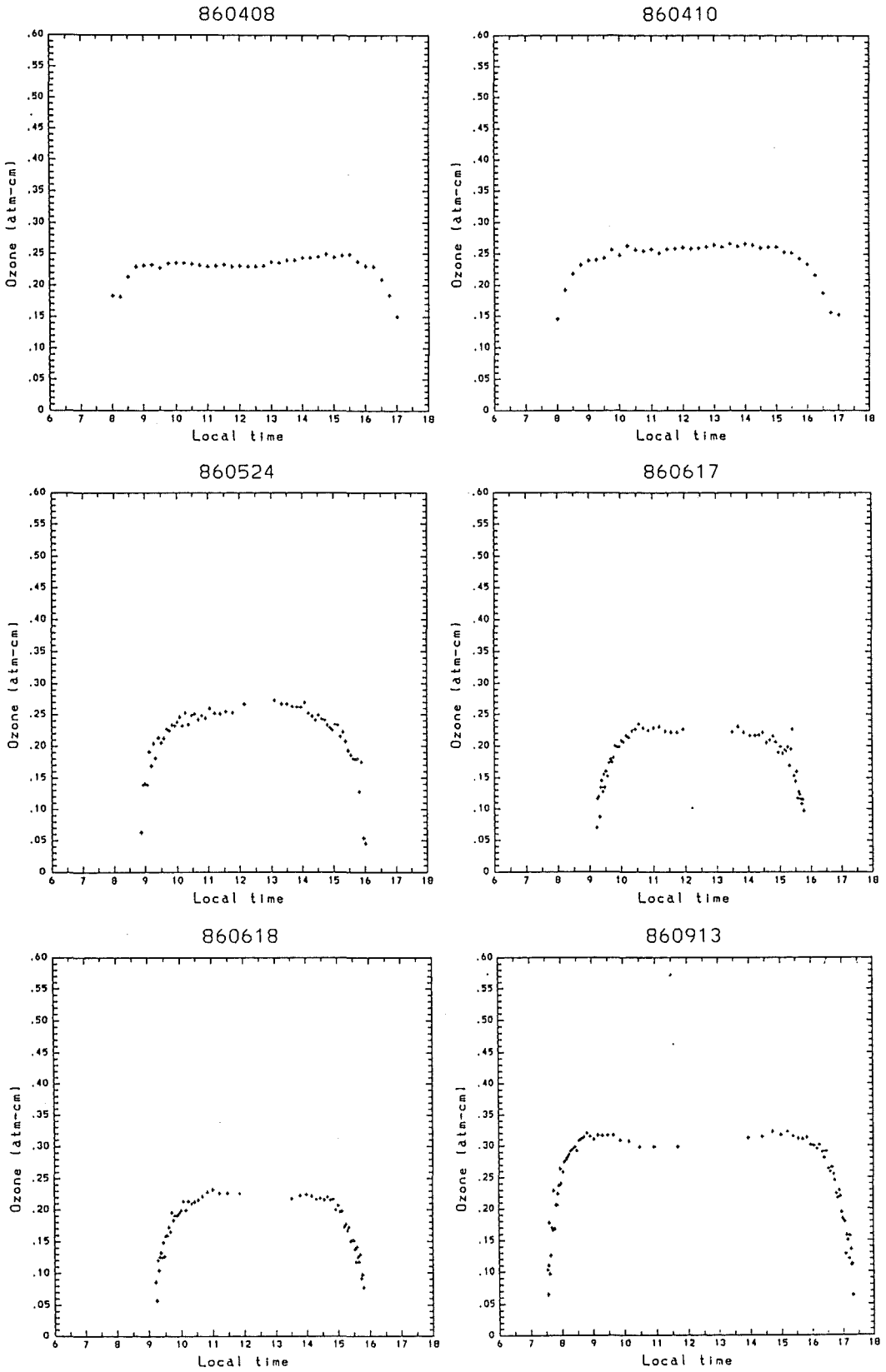

Figure 4.6: Values of total ozone calculated from the ratio of channels 2 and 3 for selected days

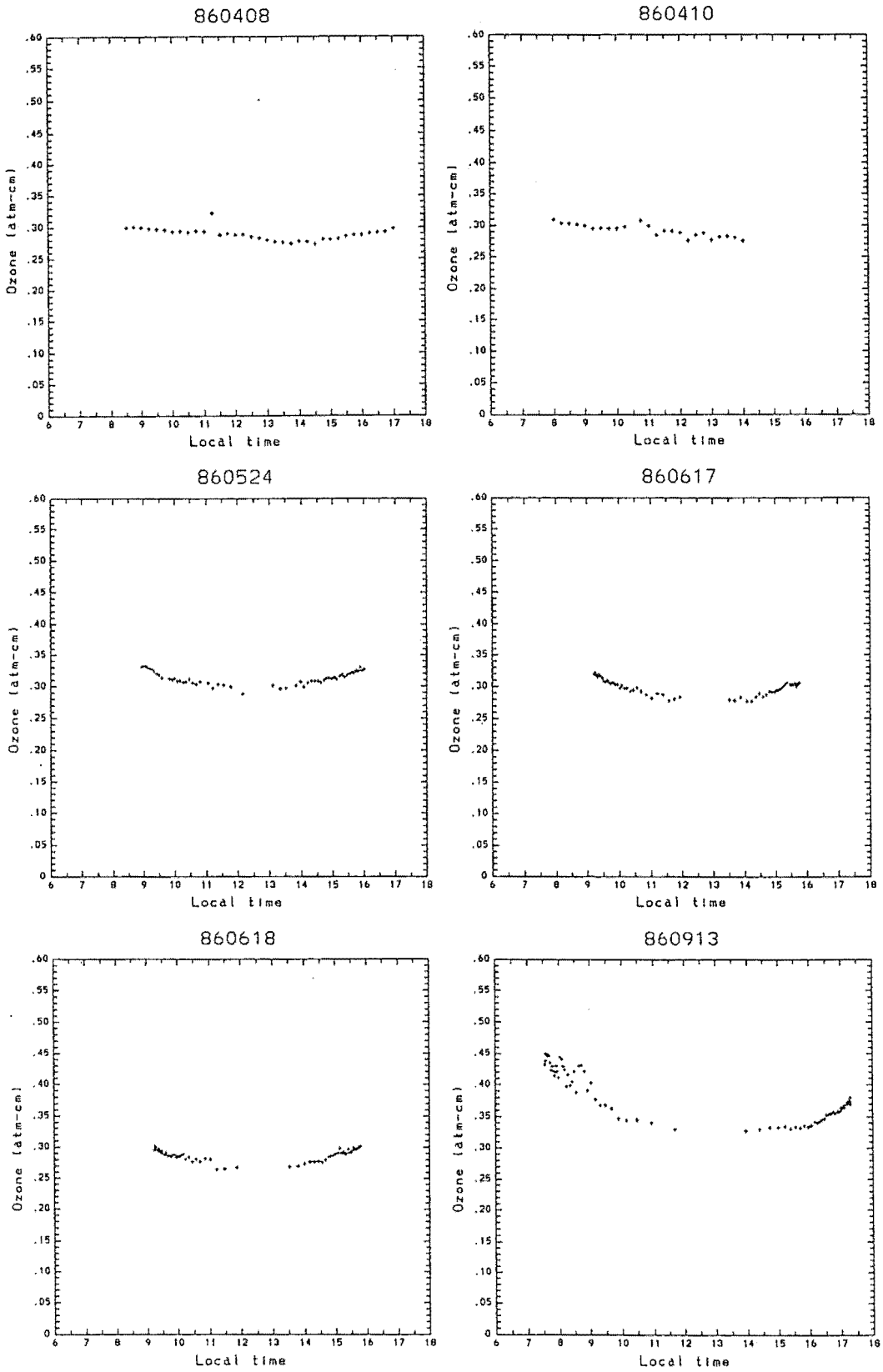

Figure 4.7: Values of of total ozone derived from measurements in the visible with the minimisation method described on page 49.

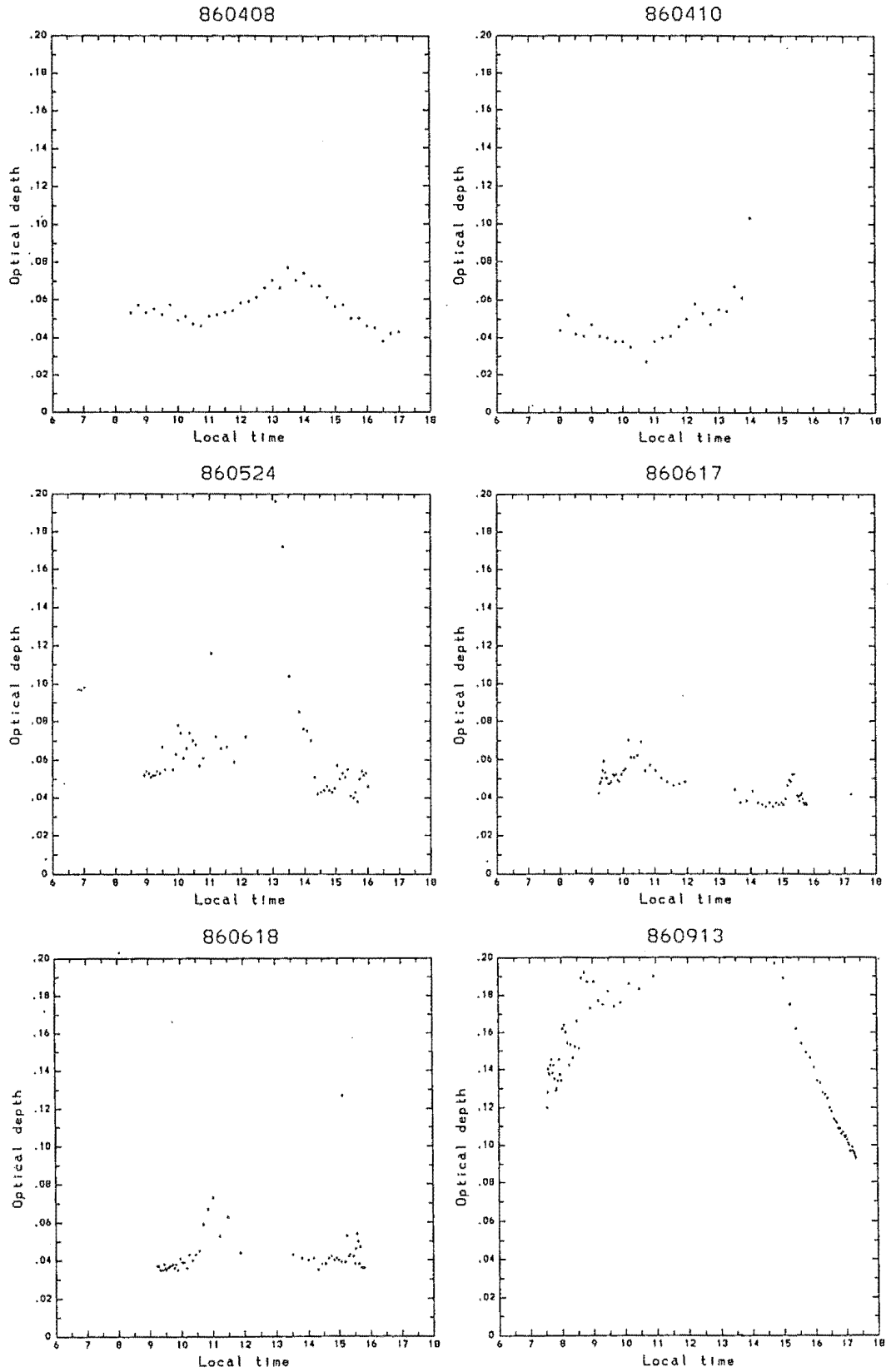

Figure 4.8: The variation in the measured aerosol optical depths at 500 nm for the days shown in Figure 4.6.

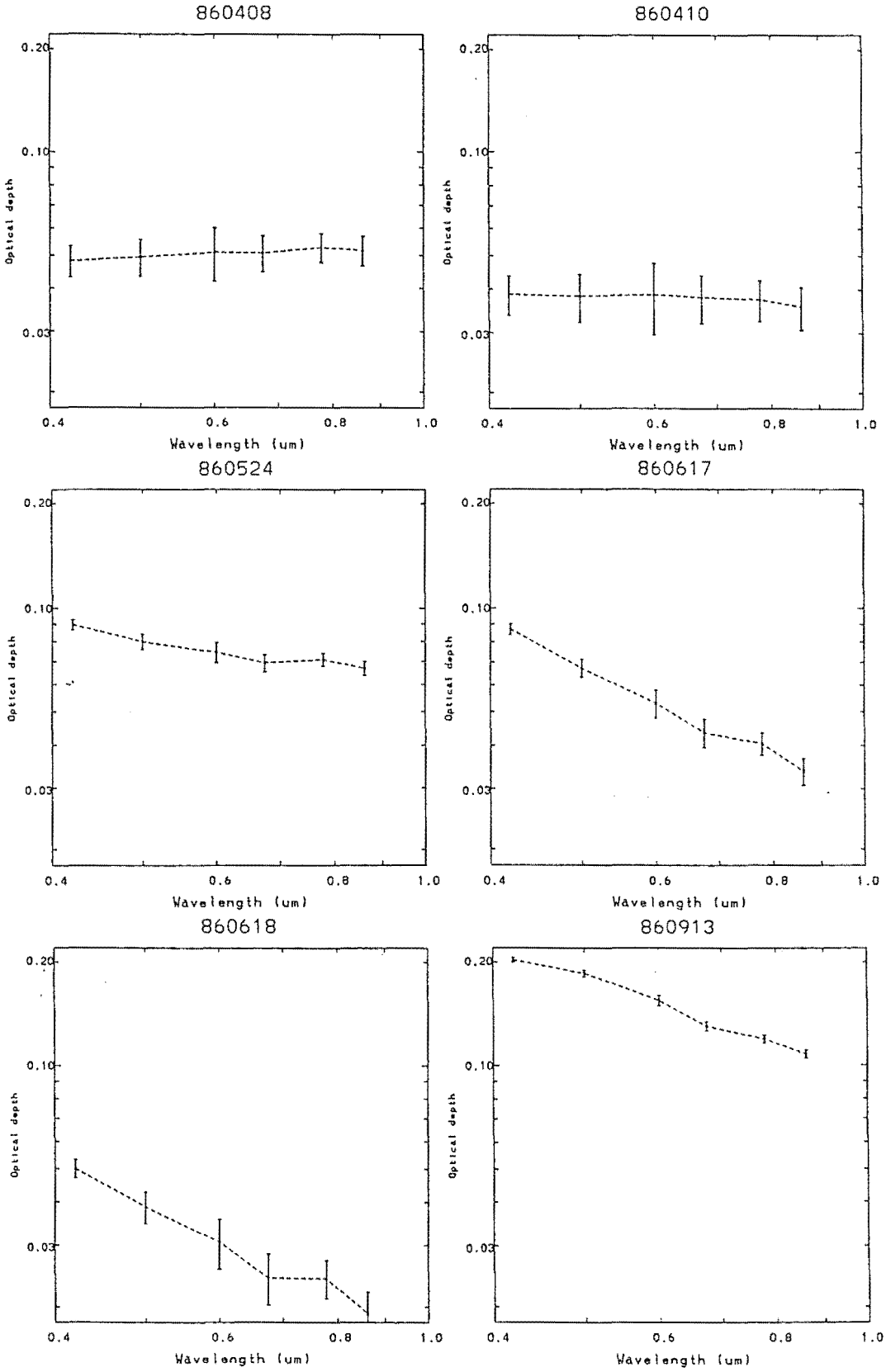

Figure 4.9: Aerosol optical depths in the visible for the days shown in Figure 4.6.

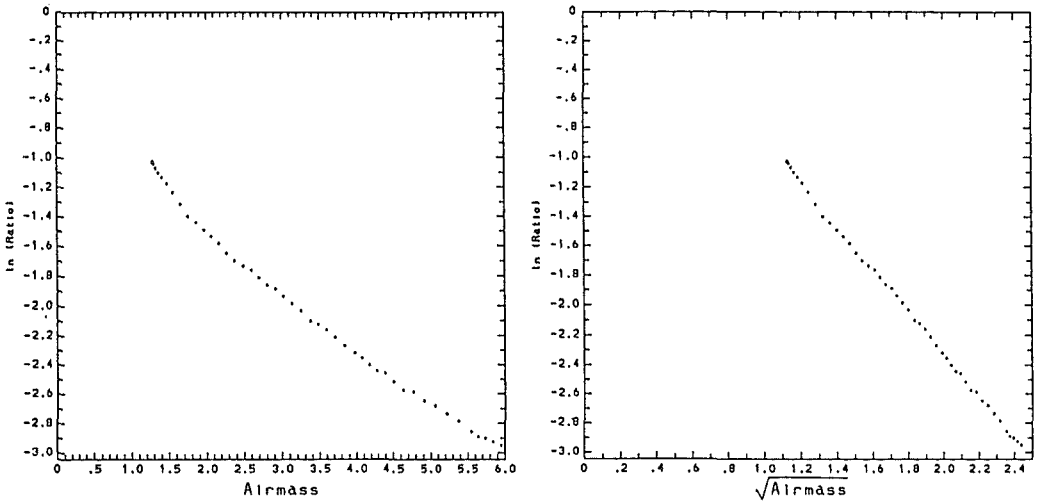

Figure 4.10: The strong water vapour absorption in the passband of the 940 nm makes the conventional Langley plot curved. The ratio of the 940 nm signal to the 862 nm signal is also curved. However if gives an almost straight line when plotted against the square root of the airmass.

contributions from molecular scattering, aerosol scattering, and the water vapour absorption. The first two contributions are linear and can be described by the Bouger law. Some way of separating them from the other component is required. The simplest way of doing this is to take the ratio of the signal on the 940 nm channel to that on the adjacent 862 nm channel. The variation in this ratio will principally be due to the water vapour absorption. A plot of the logarithm of this ratio against the square root of airmass is significantly straighter than the conventional Langley plot (Figure 4.10). This seems a good indication that if better calibrations were made for the instrument then it could indeed provide estimates of the water vapour content of the atmosphere. A more sophisticated method, that used extrapolation of the measured aerosol optical depths in the infrared channels to estimate the aerosol optical depth at 940 nm, could also be tried. Such an approach is likely to be an improvement on assuming that the aerosol optical depths at 862 nm and 940 nm are the same.

In addition the photometer was operated at two other sites. These measurements are discussed in Sections 4.3 and 4.4.

4.3 Measurements at Arrival Heights, Antarctica

The photometer was taken to the Antarctic for a period of eight weeks as part of the New Zealand Antarctic Research Programme, 1986-87 summer season (DSIR, 1986). It was installed at Arrival Heights (77°49′S, 166°39′E) a few kilometers from the United States' McMurdo station and New Zealand's Scott Base. The dates of the trip were October 20 until December 12, 1986. Observations were

20 October:	Travelled to Scott Base.
21-22 October:	On survival training course. Technician unpacked equipment at Arrival Heights.
23-24 October:	Assembled and checked photometer. Removed all-sky camera and its dome. Installed skylight and photometer.
25-27 October:	Traced faults in photometer caused by static. Solved problem of condensation on skylight.
27 October:	Technician returned to N.Z.
28-29 October:	Ran checks on alignment and programming.
30 October – 9 December:	Equipment running automatically. Checks made approximately daily.
10-12 December:	Took down and packed equipment. Replaced all-sky camera and dome.
12 December:	Returned to N.Z.

Table 4.1: Brief diary for the Antarctic trip.

made for the period 29 October until 10 December. A brief diary of the trip appears in Table 4.1. Unfortunately the NZARP research schedule did not allow the trip to be brought to an earlier date in the season so that the photometer could be in place for more of the time that the ozone hole was present.

4.3.1 Modifications required

Some modifications were required to the instrument and the program to control it. Operating the photometer in the open air was considered. The uncertainty involved in keeping a prototype instrument such as this operating at temperatures as low as -20°C was considered too great. The mechanical parts would be subject to large temperature gradients and the electronic circuits would be operating outside their specified temperature range. There was also the risk of damage to the photometer if accidentally left unattended in adverse weather conditions. It was decided therefore to install the photometer inside a laboratory in such a way that it looked out of a skylight. Unfortunately, this decision meant that very much less could be expected from absolute values of the readings from the photometer, but that relative values would still contain useful information.

The skylight was a cylindrical arrangement with twelve flat vertical panes. A drawing of the window is shown in Figure 4.11. This construction was used as the range of zenith angles over which the measurements would be taken was approximately 55–80°. The glass used was supplied by Schott of West Germany and carried the code number WG280, indicating it had a usable transmission at wavelengths longer than 280 nm. It had a transmittance of 0.95 at the shortest wavelength used by the photometer and more than 0.99 at visible and infrared wavelengths. The window assembly was bolted over a hole in the laboratory roof

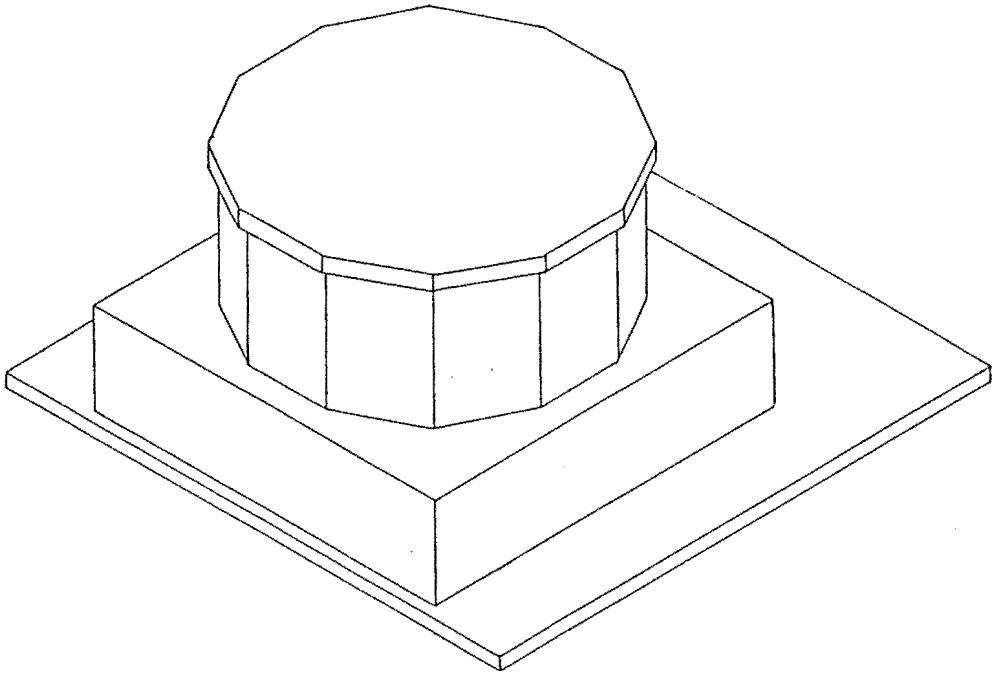

Figure 4.11: The skylight used for Antarctic measurements

that had been used for another experiment, an all-sky camera for recording auroral events.

The ceiling of the laboratory was a panel made up of 100 mm of foam insulation sandwiched between thin sheets of steel. The photometer was held up to this panel with brackets supporting the flat plate which usually formed the top of the box containing the electronic circuits for the photometer. That box was placed on a bench below the photometer because its weight was too great to be supported by the ceiling panel. Extension cords to link the photometer with its electronics were made up and checks were made that doing this did not alter any readings.

Problems encountered in setting the photometer up included one of the integrated circuits in the interface being damaged by a static electrical discharge during assembly. This was easily traced and rectified. The second problem encountered was how to prevent condensation from forming and then freezing on the inside of the skylight. After failing to find a suitable hot air blower that would keep the inside surface of the window warm enough, not only to prevent the freezing of the condensation but also limit its formation, a small cheap hair drier was bought from the US Navy store at McMurdo station and this served well until a more reliable alternative could be sent down from New Zealand.

The photometer's operating program had to be modified so that it took measurements continuously. The previous control method of using sunrise and sunset as the times to control the opening and closing of the disk data files was obviously not suitable at a station where the sun did not set. Taking measurements at all values of azimuth was the second new factor to contend with. The solution was to use midnight as the time to close the file that the day's data had been written to, open the new day's data file, and drive the azimuth motor one revolution in the

opposite direction to the sun's apparent motion in order to unwrap the cables.

The photometer performed well during the period of observations. A power surge or interruption caused the computer to fail once. The fault was discovered after a few hours and although the data file that was open at the time was not properly closed, it was recoverable. It would be possible, with a more sophisticated computer, to set the instrument up so that such an event would be less troublesome and cause no loss of data and this may well be an option to consider in the future.

4.3.2 The measurements

Because the instrument was looking through a window that was exposed to the elements on the outside and to condensation on the inside, the absolute values of the counts were less reliable than for measurements made in the open air. A plot of the typical kind of recorded optical depth with time is shown in Figure 4.12a. While the measurements were being made it was hoped that, despite the large variations in the values, a base level could be identified when they were plotted against time. This occurred on a few days, one of which is shown in Figure 4.12b. The spikes in this record are caused by the small structural rods at some of the corners of the skylight. These affected the reading over a wider interval of the azimuth angle that was anticipated. While it may be possible to do something useful with these measurements any information from them would be very poor in quality.

However, ratios of counts were better defined and these enabled signals to be used to do the simple determination of ozone with the two good ultraviolet channels. Despite short term scatter, over time scales of a few tens of minutes, the values of total ozone were remarkably self consistent. A number of days are shown in Figure 4.13. Many of the days show a characteristic pattern of values that peak around noon. These are a number of possible explanations for this. One is that the glass of the window has a transmission that is approximately 1% lower at the shorter wavelength that at the longer. of the two wavelengths used for the ozone estimate. This difference will become more significant as the path length through the glass increases, and will decrease the value of the measured response ratio. Since the window panes are vertical, this error is larger when the zenith angle is smaller, around noon. The other possible explanation is that the measurement is a real indication of a horizontal gradient in total ozone. At such a high latitude during the summer the sun's path stays low in the sky and appears to do complete circuits around the sky. This means that direct sun measurements at such a station are sampling a part of the atmosphere that is much larger in horizontal extent than at a mid-latitude station. Since the horizontal gradient of ozone at that time is an increase to the North, the variation in the retrieved ozone value may well reflect this. The two possibilities are not easy to distinguish, but the fact that the pattern is common but not universal in the readings suggest something that at least part of the effect is is dynamic rather than static. A time series of those readings taken within an hour of noon is shown in Figure 4.14. The behavior of these readings is generally consistent with satellite measurements made at the same time (Krueger et al., 1987). The rise from very low values

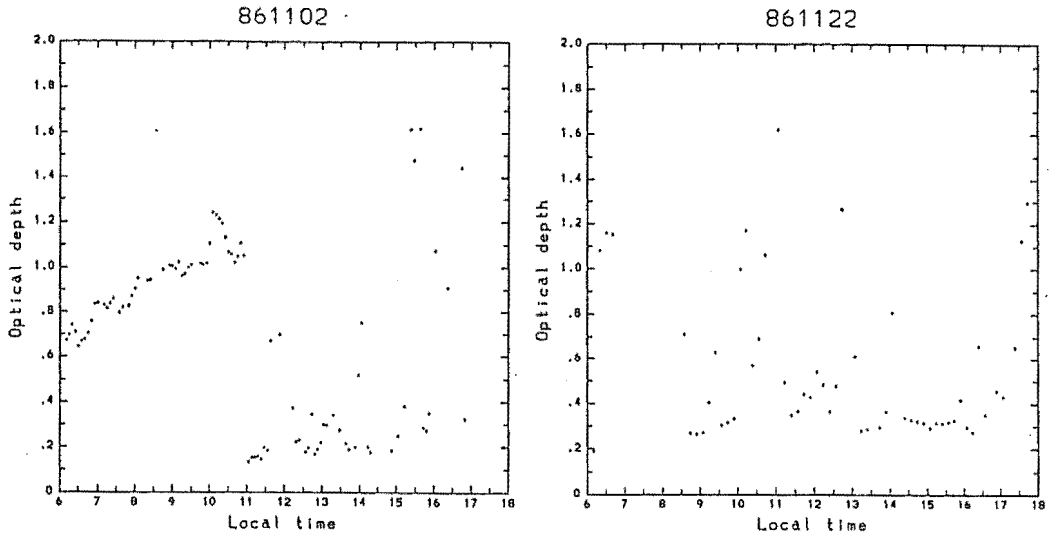

Figure 4.12: Optical depth at Arrival Heights as a function of time for two typical days.

of ozone at the beginning of November is particularly interesting. It seems that despite the poor quality of this measure it has responded appropriately to a large change in total ozone.

4.4 Measurements at Lauder

In an attempt to resolve some of the difficulties in analysing the readings taken so far, a two week period of readings was undertaken at Lauder, Central Otago (45°03′S, 169°41′E) where the Physics and Engineering Laboratory, part of the New Zealand government's Department of Scientific and Industrial Research, runs an atmospheric research station. Lauder is at a higher altitude than Christchurch and is not close to a city. The measurements were close to the summer solstice and so there was a good chance that better values to the extraterrestrial constants could be obtained. Routine measurements of total ozone are made here with an automated Dobson spectrophotometer, measurements of the vertical distribution of ozone are made with Umkher Dobson measurements, and a balloon borne electrochemical ozonesonde launched weekly.

Unfortunately, the weather was not favourable and all of the nine days that were fine enough to operate the photometer were marred by high cloud or high optical depth during all or part of the day. Figure 4.15 shows a Langley plot for a typical day. Measurements were possible on a total of just nine days. The measurements were discontinued when the automated Dobson instrument developed a mechanical fault that required spare parts to be flown from overseas.

Despite the poor weather it became apparent during the measurements that the restricted range of the photomultiplier detector circuits made it extremely difficult to take readings over the full range of airmasses encountered during a day. That range had become more of a problem because the noon airmass was so much closer to one than any of the previous readings. Some readings at low airmass were incorrect because the counters had overflowed and the problem of

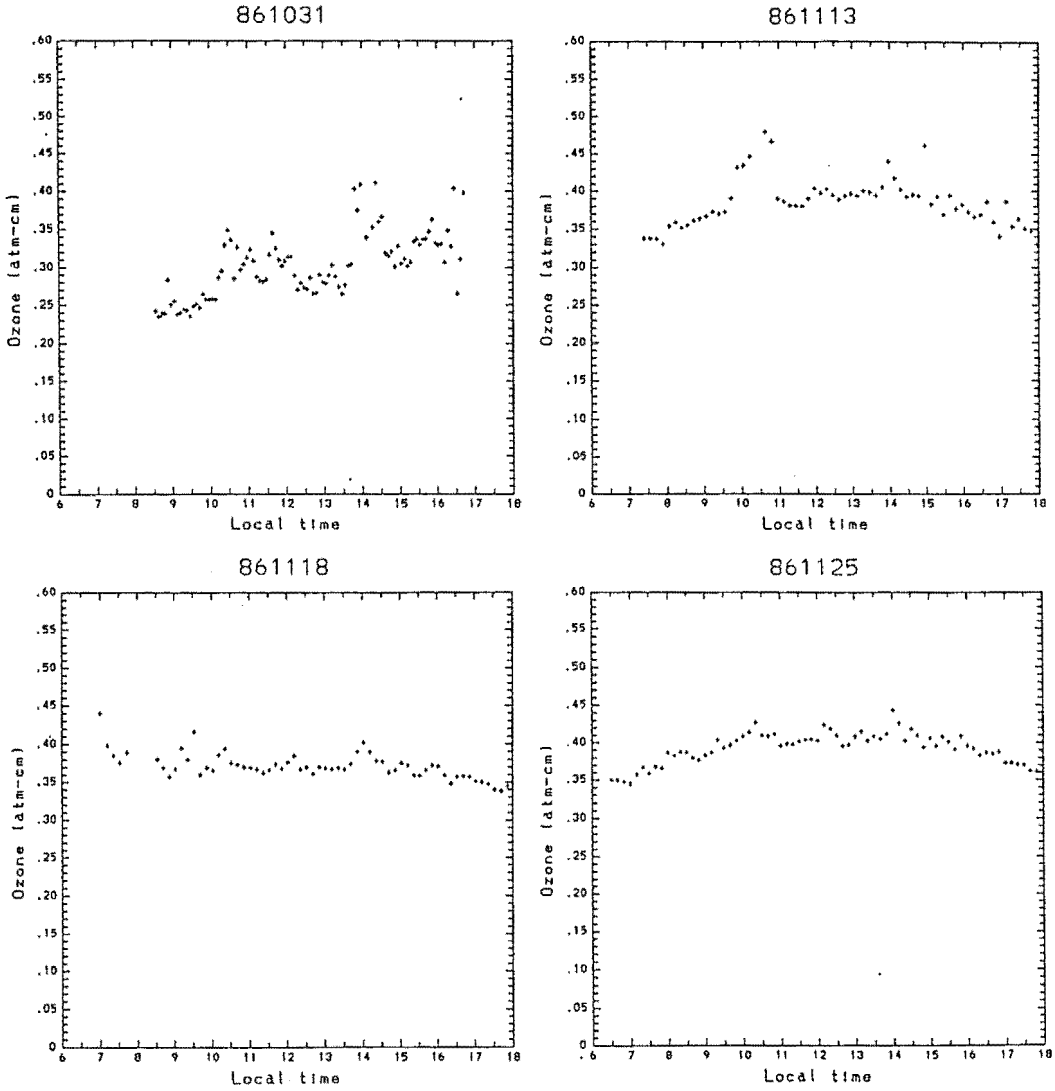

Figure 4.13: Total ozone during selected days at Arrival Heights, Antarctica. The values are derived from the ratio of channels 2 and 3.

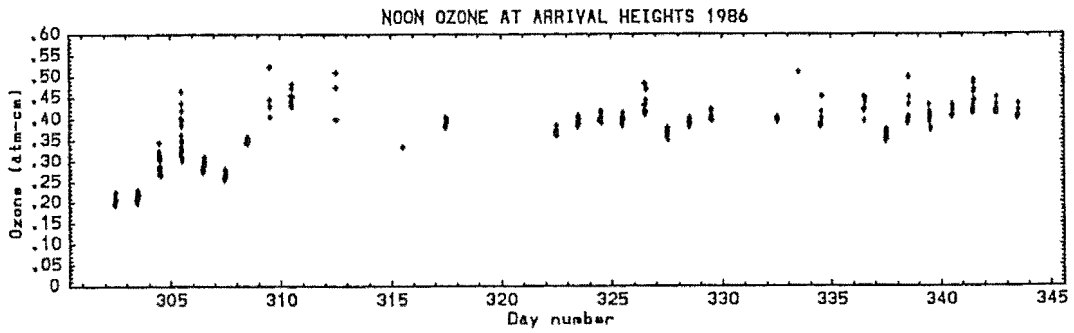

Figure 4.14: Values of total ozone at Arrival Heights for 29 October to 12 December 1986. All readings that were taken within an hour of local noon are shown.

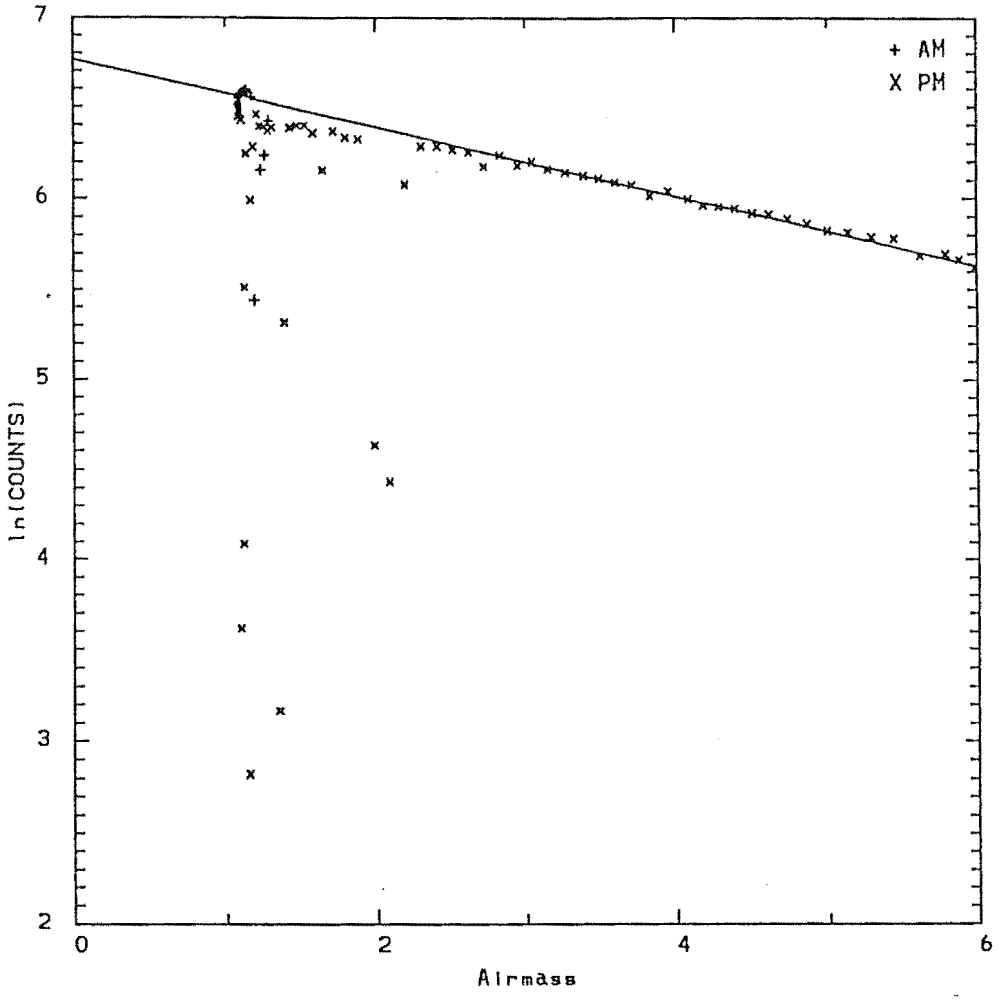

Figure 4.15: Langley plot for a typical half-day at Lauder, the afternoon of Janaury 15, 1988.

poor signals at high airmass remained. Langley plots for the four ultraviolet channels taken on the last day at Lauder illustrate this vividly (Figure 4.16).

However measured values of ozone with the photometer were stable for some of the periods of observation. The results from two such days are presented.

Figure 4.17 shows the day of January 8. This day started well with low optical depth before 0900. Both estimates of ozone produce sensible values but the value derived from the ultraviolet is too low by 30% and is decreasing considerably as the airmass increases. For the rest of the morning the optical depths are so high that neither measure of ozone gives sensible values. At 1300 the readings stabilise but with a significantly higher optical depth. This depth is decreasing with time. The ultraviolet-derived value for ozone is stable during this period at 0.25 atm-cm. whilst the methods using visible channels gives poor values that are rapidly changing. The quantity of ozone measured with the Dobson was 0.322 atm-cm or 322 Dobson units.

Figure 4.18 shows the day of 12 January. Only half a day's readings were possible before the weather clouded over. During the time of the readings both measures of ozone were changing significantly with airmass. The drift reverses

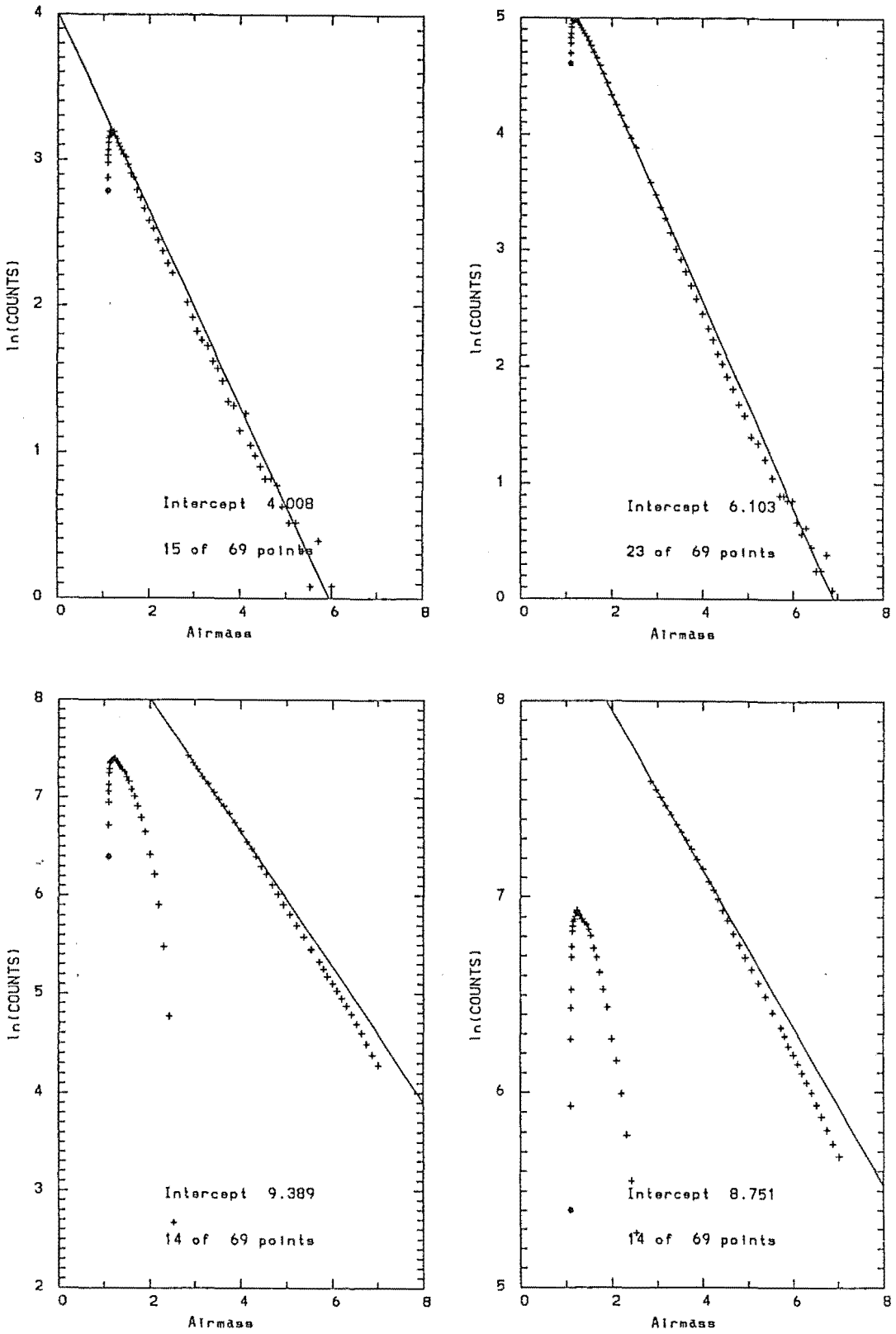

Figure 4.16: The problem of range in the photomultiplier. The four plots were taken on the morning of January 16, 1988. The photomultiplier tube voltage was set too high and the counter overflowed on the two longer wavelengths. At the other two wavelengths the airmass range of useful signals is limited by their small size. The program that produced these plots has not coped well with fitting a straight line to the points.

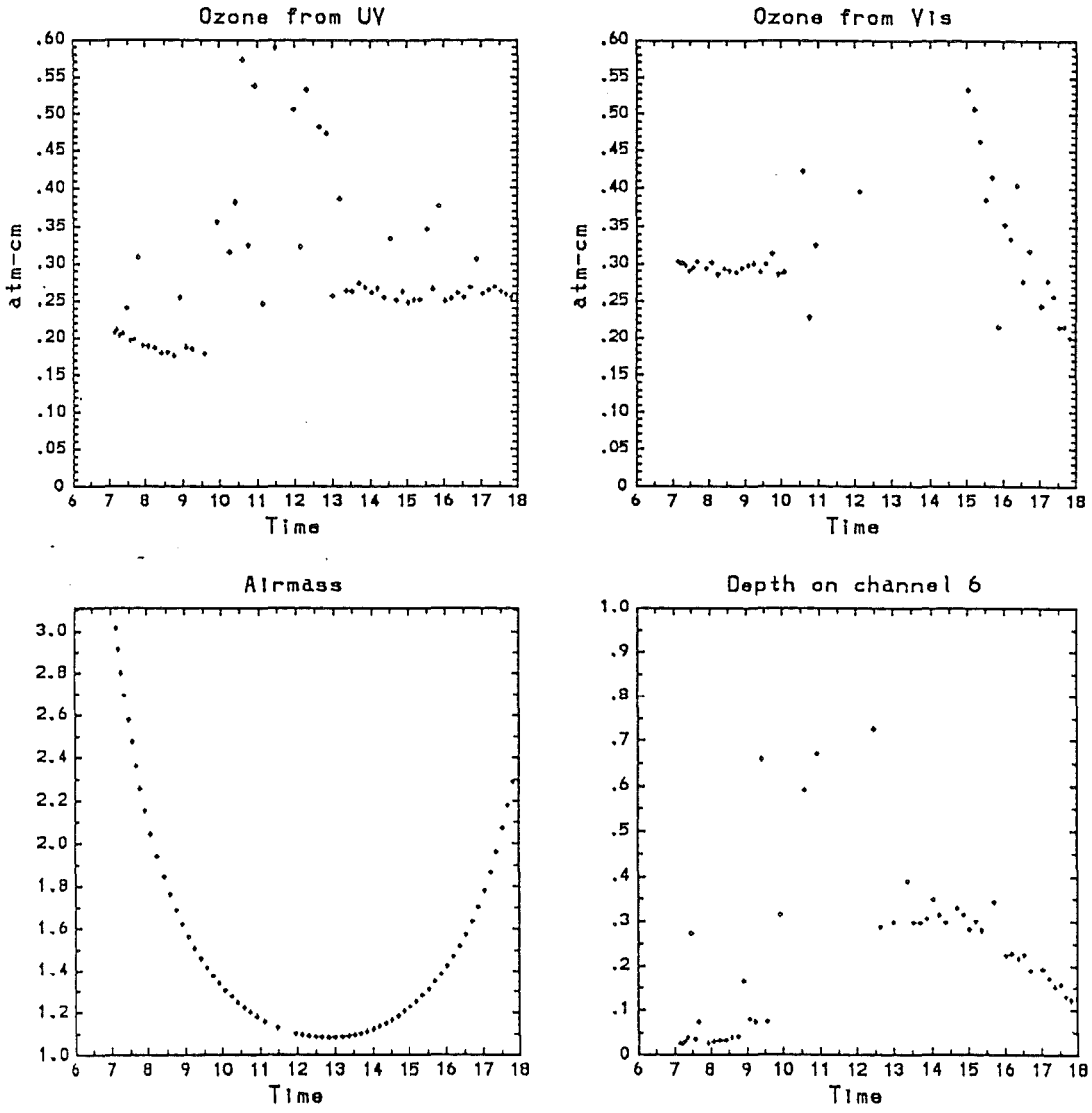

Figure 4.17: Readings at Lauder on 8 January 1988. At top left are the estimates of total ozone derived from the two ultraviolet channels. At top right are the values derived from the visible channels. Beneath these, respectively, are plots of the airmass and the optical depth on channel 6 (500 nm).

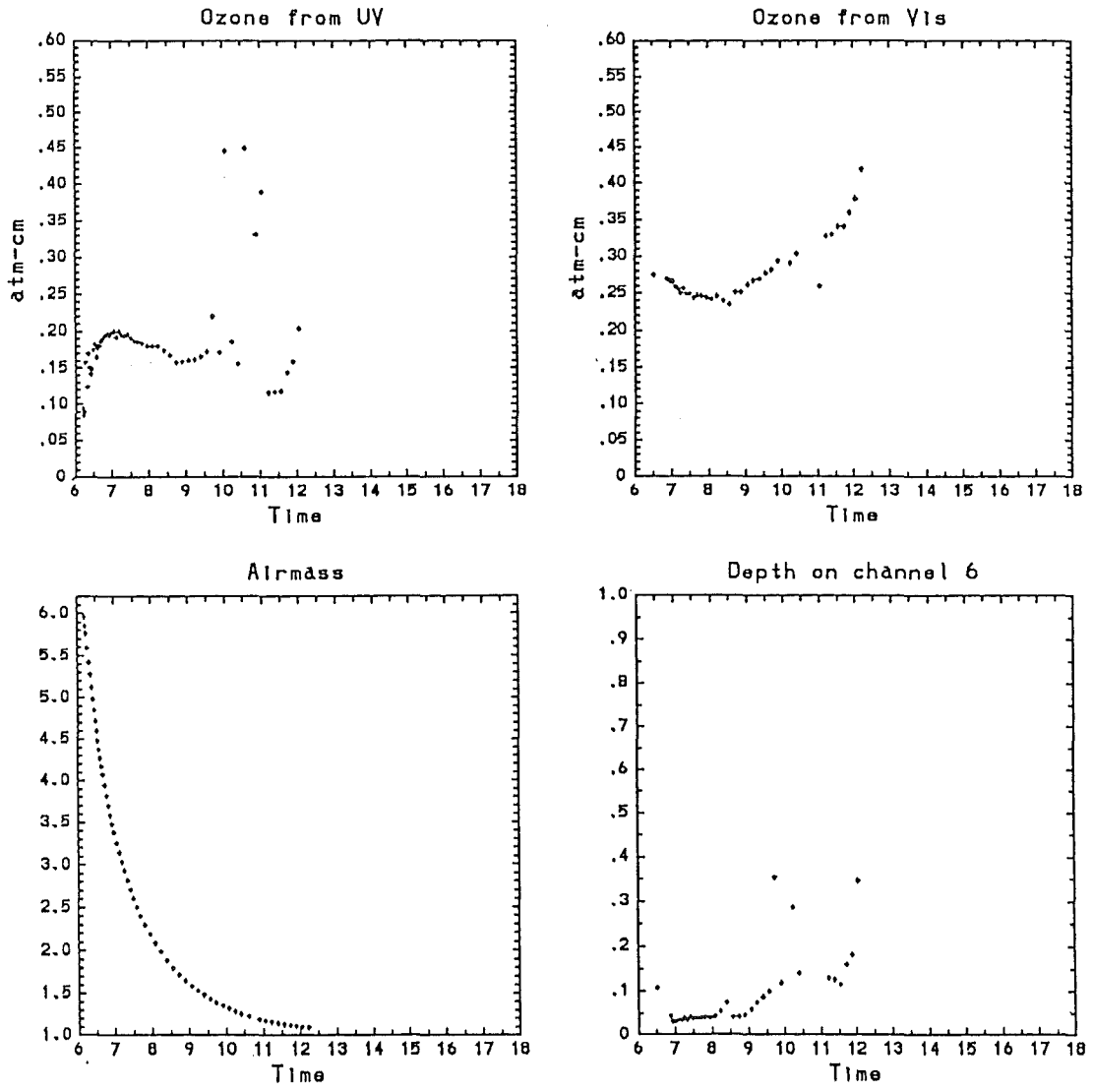

Figure 4.18: Readings at Lauder on 12 January 1988. The plots are the same as for Figure 4.17.

at the time that the optical depth starts to increase. The ultraviolet-derived value is again too low by a similar factor. The values obtained by the Dobson spectrophotometer throughout the morning were all within the range 0.283±0.002 atm-cm (283±2 Dobson units).

For the conditions encountered at Lauder, the photometer performed poorly in the determination of ozone. While the two methods for deriving ozone from its readings — from the Huggins band in the ultraviolet and the Chappuis band in the visible — both give estimates of the correct order of magnitude, there are significant systematic errors, especially in the former.

Chapter 5

Error Analysis

In this chapter the sources of error in the measurements made by the photometer are accounted for. These can be divided into errors that affect the amount of light received by the detectors, those that affect the value of the counts recorded by the photometer's computer, and those introduced in deriving the final parameters.

5.1 Errors affecting the amount of light received

This kind of error is the most difficult to quantify. The order in which they are considered follows the light path from the top of the atmosphere to the detectors. The errors due to varying atmospheric transmission and their effects on the calibration of the measurements have been discussed in Section 3.4.1 and are not considered further here.

5.1.1 Scattered light into the field of view

Much of the scattering in the atmosphere has a strong component in the forward direction. This means that some of the light travelling in the same direction as the direct beam, and received by the photometer, is scattered into the field of view and is not part of the direct solar radiation we are trying to measure. An instrumental field of view that is larger than the sun's disk will allow even more scattered light in. The effect of this light will become more significant at higher airmass as the ratio of scattered to direct radiation increases. This is one of the many reasons for limiting the airmass range over which measurements are taken. Shaw (1976) discusses calculations for a field of view with a 2.5° semi-angle, larger than that used in this photometer, at a wavelength of 371 nm. Plots of the ratio of diffuse radiation within that field of view to the direct solar radiation and the consequent error in the measured optical depth are calculated as a function of airmass and total optical depth. The error increases with total optical depth and becomes much larger at airmasses greater than five. The relative error in the measured optical depth remains roughly constant at 0.025 as long as measurements made at zenith angles greater than 80° are not used. If the field of view was larger, then the error would be greater. It is worthwhile then to keep the field of view as small

as possible so long as tracking is accurate enough to keep the sun within the field of view.

The next thing that can happen is that stray light entering the objective at angles outside the field of view can get to the detectors. The baffles in the heliostat are intended to prevent this. Their effectiveness can be checked by blocking the direct solar radiation from the instrument with an object sufficiently far away that the light reaching the instrument from other directions is not altered. The signal obtained in this manner was compared with the signal obtained with the objective completely blocked. This revealed a small but detectable difference between the two signals but it represented a small fraction of the direct signal, typically less than 0.4% at zenith angles less than 80°, in the channels that have strong signals. This means that direct-sun measurements are not affected significantly. If however, measurements of sky radiation were carried out with this instrument then the effect of this error would need further investigation.

An error peculiar to an instrument with a heliostat is that at different orientations the small polarisation that occurs on reflection at the mirrors affects the measurement in a way that depends on the relative position of the mirrors. However, since all the measurements considered in this report were direct-sun measurements the effects of this polarisation will be negligible compared to other errors considered in this section. If measurements of polarised or partially polarised radiation, such as skylight, were considered then the effects of this error may become more significant.

5.1.2 Errors due to the filter transmission

Basher (1975) found that sidebands in the filter transmission functions could cause significant errors. Compared with previous filter sets used at Canterbury, the present set is extremely well blocked. Details of the filter transmission were given in Section 2.1.2. The effect of those sidebands that were found was estimated using the model of the measurements described in Section 3.3 and are shown in Table 5.1. The infrared leakage of filter 8, which was of the most concern because it had the highest transmission ratio, contributes less than 0.5% to the total signal on that channel. Far more serious leakages exist in the two filters with the shortest wavelength passbands. This is because the ozone absorption is a rapidly varying function of wavelength and a sideband at a wavelength where ozone absorbs less strongly than at the passband (that is at a longer wavelength) begins to dominate the total response as airmass increases. The measurements made with these two filters must be treated more carefully as a consequence. The calculation of equivalent ozone absorption coefficients, described in Section 3.3, will include the effect of the sidebands.

The transmission of filters changes with temperature due to the temperature dependence of the refractive index and thermal expansion of the dielectric layers. The main effect of temperature is to shift the passband. The relative shift is linear, positive, and can be as much as $5\times10^{-5}/°C$ (Blifford, 1966). Basher (1975) measured values of approximately $3\times10^{-5}/°C$ in the filter set he used. The error due to temperature effects in the filters has been minimised by having them tem-

Filter Number	Centre Wavelengths (nm)		Transmission Ratio	Response Ratio	
	Passband	Sideband		$\mu = 2$	$\mu = 5$
1	311	365	4.4×10^{-4}	0.013	0.28
2	317	365	5.0×10^{-4}	0.0034	0.035
4	368	310	5.6×10^{-5}	1.4×10^{-6}	8.2×10^{-8}
6	500	> 1200	$*6\times10^{-4}$	4.8×10^{-4}	7.7×10^{-4}
7	600	700	9.0×10^{-5}	6.7×10^{-5}	8.1×10^{-5}
7	600	1175	1.5×10^{-4}	2.3×10^{-5}	3.2×10^{-5}
8	675	1150	0.02	0.0040	0.0046

Table 5.1: Ratios of the response in filter sidebands to the total response for that channel. The figures are calculated using the model described in Section 3.3 for an atmosphere with 0.3 atm-cm ozone. Values are given for airmasses of two and five, representing values near to the ends of the typical range over which measurements are made.

perature controlled. The temperature in the filter chamber of the photometer is 38±1°C. Assuming a similar value for the temperature coefficients of the present filter set, the passband shifts due to temperature variations during the measurements are limited to a few hundredths of a nanometre and so are insignificant. There is however the error due to the fact that the filter transmission measurements were made at a lower temperature, of around 25°C. This is because the spectrophotometer used to make the transmission measurements has no provision for maintaining the filter at a given temperature. The likely shift in passband due to a 15°C difference in temperature is a relative shift of 5×10^{-4} which is 0.15 nm for the ultraviolet filters and proportionately larger for the visible and infrared filters. The effect of such a shift has been calculated with the model described in Section 3.3 by shifting the filter transmission functions the appropriate amounts and calculating the effect this has on the response in each channel. The results are shown in Table 5.2. Given that the effect of this shift is significant in the case of the shorter wavelength filters, it was decided to use the shifted filter transmission functions in further calculations on the ground that some correction for the discrepancy between the filters' temperature for the transmission measurements and their operating temperature in the photometer is better than not correcting at all.

The transmission of the filters is also a function of the angle of incidence. The way in which this affects the measurements that were made of the filter transmission is discussed in Appendix A. Measurements of the transmission of some of the filters were made at varying angles of incidence and these showed that the principal effect of changing the orientation was to shift the central wavelength of the main passband to shorter wavelengths. A simple model (Basher, 1975) has the relative shift proportional to the square of the angle of incidence θ, according to

$$\frac{\delta\lambda_C}{\lambda_C} = -B\theta^2 \tag{5.1}$$

Filter Number	Total Response, P				Ozone Coefficient, $\overline{\alpha}_{O_3}$			
	X=0.25 cm		X=0.35 cm		X=0.25 cm		X=0.35 cm	
	$\mu = 2$	$\mu = 5$	$\mu = 2$	$\mu = 5$	$\mu = 2$	$\mu = 5$	$\mu = 2$	$\mu = 5$
2	2.0	4.4	2.8	5.9	-2.2	-2.1	-2.2	-2.1
3	0.21	1.0	0.37	1.2	-2.2	-2.2	-2.1	-2.2
4	-0.05	0.25	-0.05	0.25	-	-	-	-
5	0.21	0.42	0.22	0.42	-	-	-	-
6	0.08	0.13	0.05	0.09	-0.78	+1.3	-0.25	+1.1
7	0.16	0.23	0.17	0.25	-0.66	-0.37	-0.66	-0.30
8	0.02	0.07	0.02	0.09	-0.45	-0.56	-0.85	-0.45
9	0.03	0.06	0.04	0.06	-	-	-	-
10	0.16	0.17	0.16	0.15	-	-	-	-
11	-	-	-	-	-	-	-	-

Table 5.2: Calculated effect of filter passbands shifting with temperature. The assumed shift is $+5\times10^{-4}$. The values are the percentage changes in the total response P, and the effective ozone absorption coefficient $\overline{\alpha}_{O_3}$. These are shown for 0.25 and 0.35 atm-cm (250 and 350 Dobson units) total ozone and airmasses of two and five.

The measurements taken with the Cary spectrophotometer fitted this law well (see Figure 5.1). The value of the coefficient B was typically 0.2, similar to the values found by Basher, although some filters were 30% lower.

The angular dependence can affect the effective transmission of the filter whilst installed in the photometer in two ways. The first is that the filter must be mounted perpendicular to the principal axis of the incoming beam to prevent an unwanted shift in the passband. The precision need not be great: if the filter is aligned to a precision of just half a degree then the passband shift will be of the order of 10^{-5} or thousandths of a nanometre. The second effect is due to the fact that the light incident of the filter is not a collimated beam but contains a range of incident angles. This will shift and broaden the filter passband. As a rough approximation, the effect of a beam with a certain semi-angle is half that of tilting the filter through the same angle. In the photometer the field of view is limited to a semi-angle of 0.9° so the shift is likely to be of the order of 3×10^{-5}. For direct-sun measurements the dominating direct solar radiation is limited to a semi-angle of only 0.3° so the effect is even smaller.

The uncertainty of having a different beam geometry between the filter transmission measurement and the measurements made with the photometer could be removed by taking the transmission measurements with a collimated beam at varying angles of incidence and calculating the transmission for the beam geometry of the photometer. This is the approach used by McKenzie (1981). A more direct approach, if it were possible, would be to determine the filter transmission with a beam of identical geometry to that of the photometer by making the measurements in the instrument in which they will be used. Neither of these options was easily available to the author. However, simple checks of the effect of the spec-

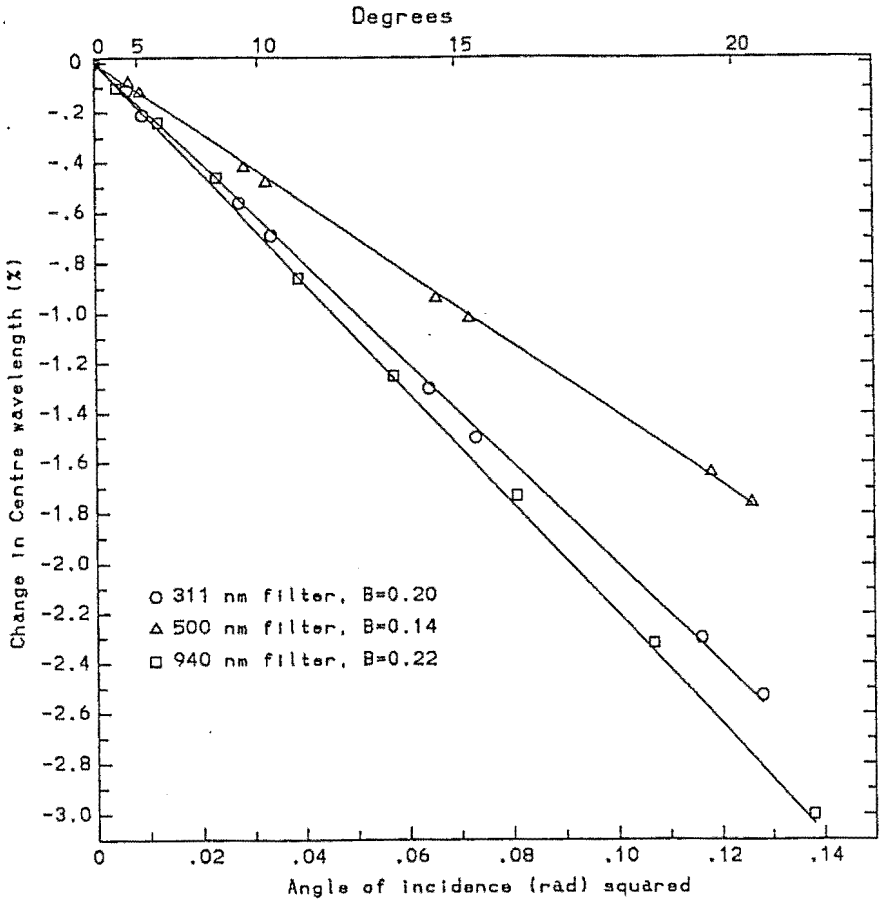

Figure 5.1: The variation of the centre wavelength of the main passbands of three of the filters. The variation is plotted against the square of the angle of incidence of the Cary's beam to check the fit of Equation 5.1.

trometer's beam geometry, described in Appendix A, failed to find any difference in the measured filter transmission.

The characteristics of interference filters are subject to changes over time. Short term changes are mainly due to absorption and desiccation of water vapour by the dielectric layers (Furman and Levina, 1971). This is minimised by hermetically sealing the filter between windows, so that the volume of air with which the filter can exchange water vapour is as small as possible. Basher (1975) estimated that a hermetically sealed window within 0.02 mm of the filter would restrict shifts in the passbands of the filter to the order of 10^{-2} nm which is adequate for use in the photometer.

There is the possibility of longer term changes in the filter characteristics. These may occur due to other processes: a failure of the seal; crystalisation in the dielectrics; or chemical interactions between layers. For this reason,the transmission characteristics of the filters used in this project were checked four years after the initial measurements were made. The central wavelength of one filter, that for

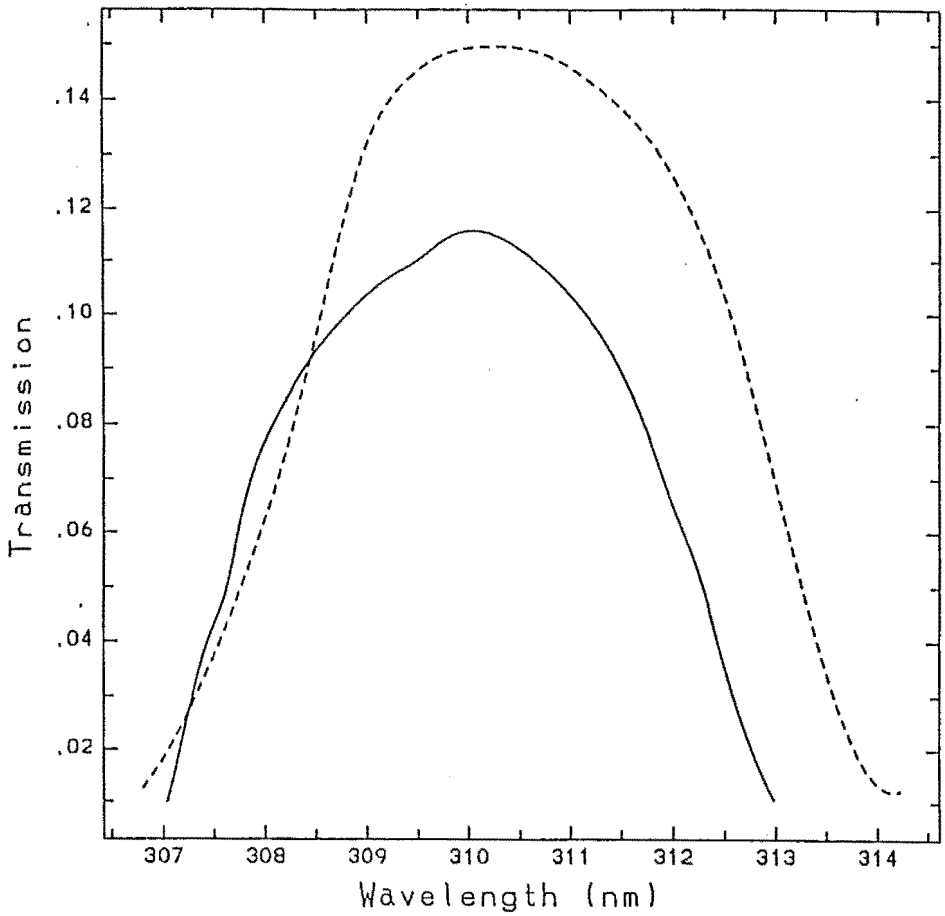

Figure 5.2: The shift in the passband of filter 1. The dashed line shows the original measurement. The solid line shows the measurement taken four years later.

the shortest wavelength, was found to have shifted from 310.5 to 309.9 nm along with a small drop in the peak transmission. This is shown in Figure 5.2. In a spectral region in which the ozone absorption changes rapidly with wavelength, this seemingly small shift decreases the total response P by as much as 30% and increases the effective ozone absorption coefficient by approximately 8%, as determined from the model of Section 3.3[1]. Values of these changes are shown in Table 5.3. As it was not clear exactly when the passband shifted the readings from that channel could not be used with any confidence. The passbands of the other filters had not detectably changed in the four years between measurements.

Since the transmission of interference filters is unlikely to be completely uniform because of the difficulty of depositing many uniform dielectric layers, the effect of this must be considered. Checks were made with the Cary spectrometer on the uniformity of some of the filters by masking the beam so that the area of the filter illuminated was similar in area to the amount that is illuminated in the photometer, approximately 20 mm^2. Different parts of the filter were used but no difference in the main passband characteristics, peak transmission, centre

[1]By comparing the integrated response obtained for the original and shifted filter transmissions.

Total	Total Response, P		Ozone Coefficient, $\overline{\alpha}_{O_3}$	
Ozone	$\mu = 2$	$\mu = 5$	$\mu = 2$	$\mu = 5$
0.25	-40	-50	+7.9	+8.3
0.35	-42	-54	+7.6	+8.4

Table 5.3: Calculated effect of filter 1 passband shift. The shift is as shown in Figure 5.2. The values are the percentage changes in the total response P, and the effective ozone absorption coefficient, $\overline{\alpha}_{O_3}$, and are shown for 0.25 and 0.35 atm-cm (250 and 350 Dobson units) total ozone and airmasses of two and five.

wavelength, or bandwidth, were found. To reduce the possible errors due to filter non-uniformities the distance between the filters and the detectors was kept as small as possible so that the part of the filter used does not depend on the direction of the incident radiation, and the filters held with a fixed orientation in the filter wheel so that the same part of each filter is always used. The filters also move during the measurement, so that the filter characteristics are averaged out as the radiation scans across the filter, reducing the error further.

5.2 Errors affecting values of counts

In this section those errors that affect the values of the counts for a given distribution of light are considered.

5.2.1 Variations in the detectors

The first of these is variations in the sensitivity of the detectors. If this changes at all in response to anything but the incident light intensity then the assumption that knowing the detector signal means knowing the light intensity is invalid unless the effect is quantified and compensated for.

The colour-voltage effect of the photomultiplier tube.

It was originally intended that the voltage divider for the photomultiplier tube be built with zener diodes instead of resistors on the first two stages[2]. On previous University of Canterbury photometers this was done to stabilise the voltage on those first stages (Matthews, 1971; Basher, 1975). The reason for doing this is that the relative spectral sensitivity of the tube can be a function of the voltage on these two stages (Carleton, 1974). This is known as the colour-voltage effect and arises because the performance of the cathode and the first dynode change as the electric field around them changes. There are several reasons for this. The effective electron affinity[3] is reduced at higher fields. This affects the sensitivity at all photon energies but has a greater effect in the spectral region on the longer

[2]That is the cathode to first dynode and the first to second dynode.

[3]Electron affinity is the energy required to eject an electron from the cathode.

wavelength side of the peak sensitivity, where the photon energies are close to the energy required to emit photoelectrons. The second effect is that the collection efficiency of faster photoelectrons at the first dynode is better at high fields. This improves sensitivity on the short wavelength side of the sensitivity curve were photon energies are large enough to produce the more energetic photoelectrons. The combined effect of these two factors is to broaden the sensitivity curve at higher fields. However, a more significant effect is that with different electric fields around the cathode and first dynode, the trajectories of the electrons emitted is different and those that are collected by the dynode will come from a slightly different area of the cathode, which may be more or less sensitive at a given wavelength. This is because the spectral sensitivity of the cathode surface is non-uniform[4]. This last effect means that the magnitude of the colour-voltage dependence varies from tube to tube. In order to establish their importance for the particular 1P28 tube used in the photometer, a closer look at the measurements taken to establish the variation in gain with voltage (described in Section 4.1) was made. When the data were taken and plotted (Figure 4.1) there appeared no difference in the voltage dependence of individual channels. However, by plotting ratios of channels a difference can be detected. Figure 5.3 shows this for the three channels that were plotted in Figure 4.1. There is definitely a colour-voltage effect for this tube which, except at small voltages where digital noise has affected the ratios, is approximately linear with voltage. The ratios of some channels vary by $\pm 8\%$ over the full voltage range. This is an intolerably large error. However, the atmospheric measurements that were made with the instrument were made with photomultiplier supply voltages in the range 700–900 V, over which the ratios vary by considerably less. It was found that the signal for each channel still followed the power law (Equation 4.1) well but with slightly different coefficients. The process of adjusting counts taken at a given voltage to an equivalent count at a standard voltage was modified accordingly. In doing this it is assumed that the wavelengths contributing to the measured signal on a given channel are dominated by the wavelengths in the filter passband. If a measurement was made which was dominated by some other wavelength then the measurements will be affected by a different amount and the adjustment incorrect[5]. The maximum change in any of the photometer measurements due to this new correction was 0.8%. It seems reasonable to assume that, despite the assumptions made in applying the correction, it will have removed at least 90% of the error, leaving a residual error of 0.08% or less.

Also of concern in relation to making accurate measurements with the photomultiplier tube are short term changes in the supply voltage. Such changes cause changes in the gain of photomultiplier tube according to

$$\frac{\mathrm{d}G}{G} = N\frac{\mathrm{d}V}{V} \tag{5.2}$$

[4]This is why it is so important to ensure that the same area of the cathode is illuminated for all measurements.

[5]What has been done is to correct all measurements on the assumption that the wavelengths contributing to the signal are the same as for the calibration measurements with a tungsten lamp.

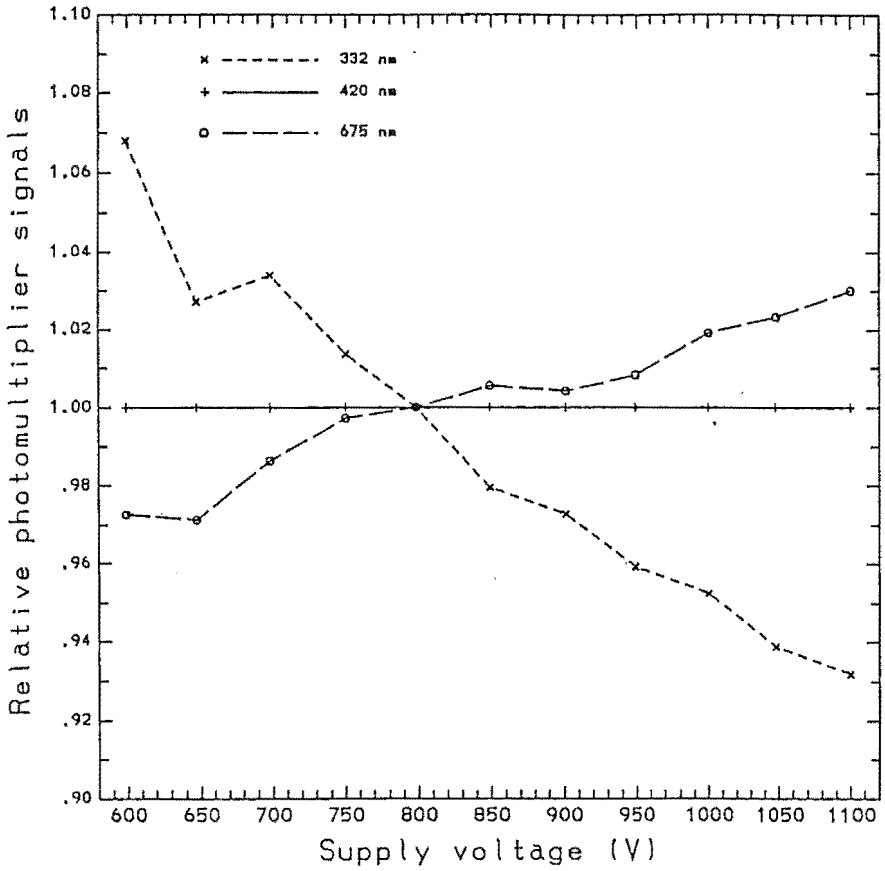

Figure 5.3: The colour-voltage effect for the photomultiplier tube. The ratio of the count on each channel to that on the 420 nm channel is shown as a function of supply voltage. The ordinate of each line has been scaled so that the point for 800 V is at 1. The data used are the same as for Figure 4.1.

which comes from differentiating Equation 4.1. The stabilisation of the power supply is 0.02%, over a period of a second, which gives a gain stability of 0.2% on that time scale. Changes to the supply voltage over longer times are of less concern as they affect the magnitude of all signals in the same way. While this means that quantities such as optical depths will be in error, most of the parameters derived from the measurements depend on the ratios between channels.

The photodiode measurements also have a variable gain. This is adjusted with a variable resistor in the amplifier circuit. Once it was set at a suitable value determined from the first few days of operation of the photometer, it was not changed at all.

The output signals of both detectors include a component that is independent of the radiation level, known as the dark signal. In the photomultiplier tube this is due mainly to the thermionic emission of electrons from the cathode which is dependent on temperature and gain. Other contributions come from ohmic leakage and various other effects such as internal fluorescence, residual gas ionisation, and ionic currents in the glass walls of the tube. For the diode the dark signal is the result of an offset in the amplifying circuit. These signals would be a significant

source of error if they were not continuously monitored by having a twelfth channel that is blocked off. The first step in analysing the readings is to subtract this dark reading from the counts.

The photodiode has a significant temperature coefficient. This varies, and even changes sign, with wavelength. The values quoted in the manufacturer's specifications are -0.1%/°C at 350 nm and +0.5%/°C at 900 nm. This has very little effect as the diode is in the filter chamber whose temperature is controlled to the nearest degree.

The photomultiplier tube is not thermostatically controlled. Its gain is temperature dependent and is of the order of 10^{-3}/°C (Philips, 1970). The maximum range of temperature that the photomultiplier tube operates at is 20 to 30°C which implies that gain changes of the order of 1% are possible. However on a given day the temperature inside the photometer will be stable to a few degrees so this error will be reduced somewhat, especially if the instrument has been running for long enough for it to reach equilibrium temperatures.

The linearity of the photodiode is better than 1% over six orders of magnitude in response, although less of this range can be used in this instrument because of limitations of the digital recording of the signal.

The whole of the photosensitive surface of the diode, a circle with a diameter of 5 mm, was illuminated as there was no aperture to limit the illumination to any one part of the surface. This means that any surface non-uniformity is not important in this application.

The linearity of the photomultiplier tube is limited at the low end of its working range by the dark current. Since the dark current is measured and corrected for this is of no concern in this instrument. At the high end of the range linearity is limited by the need to keep the anode current a small fraction of the total bleeder current in the voltage divider. The bleeder current at a typical working voltage of 800 V is 0.8 mA. If the current drawn at any point from the divider is a significant fraction of this then the current in the divider's resistors, and hence the voltage across them, is modified. The error shows up in the final stages and at the anode because that is where the currents are largest. Philips (1970) gives an expression for the relative gain change $\mathrm{d}G/G$, as a function of the anode current i_a, the bleeder current i_b, the number of stages N, and the mean gain per stage δ

$$\frac{\mathrm{d}G}{G} = \frac{i_a}{i_b}\left[\frac{N}{N+1} - \frac{1}{(N+1)(\delta-1)}\right] \tag{5.3}$$

For the 1P28 photomultiplier tube, $N = 9$ and δ can be calculated from the specified current amplification A, since $A = \delta^N$. Values of δ for different supply voltages and the consequent gain changes are shown in Table 5.4. The gain inaccuracy can be approximated with

$$\frac{\mathrm{d}G}{G} = 0.85\frac{i_a}{i_b} \tag{5.4}$$

The maximum count that can be measured with the digital counters in the 20 ms timing interval corresponds to an anode current of 20 μA. At a typical supply voltage of 800 V this is 2% of the bleeder current. At this point the inaccuracy

Supply Voltage	Total current amplification A	Mean gain per stage δ	Relative gain change dG/G
500 V	9×10^3	2.75	$0.84i_a/i_b$
600 V	3×10^4	3.14	$0.85i_a/i_b$
700 V	9×10^4	3.55	$0.86i_a/i_b$
800 V	2.5×10^5	3.98	$0.87i_a/i_b$
900 V	5×10^5	4.30	$0.87i_a/i_b$
1000 V	1.2×10^6	4.73	$0.87i_a/i_b$

Table 5.4: Gain changes for the photomultiplier tube due to excessive anode current modifying the voltages in the final stages. The gain changes are proportional to the ratio of anode current i_a to the bleeder current in the voltage divider i_b, and are calculated using Equation 5.3.

Supply Voltage (V)	Bleeder Current (mA)	Anode current, i_a (μA)	
		$dG/G = 1\%$	$dG/G = 0.1\%$
500	0.5	5.8	0.6
600	0.6	7.1	0.7
700	0.7	8.2	0.8
800	0.8	9.4	0.9
900	0.9	10.6	1.1
1000	1.0	11.8	1.2

Table 5.5: Limits on the photomultiplier anode current to keep the inaccuracy in gain to 1% and 0.1%.

in the total gain of the tube is around 1.7%. Using the results in Table 5.4 the maximum allowed currents to limit the inaccuracy to 1% and 0.1% respectively are shown in Table 5.5. These limits could be increased by increasing the bleeder current, either for the whole voltage divider by increasing the output current of the high voltage power supply, or just on the final stages by supplying them with a different power supply.

5.2.2 Conversion to digital signals

The next step in the measurement process, the conversion of the output signals to digital form, also introduces errors. For the photodiode the voltage controlled oscillator has a linearity over the range 0–100 kHz of better than 0.03% so this is not a significant source of error. The linearity of the current to frequency circuit, used to convert the photomultiplier tube signal, is shown in Figure 5.4. The performance of the circuit becomes slightly non-linear at input currents below 1 nA. The range of currents over which it is used is in the photometer is approximately 2 nA–30 μA, this being the range that the digital circuits are set up to measure.

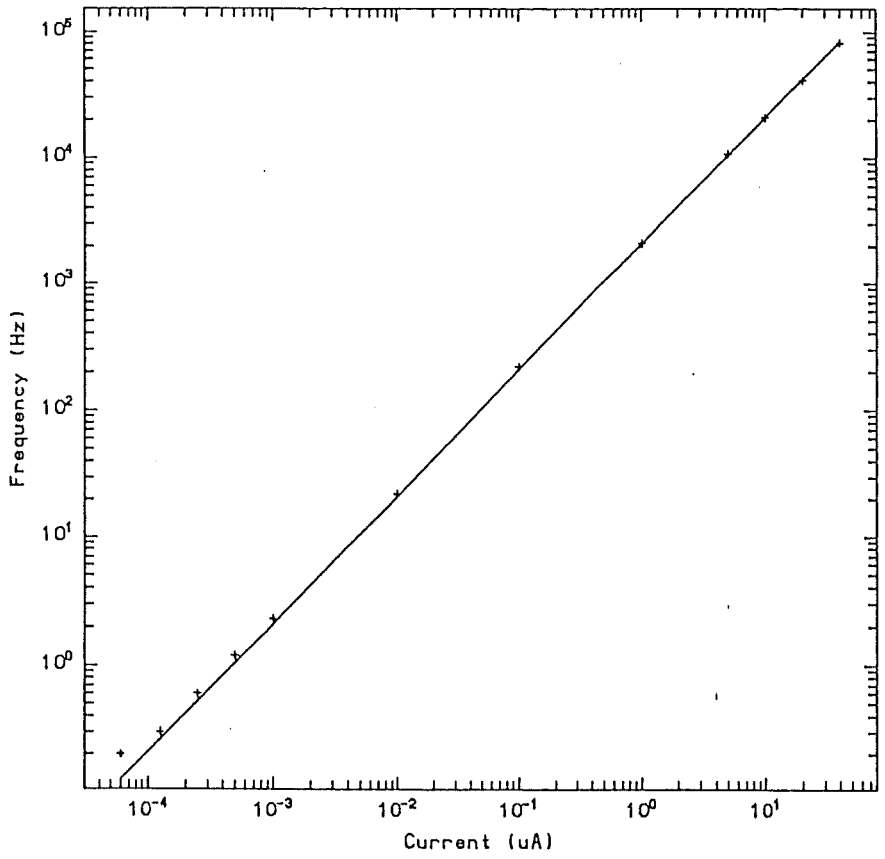

Figure 5.4: The linearity of the current to frequency circuit.

Within this range the linearity of the circuit is better than 0.5%.

The final step in the conversion of the analogue signal from the detectors to the digital counts relies on a consistently accurate integration time during which the output pulses from the frequency circuits are counted. The times were generated by a monostable circuit which produced a timed interval of 20 $\pm$ 0.1 ms. The uncertainty of any given interval is thus $\pm$0.5% but since most measurements are made over a number of intervals, typically 10-20, this error is reduced by approximately half an order of magnitude.

As long as the counters do not overflow during a single timed interval, something that is avoided by having the detector gains set at suitable values, the only error in the conversion to a digital count is the rounding error from taking only whole numbers. This becomes significant at low count rates. If all the counts are low then the controlling program of the photometer will take counts over a larger number of filter wheel revolutions to reduce the error. For example, if the count rate on a given channel is only 50 pulses in the 20 ms interval then the digital error in a measurement made on just one timed period is an unacceptable 2%. If that measurement is taken as the aggregate over ten wheel cycles then the error is 0.6%. If the magnitude of all the signals could be somehow made similar, then the digital error need not be of concern. There is however a considerable variation in the magnitude of the signals, especially in the ultraviolet channels. This means

that the range of airmass over which a useful measurements can be taken is limited on some channels. Instances of this were discussed in Chapter 4.

In summary, the error in any value recorded by the photometer is dependent on the operating conditions. If there are no problems with the magnitude of the signal being too large or too small, then errors due to other effects can be limited to approximately 2% for the photomultiplier tube and 1% for the photodiode. If the the photomultiplier is operated at currents of 10 nA or higher then an additional error is introduced of 1%.

5.3 Errors introduced in calculations

There are several sources of error introduced in the calculations. The most significant error introduced in reducing the data is the uncertainty in the experimentally determined extraterrestrial responses P_0^i, of the instrument. The sources of this error are discussed in Section 3.4.1 and their magnitude is given in the previous chapter.

In Chapter 3 mention was made of the depolarisation correction to the Rayleigh scattering coefficient. This is discussed more fully here as it has been the cause of recent debate. In the scattering from an isotropic molecule, the light scattered at right angles to an unpolarised incident beam is totally polarised, with its electric field perpendicular to the plane of scattering. The effect of anisotropy is to allow some of the opposite polarisation to be scattered in this direction. The depolarisation factor ρ of the light scattered at right angles, defined as the ratio of the parallel to the perpendicular component, is a measure of the effect of the anisotropy. Cabannes (1921) showed that in this direction the light scattered by the anisotropic molecule exceeds that scattered by an isotropic molecule by a factor $\frac{6+6\rho}{6-7\rho}$. King (1923) showed that the factor was different for total scattering, being $\frac{6+3\rho}{6-7\rho}$, because the angular distribution of the scattered light is changed. Neither of these workers had considered molecular rotation, the effect of which is to produce two side bands in the radiation radiated by the molecules with wavelength slightly to each side of the incident wavelength. These side bands form the Raman rotational spectrum of the molecule. There has in recent years arisen a confusion about whether the Raman bands should be included in the measurement of the depolarisation ratio or not. This is because molecular spectroscopists reserve the term Rayleigh scattering for the scattering that occurs with no shift in wavelength, that is excluding the Raman scattering. Some workers, Hoyt (1977), Fröhlich and Shaw (1980), have excluded the Raman lines by using laser measurements of the depolarisation of elastically scattered light. The polarisation corrections they used (1.02) were significantly lower than the value of 1.06 used in older calculations such as Penndorf (1957) and Elterman (1968). There was the suggestion that these differences could explain some of the problems in calibrating sun photometers. Measurements of depolarisation ratios are not always clear on whether the Raman lines were included or not, and there is also the possible confusion of measurements taken with polarised sources of light. Differences between depolarisation ratios can be accounted for (see Young, 1980) but only if one is aware that

there are different values. Since, in atmospheric applications, the interest is in the total radiation scattered, the Raman components should be included. In many cases it is unlikely that the Raman components are able to be differentiated from the rest of the scattered radiation anyway, as in broad band measurements. Young (1981a, 1981b) has written papers carefully explaining the issue in order to clear the confusion and arrive at the best value for the correction. His conclusion is that the best values for depolarisation lie between the old and new values. Nicolet et al. (1982) responded to this by taking a median value of 1.03 ± 0.01. Recently a calculation of the scattering cross sections that includes the wavelength variation of the depolarisation correction has been published (Bates, 1984), and it is these that are used in this project (see Table 3.1). The agreement between these and experimental values is claimed to be rather better than 1%. The correction factor used lies in the range 1.05 ± 0.005 in the wavelength range of the photometer (300–1000 nm) and so is consistent with Young.

Another parameter introduced in the calculations is the airmass. The functions used to describe it were described in Section 3.1. The airmass for Rayleigh or molecular scattering was approximated by the function given in Equation 3.9. Kasten (1966) estimates that for zenith angles less than 86° the deviation from his calculated airmass is less than 0.1%. However these calculations are for a standard atmosphere and so the airmass should not be considered to be that precise for a real atmosphere. At small airmass there should be little problem but at airmass greater than five all the airmass functions (Equations 3.9, 3.10, and 3.11) should be viewed as good approximations accurate to a percent or so.

The ozone absorption coefficients are based on laboratory measurements. There have been a number of measurements (Griggs, 1968; Simons et al., 1973; various papers in IOC, 1984) that are more recent than the ones used in this project (Valley, 1965). However they have either been made at room temperatures, which are significantly different from the temperatures in the lower stratosphere, or the values themselves have not been published. The temperature dependence of the coefficients is complex. The maxima tend to decrease in absorption with increasing temperature whilst the minima increase. This can be interpreted as the effects of a large number of overlapping lines which are broadening as temperature increases. Measurements taken at room temperatures can be corrected to other temperatures by using the Vigroux measurements at different temperatures, as is done in Klenk (1980) for satellite and Dobson bands, but it is a complex procedure and considered to be beyond the scope of this project.

Even if the values of ozone absorption coeficient α_{O_3}, were perfect there is still the error in determining the calculated values of the equivalent ozone absorption coeficient $\overline{\alpha}_{O_3}$, for each filter. The uncertainties in the filter transmission measurements — from both the transmission values and the their wavelength calibration — can cause significant changes in these values, as is demonstrated in the results shown in Tables 5.3 and 5.2. Consequently the equivalent absorption coefficients may be in error by several percent. It is only by improving the performance and calibration of the photometer, especially in the ultraviolet, that the effect of this particular error can be quantified. If the errors in the filter transmission measurements are found to be too large, then a more accurate measurement, made at the

same temperature that the filters operate at in the photometer would be required.

Chapter 6

Discussion

6.1 The photometer's design

The idea of providing a sun photometer with bands over such a wide range of wavelengths is an ambitious one. To have in a single instrument, that is relatively portable, the ability to measure both aerosol characteristics and the quantity of atmospheric ozone is a distinct advantage over having two separate instruments. Even an accuracy of 10% in the measured value of ozone means that the errors in measured aerosol optical depths at those wavelengths in the visible that ozone absorbs are reduced. Despite some remaining difficulties, the photometer has gone part of the way to doing this.

Having an automated instrument is a significant advantage over an instrument that has to be operated manually. It allows readings to be taken far more frequently and the data to be recorded automatically. The only reason why the computer controlling the instrument, in this case, could not do some simple analysis of the results, as they are taken, is the poor calibration of the extraterrestrial constants. If that difficulty were overcome then a direct readout of the parameters of interest could be made almost instantaneously. The raw data could still be recorded in a way that allowed a re-analysis of the calculations. This has been achieved in the semi-automation of Dobson spectrophotometers which can take a measurement and then provide a direct readout of the quantity of ozone. This is a vast improvement over the skilled operations required to take a measurement with the unmodified Dobson instruments.

However the photometer's design has a number of disadvantages. It was designed to measure both aerosol characteristics and to determine ozone. By nature, anything that is designed to do more than one thing will often perform less well than a single purpose design, and this photometer is no exception.

Firstly, the photometer is more complex than it would be if it had only one function. By having a large number of filters, it has to be physically bigger than previous instruments. This makes it less portable than a filter instrument designed to do one thing, such as the previous University of Canterbury ozone photometers or a Volz sun photometer. It can still be moved by one person, which means it is much more portable than a Dobson spectrophotometer.

Using a heliostat that tracks the sun, rather than pointing the whole instru-

ment with an equatorial mount, introduces the complications of extra optical surfaces in the light path and the fact the light path is not identical for all measurements. The mirrors in the heliostat must be aligned to better than a few minutes of arc to be sure that the light path is correctly aligned. A sun photometer that is light enough to be tracked by turning it on an equatorial mount has a much simpler light path.

Having two detectors increases the alignment problems. Care must be taken to ensure that the field of view of the two are identical in size and position.

The error that was made with the photomultiplier tube voltage divider, described in Section 5.2.1, did not cause large errors in the measurements made with the instrument but there is no doubt that this is the sort of situation that is far better to avoid than to have to correct for.

One disadvantage with having a larger number of channels is that this inevitably means that there is a range of signal strength from channel to channel and that the detectors and the way the signal is recorded must cope with this range. When those signals also start to vary the range required of the detector circuits is further increased. This means that precision and accuracy are sacrificed on some channels because the signal becomes small compared with the noise. Because the filter bandwidths and the spectral irradiance are similar over much of the visible and infrared, and because attenuation by the atmosphere at these wavelengths is not large, the range of the detector circuits is adequate in these regions. However in the ultraviolet, the range in signal strengths is much larger and it is the weakest signals that are attenuated the most by the atmosphere, meaning that they vary the most during the course of a day. Even though significant reductions in the range required were achieved by the author, the limit on dynamic range imposed by the digital counters used cannot cope with the range of signal expected of it. This means that it is impossible to set the gain of the photomultiplier tube at a suitable value for a whole day's readings. In the same day that the signal on one channel is being lost due to noise or scattered light at high airmass, problems are encountered with the digital counter overflowing on other channels at lower airmass. If the photomultiplier tube's gain is set lower to eliminate the overflow then the weaker signals are useful over an even smaller range. The weakest signal of all was at the shortest wavelength and even if the passband of that filter had not shifted the readings were of limited use.

The solution to the problem is to increase the range over which useful measurements can be made. There are two ways of approaching this. One is to increase the number of bits available in the digital counter. The number of bits in the counter is currently eleven and accumulated sums are stored in a sixteen bit register. If these values were increased then the gain of the photomultiplier tube could be increased without causing overflows of the counts from the stronger signals.

A second solution is to provide a way that the computer can control the voltage applied to the photomultiplier. Then it could set the voltage to an appropriate value, determine by trial readings, to make each measurement. A system such as this is used in the automated Dobson spectrophotometers, although it made much simpler in that instrument by the fact that the aim is to establish that two signals are equal rather than measure the absolute value of any one signal.

6.2 Conclusions

It has been shown that the photometer can provide measurements of atmospheric ozone and aerosol characteristics. Even with a value for ozone that is not very precise, the aerosol optical depths in the visible are more useful than if a value to the ozone content has to be assumed. This project has highlighted the difficulties in setting up and calibrating a new type of instrument.

The loss of the information from the shortest wavelength channel centred on 311 nm was significant. A full measurement of the filters transmission function with wavelength is time-consuming, requires that the filter be removed from the instrument and so cannot be carried out frequently. The shift has compromised the ability of the photometer to provide good estimates of ozone. It would have been the most sensitive to ozone, with an ozone absorption coefficient larger than any of the other channels by a factor of three or more.

The second limitation is the accuracy of the extraterrestrial constants. This was a matter of logistics. As the photometer was a prototype, it was not considered practicable to operate it at remote sites where the technical support to cope with any difficulties was not available. Since previous University of Canterbury photometers have been adequately calibrated in Christchurch, it was assumed that sufficient readings in Christchurch would provide good enough extraterrestrial constants. However these instruments were easier to calibrate because one was only interested in the ratios of extraterrestrial constants in order to determine total ozone. The absolute values of these constants were not as important as the wavelengths of the channels were sufficiently close that one could expect much less in the way of variation between channels except from changes in ozone. To be able to make measurements of aerosol optical depths one must have an absolute calibration for each channel of interest and this proved much more difficult to do than was anticipated. The measurements that were undertaken at Lauder in an attempt to rectify the problem did not provide good enough readings to do so.

The channels in the ultraviolet had broader bandwidths than would be used in an instrument designed solely for the determination of ozone. Previous University of Canterbury photometers used bandwidths of approximately 2 nm whilst this one uses widths of 5 nm. Because of the difficulties with the loss of the 311 nm channel, the problem of insufficient range and the low accuracy of extraterrestrial responses, the precision with which which such broad filters can determine the quantity of ozone has not been determined. The effective ozone absorption coefficients vary significantly with ozone and airmass for these filters. Their usefulness depends heavily on the accurate calculation of the effective absorption coefficients and their variation. These calculations in turn require good values for the ozone absorption coefficient as a function of wavelength at a temperature applicable to stratospheric conditions and accurate measurements of the filter transmission at the temperature at which they are operated. When the instrumental problems have been solved it may well be that better measurements of both these functions will be required to improve the performance of the photometer in determining ozone.

The design of the instrument was one of compromises and so the objective of

looking at the interaction of ozone absorption and aerosol scattering was rather ambitious. The photometer can provide measures of both but since its ozone measurement must be less reliable it can do little in quantifying the effect of aerosol scattering on ground based ozone measurement. If the sole objective were to investigate the way in which ground based ozone measurements are affected by aerosol scattering, then measurements with a much better wavelength resolution at several points in the range 300–340 nm would do the job. A measurement of the ultraviolet spectrum in the direct solar beam or in zenith skylight over these wavelengths would allow an even more reliable investigation of these effects.

In the converse problem the photometer is more useful. Even a crude measurement of ozone such at this photometer is able to make can improve the accuracy of aerosol optical depths in the region around 600 nm over the usual method of assuming a typical value for ozone.

Despite its shortcomings the photometer can produce useful measurements. The visible channels provided the same sort of information on optical depth that a simpler sun-photometer could provide. Despite the loss of an important channel, measures of ozone were made. While these do suffer from significant systematic errors, the ways in which they can be improved are known. If these improvements can be made then the result will be a useful and portable instrument which could provide good values of both total ozone and aerosol characteristics.

Appendix A

Measurements of the filter transmission

The author measured the transmission functions of each of the interference filters. The instrument used to do this was a Cary 14 spectrophotometer owned by the Condensed Matter research group of the Physics Department of the University of Canterbury. This uses a variety of radiant sources and detectors to cover a range of wavelengths from 0.19 to 2.6 μm. The source used in this work was a quartz iodine lamp and the detectors were a photomultiplier tube of the same type as the one in the photometer (an RCA 1P28) and a lead sulphide detector for the infrared. The spectrophotometer uses a scanning monochromator consisting of a quartz prism and an echelette grating to produce a beam of known wavelength. This beam is passed alternately through a sample and a reference chamber by a mechanical chopper. The ratio of the two intensities, as measured by the detector in use, provides a measure of the transmission of the sample. The transmission is shown on a scale as an optical density[1] from zero to two. The scale could be read directly or pens attached to the instrument to record the values on chart paper. Both the chart and the monochromator could be driven at a constant speed to provide a plot of optical depth as a function of wavelength. Wavelength calibration was achieved by comparison with the known lines in a Mercury lamp and was good to ± 0.1 nm as long as care was taken to eliminate the effects of slack in the gear trains that drive the monochromator and chart. This was done by always driving the wavelength gear train in one direction only, the same direction used to make the calibrations of wavelength, and by ensuring that there is no slack in the chart drive at the start of a scan.

Since the low transmission parts of the filter spectra had to be checked, the limit of only 1% transmission had to be circumvented. This was achieved by the positioning of neutral density filters in the reference beam. These filters consisted of layers of stainless steel gauze held together in a configuration that gave an

[1]Optical density is the negative of the common logarithm of the transmission, that is an optical density of x corresponds to a transmission of 10^{-x} . The Cary can in fact be converted to read transmission directly, which would have been slightly more convenient, by the substitution of the potentiometer which provides the feedback by which the pen carriages are positioned, but this was not available to the author.

integral optical density of either one or two and were oriented to avoid any Moiré fringes. One or more of these filters could be placed in the reference beam to provide an optical density in that beam of as much as four. Since the Cary records the ratio of sample beam intensity to that of the reference beam this meant that the filters could be checked to optical densities of 5 or 6, that is to transmissions of 10^{-5} or 10^{-6}. The limit depends on the noise limit of the instrument, due to internally scattered light and electrical noise in the various circuits.

The resolution of the measurements was variable. This is because of a complex servo slit system that the Cary uses to compensate for the variations in the spectral sensitivity of the detector and the intensity of the source in use at the time. The slits, two in the light path of each beam, are adjusted to keep the amplified electrical output of the detector at a constant level. That means that if either of the beams is attenuated, the source become weaker, or the detector becomes less responsive at a particular wavelength then the slits will widen to compensate. This allows a wider range of wavelengths into the beam. There is a fixed relationship between the slit width and resolution at a given central wavelength, defined by the dispersion of the monochromator. This is of considerable importance when the measurements of the low transmission parts of the filters are scanned with the neutral density filters in place, as the transmitted beams have low intensity. Fortunately the operator is not completely at the mercy of the instrument in this respect. There are several instrumental parameters that can be modified to increase the signal and hence decrease the slit widths and increase the resolution. These are:

- Increasing the voltage supplied to the lamp being used as the source to increase its intensity.
- Increasing the amplification of the detector feedback signal that is supplied to the slit servo system.
- If the photomultiplier tube is being used as the detector, increasing the voltage supplied to it to increase its gain.

Each of these can be adjusted to help achieve the required resolution, but the second and third do so at the expense of increased noise in the recorded signal.

The need to be aware of the resolution for a particular measurement was increased by the nature of the filter transmission curves. When the transmission varies slowly or linearly with wavelength there is little error from a finite bandwidth and so no need for concern. If however the transmission is more complex then a finite resolution will introduce an error into the measurement because it is an average over the range of wavelengths in the beam. The transmission of the filters resemble exponential functions of wavelength of the form

$$T = \exp(a_1\lambda + a_0) \tag{A.1}$$

in the skirt regions to either side of the passband[2]. The relative error in the measured value T_m, of such a transmission function made with a finite bandwidth

[2]That is, plots of optical density or logarithmic plots of transmission appear almost linear in these regions.

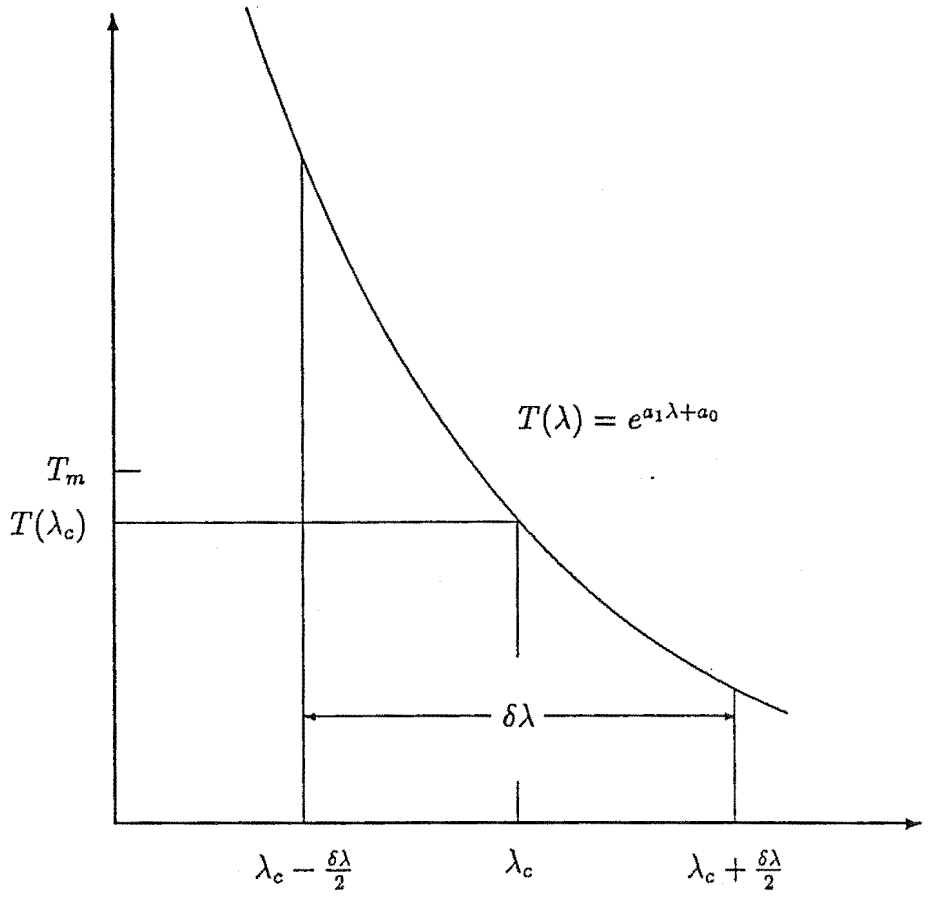

Figure A.1: The error in measuring a transmission that is an exponential function of wavelength $T = a_1\lambda + a_0$, with a finite resolution $\delta\lambda$. The result T_m, of the measurement centred at λ_c is represented by the average of the function between $\lambda_c - \frac{\delta\lambda}{2}$ and $\lambda_c + \frac{\delta\lambda}{2}$. This differs from the actual value of the function at λ_c by a factor of $\frac{\sinh\xi}{\xi}$ where $\xi = a_1\frac{\delta\lambda}{2}$.

$\delta\lambda$, can be calculated (see Figure A.1) and is equal to

$$\delta T = \frac{T_m - T}{T} = \frac{\sinh\xi}{\xi} - 1$$
$$\text{where } \xi = \frac{a_1\delta\lambda}{2} \tag{A.2}$$

This relationship can be used to determine the resolution required to keep the error acceptable. The regions to either side of the main passband of each filter are extremely steep and care must be taken to manage the instrument, using the steps listed above, so as to keep the error within reasonable bounds. As an example the resolution errors at selected points in the skirt region on one side of the passband of filter 4 (368 nm) are shown in Table A.1. The effect of the Cary's beam geometry on the measurements is important. The transmission of an interference filter is a function of the angle of incidence. Normal incidence was assured for the measurements by checking that the reflected image of the entrance slit in the sample chamber coincided with the slit. There is the possibility that

Wavelength, λ_c (nm)	373.6	377.6	384.9	396.2
Measured Transmission, T_m	0.251	0.0316	1.0×10^{-3}	3.2×10^{-5}
Resolution, $\delta\lambda$ (nm)	0.1	0.2	0.5	1.2
Gradient, a_1 $(\text{nm})^{-1}$	0.20	0.57	0.34	0.29
Error, δT (%)	0.002	0.05	0.12	0.5

Table A.1: The resolution error in transmittance measurements for filter 4. The wavelengths shown represent points progressively further from the main peak. The resulution gets worse as the transmission decreases.

there is an error in the measured filter transmissions due to the range of angles of incidence in the Cary's beam. The beam has a rectangular geometry with different semi-angles of 4° and 1.5° in the horizontal and vertical respectively. Some idea of the magnitude of the effect can be obtained by placing masks at the entrance slits of each chamber to remove the outer, more divergent, parts of the beams and repeating the measurements. Care is needed when masks are used that the balance between the reference and sample beams is not lost. For this reason, and because the signals are made smaller by the masks, these measurements are less precise than when the full beams are used. They did show, however, that the main features of the transmission curves, the central wavelengths, peak transmission, and bandwidths did not change within the accuracy of the measurements. As a further check, the measurements that were made with the filters deliberately tilted, reported in Section 5.1.1, establish the magnitude of the angle dependence. Using the same approximation to estimate the effect of a range of incident angles, the passband shifts due to the Cary's beam are of the order of 0.05%.

Appendix B

Programs for the photometer

Included in this appendix are further details of the programs used for the photometer.

B.1 Machine code routines

The assembler used to write the machine code routines was MAE, a Macro Assembler and Editor produced by Eastern House Software. The input to the assembler is a program consisting of the following

Op-code mnemonics: consisting of three letters. Each of these corresponds to an operation that the processor can perform and which is assigned a singe byte operation code. The mnemonics for the op-codes are standard abbreviations for the 6502 processor and are common to all 6502 assemblers. Some of the operations must be followed by parameters, of either one or two bytes, representing data or a memory location. The assembler allows these to be defined in a number of ways, as a binary, decimal, or hexadecimal number or with an alphanumeric label.

Assembler directives: consisting of a period and two letters. These are instructions to the assembler that are not reflected directly in the output. Examples are the definitions of labels, the inclusion of another file, or details of where the output should go.

Comments: being anything following a semi-colon on a given line. A liberal commenting policy is advisable to aid the readability of the routines.

Although the programs are still more difficult to read and work with than a high level programming language they are a considerable improvement on working with the raw machine code sequences of code bytes. The ability to have meaningful alphanumeric labels representing memory locations is especially helpful, be they locations used for data storage or specific point in the routines themselves. The assembler produces machine code output in an process similar to the way that a compiler[1] produces object code from a program written in a high level language.

[1]The operation of an assembler is simpler because there is a one-to-one correspondence between the mnemonics in the input and the operation codes in the output.

Source listings for the routines follow.

The Initialisation Routines

Routines to configure each of the Peripheral Interface Adapters correctly for the use to which it is to be put. Most of the other routines will call the appropriate initialisation to ensure correct configuration.

```
--------------------FILE PIA.SRC--------------------
0010 .
0020 ;SUBROUTINES TO CONFIGURE EACH PIA
0030 .
0040 ;DATE 84-1218
0050 .
0060 PIACONF    JSR PHCONF
0070            JSR ADCONF
0080            JSR PDCONF
0090            JSR CLCONF
0100            RTS
0110 .
0120 .
0130 PHULT      .DE $9000           ;PHOTOMULTIPLIER TUBE
0140 .
0150 ;PA0-7 I/P BITS 0-7 OF COUNT
0160 ;PB0-3 I/P BITS 8-10 OF COUNT
0170 ;PB6 I/P FILTER PULSE (+VE 12/REV)
0180 ;PB7 I/P COUNT FLAG (H=COUNTING)
0190 ;CA1 I/P COUNT OVERFLOW (BIT 11)
0200 ;CA2 O/P CLEAR COUNTER (-VE PULSE)
0210 ;CB1 I/P CYCLE PULSE (-VE 1/REV)
0220 ;CB2 O/P START COUNT (-VE PULSE)
0230 .
0240 PHCONF     LDA #0
0250            STA PHULT+1
0260            STA PHULT+3
0270            STA PHULT           ;A PORT INPUT
0280            STA PHULT+2         ;B PORT INPUT
0290            LDA #%00101110
0300            STA PHULT+1         ;CA1 ACTIVE^ CA2 O/P PULSE
0310            STA PHULT+3         ;CB1 ACTIVE^ CB2 O/P PULSE
0320            RTS
0330 .
0340 .
0350 A/D        .DE $9004           ;A TO D CONVERTER,ETC
0360 .
0370 ;PA0-7 I/P DATA FROM A/D
0380 ;PB0-2 O/P ADDR TO A/D
0390 ;PB6 I/P ZENITH MOTOR LIMIT (ACTIVE L)
0400 ;PB7 I/P AZIMUTH MOTOR LIMIT (ACTIVE H)
0410 ;CA1 I/P END OF CONVERSION (ON ^)
0420 ;CA2 O/P SHUTTER SOLENOID DRIVE (H=SHUT)
0430 ;CB2 O/P ADDR LATCH,START OF CONVERSION
0440 .
0450 SHUTTER    .DE ADPAR           ;0=OPEN,OTHERWISE CLOSE
0460 .
0470 ADCONF     LDA #0
0480            STA A/D+1
0490            STA A/D+3
0500            STA A/D             ;PB0-7 INPUT
0510            LDA #%111
0520            STA A/D+2           ;PB0-2 O/P,PB3-7 I/P
0530            LDA #%11111111
0540            BIT SHUTTER         ;OPEN SHUTTER?
0550            BNE S               ;NO,LEAVE CA2 HIGH
0560            AND #%11110111      ;YES,MAKE CA2 LOW
0570 S          AND #%00111110      ;CA1 ACTIVE^,CA2 O/P
0580            STA A/D+1
0590            LDA #%00101100
0600            STA A/D+3           ;CB2 O/P PULSE
0610            RTS
0620 .
0630 .
0640 PHDIO      .DE $900C           ;PHOTODIODE
0650 .
0660 ;PA0-7 I/P BITS 0-7 OF COUNT
0670 ;PB0-2 I/P BITS 8-10 OF COUNT
0680 ;PB7 I/P COUNT FLAG (H=COUNTING)
0690 ;CA1 I/P COUNT OVERFLOW (BIT 11)
0700 ;CA2 O/P CLEAR COUNTER (-VE PULSE)
0710 ;CB2 O/P START COUNT (-VE PULSE)
0720 .
0730 PDCONF     LDA #0
0740            STA PHDIO+1
0750            STA PHDIO+3
0760            STA PHDIO           ;A PORT INPUT
0770            STA PHDIO+2         ;B PORT INPUT
0780            LDA #%00101110
0790            STA PHDIO+1         ;CA1 ACTIVE^,CA2 O/P PULSE
0800            STA PHDIO+3         ;CB1 ACTIVE^,CB2 O/P PULSE
0810            RTS
0820 .
0830 .
0840 CLOCK      .DE $9010           ;REAL TIME CLOCK
0850 .
0860 ;PA0-3 I/P D0-3 DATA FROM CLOCK
0870 ;PA4-7 I/P CONSTANT $3
0880 ;PB0-3 O/P ADDRESS TO CLOCK
0890 ;PB4 O/P WRITE
0900 ;PB5 O/P HOLD
0910 ;PB6 O/P READ
0920 ;CA1 I/P D1 (1 HZ PULSES)
0930 ;CA2 I/P D2 (1/60 HZ PULSES)
0940 .
0950 CLCONF     LDA #0
0960            STA CLOCK+1
0970            STA CLOCK+3
0980            STA CLOCK           ;A PORT INPUT
0990            LDA #%11111111
1000            STA CLOCK+2         ;B PORT OUTPUT
1010            LDA #%100
1020            STA CLOCK+1
1030            STA CLOCK+3
1040            LDX CLOCK+2         ;CLEAR CRB FLAGS
1050            CMP CLOCK+3
1060            BEQ R
1070            LDA #%100
1080            STA ERROR
1090 R          RTS
1100 .
```

The Buffer Routines

This consists of definitions of the various locations in the data buffer used to communicate with the BASIC operating system and a routine to display its contents with appropriate labels.

```
--------------------FILE BUD.SRC--------------------
0020            ;ASSIGN BUFFER LABELS
0030            ;IN TAPE BUFFER #2
0040 .
0050            ;DATE 84-1218
0060 .
0070 BUFFER     .DE $0381
0080 .
0090 PDBUFF     .DE BUFFER              ;24 BYTES FOR PD COUNTS
0100 PHBUFF     .DE PDBUFF+24           ;24 BYTES FOR PH COUNTS
0110 SHBUFF     .DE PHBUFF+24           ;8 BYTES FOR MOTORS
0120 ADBUFF     .DE SHBUFF+8            ;8 BYTES FOR A/D
0130 CLBUFF     .DE ADBUFF+8            ;13 BYTES FOR CLOCK
0140 FWPAR      .DE CLBUFF+16           ;2 BYTES FOR FW ROUTINE
0150 ADPAR      .DE FWPAR+2             ;2 BYTES FOR AD ROUTINE
0160 SHPAR      .DE ADPAR+2             ;2 BYTES FOR SH ROUTINE
0170 ERROR      .DE SHPAR+2             ;TO STORE ERROR CODES
0180 .
0190 DISBUF     ;DISPLAY BUFFER ON SCREEN
0200 .
0210 ;ROM ROUTINES
0220 ;-------------
0230 WRCHR      .DE $F266               ;WRITES A AS ASCII CHAR
0240 DISPH      .DE $D4F7               ;MEMORY DISPLAY
0250 DSPACE     .DE $D52E
0260 SPACE      .DE $D531
0270 CRLF       .DE $D534
0280 .
0290            LDA #0                  ;INITIALISE COUNTER
0300            PHA
0310 H          LDA #H,BUFFER
0320            STA *$FC
0330            LDA #L,BUFFER
0340            STA *$FB                ;SET POINTER TO BUFFER
0350            PLA                     ;GET COUNTER
0360            PHA                     ;KEEP COPY
0370            TAX
0380            ASL A
0390            ASL A                   ;MULTIPLY COUNTER BY 4
0400            CLC
0410            ADC *$FB
0420            STA *$FB                ;ADD TO POINTER
0430            LDA #0
0440            ADC *$FC
0450            STA *$FC
0460            LDA HEADING,X           ;GET HEADING 1ST CHAR
0470            BNE T                   ;IS IT A ZERO BYTE?
0480            JSR DSPACE              ;YES, PRINT SPACES
0490            CLC
0500            BCC U
0510 T          JSR WRCHR               ;NO, WRITE 1ST CHAR
0520            LDA HEADING+1,X         ;GET 2ND CHARACTER
0530            JSR WRCHR               ;WRITE IT
0540 U          LDA #8                  ;# OF BYTES TO DISPLAY
0550            JSR DISPH               ;PRINT BUFFER CONTENTS
0560            JSR CRLF
0570            PLA                     ;GET COUNTER
0580            CLC
0590            ADC #2                  ;INCREMENT BY 2
0600            PHA                     ;SAVE ON STACK
0610            CMP #22                 ;FINISHED?
0620            BCC H                   ;NO, DO NEXT LINE
0630            PLA                     ;YES
0640            RTS
0650 .
0660 HEADING    .BY 'PD' 0 0 0 0
0670            .BY 'PH' 0 0 0 0
0680            .BY 'SHADCL' 0 0 'HI'
```

The Clock Routines

A routine to read the clock and put the data in the buffer as well as one to do the opposite. The latter must configure the PIA differently, so that data can be written to the clock on lines that are usually designated as input only, and so is longer.

```
--------------------FILE CLR.SRC--------------------
0040            ;DATE84-1211
0050 .
0060 READCL     ;ROUTINE TO READ REAL TIME CLOCK
0090            JSR CLCONF              ;CONFIGURE THE PIA
0220 .
0230            LDX #0
0240            LDY #%00100000
0250            STY CLOCK+2             ;HOLD CLOCK
0260            LDY #49                 ;WAIT 150 USEC
0270 YLOOP      DEY
0280            BNE YLOOP               ;NOT FINISHED
0290            LDY #%01101100
0300 C          STY CLOCK+2             ;OUTPUT ADDRESS
0310            NOP                     ;WAIT 6 USEC
0320            NOP
0330            NOP
0340            LDA CLOCK               ;READ DATA
0350            STA CLBUFF,X            ;STORE IT
0360            INX                     ;BUFFER INDEX
0370            DEY                     ;CLOCK ADDRESS
0380            TYA
0390            CMP #%01011111          ;FINISHED?
0400            BNE C                   ;NO,DO NEXT READ
0410            STY CLOCK+2             ;YES RELEASE HOLD
0480            RTS
0490 .
```

```
--------------------FILE SCL.SRC--------------------
0010 SETCL      ;ROUTINE TO WRITE DATA TO CLOCK
0050 .
0060            ;DATE 84-1211"
0070 .
0080 ;RECONFIGURE THE PIA
0090            LDA #0
0100            STA CLOCK+1
0110            STA CLOCK+3
0120            LDA #%11111111
0130            STA CLOCK               ;A PORT OUTPUT
0140            STA CLOCK+2             ;B PORT OUTPUT
0150            LDA #%100
0160            STA CLOCK+1
0170            STA CLOCK+3
0180            LDX CLOCK+2             ;CLEAR FLAGS
0220            LDX #0
0230            LDY #%00100000
0240            STY CLOCK+2             ;HOLD
0250            LDY #49                 ;WAIT 150 USEC
0260 Y          DEY
0270            BNE Y                   ;NOT FINISHED
0280            LDY #%00101100          ;HOLD & 1ST CLOCK ADDR
0290 CLWR       LDA CLBUFF,X            ;GET DATA
0300            STY CLOCK+2             ;WRITE ADDRESS
0310            STA CLOCK               ;WRITE DATA
0320            TYA
0330            ORA #%00010000
0340            STA CLOCK+2             ;WRITE LINE HIGH
0350            NOP
0360            STY CLOCK+2             ;WRITE LINE LOW
0370            INX                     ;DATA INDEX
0380            DEY                     ;CLOCK ADDRESS
0390            TYA
0400            CMP #%00100000          ;FINISHED?
0410            BNE CLWR                ;NO, DO NEXT WRITE
0420            LDY #%01011111
0430            STY CLOCK+2             ;YES, RELEASE HOLD
0435            JSR CLCONF              ;CONFIGURE FOR READ ONLY
0440            RTS
```

The Analogue to Digital Converter Routines

The main routine reads just one channel of the A–D converter. A routine that uses that to read all of the channels was written as well as one that could be called like a function from BASIC.

Also in this file are routines to operate the photomultiplier tube protection shutter which is controlled by a line on the same PIA.

```
--------------------FILE AD.SRC--------------------
0010 ;ROUTINES TO READ THE A TO D
0020 .
0030 ;DATE 84-1218
0032 .
0034 ADCHAN    .DE ADPAR+1
0040 .
0050 ADUSR     ;TO BE CALLED FROM BASIC BY USR(CHAN #)
0060           JSR $C92D           ;FP TO INTEGER ($11)
0070           LDA $11             ;GET CHANNEL NO.
0071           STA ADCHAN
0080           JSR READAD
0085           TAY                 ;Y HOLDS LOW BYTE
0090           LDA #0              ;A HOLDS HIGH BYTE
0100           JMP $C4DC           ;INTEGER TO FP,RETURN
0110 .
0120 ADALL     ;READS AND STORES CHANNELS 0-7
0130           LDA #7
0131           STA ADCHAN
0140 J         JSR READAD
0150           DEC ADCHAN
0170           BPL J
0180           RTS
0190 .
0200 .
0210 READAD    ;READS ONE CHANNEL OF A/D
0230           JSR ADCONF
0240           LDA A/D             ;CLEAR CRA FLAGS
0245           LDX ADCHAN          ;GET CHANNEL #
0250           STX A/D+2           ;O/P CHAN.#,START CONV'N
0260 EOCN?     BIT A/D+1           ;IS CONVERSION DONE?
0270           BPL EOCN?           ;NO,LOOK AGAIN
0280           LDA A/D             ;YES,READ DATA
0290           STA ADBUFF,X        ;STORE DATA IN BUFFER
0300           RTS
0310 .
0320 OPEN      ;ROUTINE TO OPEN SHUTTER
0330           LDA #0
0340           STA SHUTTER
0350           JSR ADCONF
0360           RTS
0370 .
0380 CLOSE     ;ROUTINE TO CLOSE SHUTTER
0390           LDA #$FF
0400           STA SHUTTER
0410           JSR ADCONF
0420           RTS
0430 .
```

The Motor Routines

The routine to move the motors is the largest of the group. It must keep track of the current position of both motors and compare them with the positions desired to establish the direction to move each motor. At each step the limit switches must be checked and a step only allowed to proceed if it is in the opposite direction to that which activated the switch. A delay is put after each step because the speed at which the motors can be reliably stepped is finite[2]. A second routine uses the first to drive the motor back onto their limit switches: that is, to zero them.

[2]The motors could be moved faster if a routine could ramp their speed, that is slowly increase at the start of the move and decrease at the end. This would be worth pursuing if applications of the photometer required higher scan speeds.

```
--------------------FILE SM.SRC--------------------
0010 STEPH      ; STEPPING ROUTINE
0020 .
0030            ;DATE84-1218A
0040 .
0050 MOTORS     .DE $9008          ;MOTOR ADDRESS
0060            ;D7 ZEN DIR'N,D1 AZI DIR'N
0070            ;1=FORWARD,0=BACK
0080            ;D6 ZEN CLOCK,D0 AZI CLOCK
0090            ;PULSE LOW TO STEP
0100 .
0110 ;FOUR 2 BYTE COUNTS TO KEEP TRACK OF MOTORS
0120 DPZEN      .DE SMBUFF         ;DESIRED POS'N,ZEN MTR
0130 DPAZI      .DE SMBUFF+2       ;DESIRED POS'N,AZI MTR
0140 CPZEN      .DE SMBUFF+4       ;CURRENT POS'N,ZEN MTR
0150 CPAZI      .DE SMBUFF+6       ;CURRENT POS'N,AZI MTR
0160 .
0170 LDZEN      .DE SMPAR          ;TO STORE LAST
0180 LDAZI      .DE SMPAR+1        ;DIRECTIONS STEPPED
0190 .
0200            LDA #0
0210            STA ERROR
0220 .
0230 LIMIT      .DE A/D+2          ;ON B SIDE OF A/D PIA
0240            ;ZEN LIMIT PB6 LOW
0250            ;AZI LIMIT PB7 HIGH
0260            JSR ADCONF         ;CONFIGURE THE A/D PIA
0270 .
0280            LDX #$FF           ;INITIALISE
0290 .
0300 .
0310 ZENTEST    LDA DPZEN+1        ;ZEN MOVE REQ'D?
0320            CMP CPZEN+1        ;COMPARE HIGH BYTES
0330            BNE ZENDIR
0340            LDA DPZEN          ;HIGH BYTES EQUAL,
0350            CMP CPZEN          ;SO COMPARE LOW BYTES
0360            BEQ ZENEND         ;NO MOVE REQUIRED
0370 .
0380 ZENDIR     LDA #$FF           ;C=1,FORWARD
0390            BCS ZENLIM
0400            LDA #$7F           ;C=0,BACKWARD
0410 ZENLIM     BIT LIMIT          ;IS LIMIT SWITCH ACTIVE?
0420            BVS ZENMOVE        ;NO,UPDATE LD,DO STEP
0430            TAY
0440            LDA ERROR          ;GET ERROR CODE
0450            ORA #1             ;UPDATE IT
0460            STA ERROR          ;STORE IT
0470            TYA
0480            CMP LDZEN          ;SAME DIR'N AS LAST STEP?
0490            BNE ZENSTEP        ;NO,DO STEP
0500            ASL A              ;C_DIR'N
0510            BCS ZENEND
0520            LDA #0             ;LAST STEP BACK CPZEN_0
0530            STA CPZEN
0540            STA CPZEN+1
0550 ZENEND     LDX #0             ;TO FLAG END OF ZEN
0560            BEQ AZITEST
0570 .
0580 ZENMOVE    STA LDZEN          ;RECORD DIRECTION
0590            TAY
0600            LDA ERROR          ;GET ERROR CODE
0610            AND #$FE           ;CLEAR BIT 0
0620            STA ERROR
0630            TYA
0640 ZENSTEP    STA MOTORS         ;WRITE DIR'N TO MOTOR
0650            AND #$BF
0660            STA MOTORS         ;CLOCK DOWN
0670            ORA #$7F
0680            STA MOTORS         ;CLOCK UP
0690            ASL A              ;C_DIR'N
0700            BCS INCZ           ;UPDATE CPZEN
0710            LDA CPZEN
0720            BNE DECZ
0730            DEC CPZEN+1
0740 DECZ       DEC CPZEN
0750            BCC AZITEST
0760 INCZ       INC CPZEN
0770            BNE AZITEST
0780            INC CPZEN+1
0790 .
0800 .
0810 AZITEST    LDA DPAZI+1        ;AZI MOVE REQ'D?
0820            CMP CPAZI+1        ;COMPARE HIGH BYTES
0830            BNE AZIDIR
0840            LDA DPAZI          ;HIGH BYTES EQUAL,
0850            CMP CPAZI          ;SO COMPARE LOW BYTES
0860            BEQ AZIEND         ;NO MOVE REQUIRED
0870 .
0880 AZIDIR     LDA #$FF           ;C=1,FORWARD
0890            BCS AZILIM
0900            LDA #$FD           ;C=0,BACKWARD
0910 AZILIM     BIT LIMIT          ;IS LIMIT SWITCH ACTIVE?
0920            BPL AZIMOVE        ;NO,UPDATE LD,DO STEP
0930            TAY
0940            LDA ERROR          ;GET ERROR CODE
0950            ORA #2             ;UPDATE IT
0960            STA ERROR          ;STORE IT
0970            TYA
0980            CMP LDAZI          ;SAME DIR'N AS LAST STEP?
0990            BNE AZISTEP        ;NO,DO STEP
1000            LSR A
1010            LSR A              ;C_DIR'N
1020            BCS AZIEND
1030            LDA #0             ;LAST STEP BACK CPAZI_0
1040            STA CPAZI
1050            STA CPAZI+1
1060 AZIEND     CPX #0             ;IS ZEN FINISHED ALSO?
1070            BNE STEPDEL        ;NO, DELAY
1080            RTS ;YES, ALL DONE !
1090 .
1100 AZIMOVE    STA LDAZI          ;RECORD DIRECTION
1110            TAY
1120            LDA ERROR          ;GET ERROR CODE
1130            AND #$FD           ;CLEAR BIT 1
1140            STA ERROR
1150            TYA
1160 AZISTEP    STA MOTORS         ;WRITE DIR'N TO MOTOR
1170            AND #$FE
1180            STA MOTORS         ;CLOCK DOWN
1190            ORA #$FD
1200            STA MOTORS         ;CLOCK UP
1210            LSR A
1220            LSR A              ;C_DIR'N
1230            BCS INCA           ;UPDATE CPAZI
1240            LDA CPAZI
1250            BNE DECA
1260            DEC CPAZI+1
1270 DECA       DEC CPAZI
1280            BCC STEPDEL
1290 INCA       INC CPAZI
1300            BNE STEPDEL
1310            INC CPAZI+1
1320 .
1330 STEPDEL    LDY #250           ;DELAY
1340 D          NOP
1350            NOP
1360            NOP
1370            NOP
1380            NOP
1390            NOP
1400            NOP
1410            NOP
1420            DEY
1430            BNE D
1440            JMP ZENTEST        ;BACK TO START
1450 .
1460 ZERON      ;ROUTINE TO "ZERO" MOTORS
1470            LDA #$40           ;LOAD ALL HIGH BYTES
1480            STA CPZEN+1
1490            STA CPAZI+1
1500            STA DPZEN+1
1510            STA DPAZI+1
1520            LDA #0             ;LOAD LOW BYTES
1530            STA CPZEN
1540            STA CPAZI
1542            STA LDZEN          ;IGNORE LIMITS IF THEY
1543            STA LDAZI          ;ARE ACTIVE AT PRESENT
1550            LDA #32            ;STEP 32 STEPS FORWARD
1560            STA DPZEN          ;TO ENSURE MOTORS ARE
1570            STA DPAZI          ;FREE OF LIMITS
1580            JSR STEPH          ;DO STEPS
1590            LDA #0             ;LOAD DP WITH ZERO
1600            STA DPZEN+1
1610            STA DPAZI+1
1620            STA DPZEN
1630            STA DPAZI
1640            JSR STEPH          ;STEP BACK TO LIMITS
1650            RTS
1660 .
```

The Filter Wheel Routine

The operations performed by this routine to obtain the counts from the detector circuits are described in Section 2.3.2.

```
--------------------FILE FW.SRC--------------------
0010 FWHEEL    ;ROUTINE TO TAKE COUNTS FROM FILTER WHEEL
0020 .
0030           ;DATE 84-1221
0040 .
0050 NO.CYC    .DE FWPAR
0060 MAXCOUNT  .DE FWPAR+1
0070           JSR PHCONF
0080           JSR PDCONF
0090           LDX #0
0100           LDY #0
0110           LDA #0
0115           STA ERROR
0120 P         STA PHBUFF,Y
0130           STA PDBUFF,Y
0140           INY
0150           CPY #24
0160           BCC P
0170 .
0180           LDA PHULT          ;PULSE CA2, CLEAR COUNTER
0190           LDA PHDIO          ;PULSE CA2, CLEAR COUNTER
0200           LDA PHULT+2        ;CLEAR CRB FLAGS
0210           LDA PHDIO+2        ;CLEAR CRB FLAGS
0220 .
0230 CYCLE?    BIT PHULT+3        ;HAS CYCLE PULSE ARRIVED?
0240           BPL CYCLE?         ;NO, LOOK AGAIN
0250           INX                ;CYCLE COUNT
0260           LDY #$0            ;2*CHANNEL #
0270 FILTER?   BIT PHULT+2        ;HAS FILTER PULSE ARRIVED?
0280           BVC FILTER?        ;NO, LOOK AGAIN
0290           JSR FWDEL          ;DELAY 10MS
0300           STA PHULT+2        ;START PH COUNT
0310           STA PHDIO+2        ;START PD COUNT
0320 PHEOC?    BIT PHULT+2        ;IS PH COUNT DONE?
0330           BMI PHEOC?         ;NO, LOOK AGAIN
0340 PDEOC?    BIT PHDIO+2        ;IS PD COUNT DONE?
0350           BMI PDEOC?         ;NO, LOOK AGAIN
0360           BIT PHULT+1        ;DID PH COUNT OVERFLOW?
0370           BPL Q              ;NO, OK
0380           TYA
0390           LSR A              ;GET CHANNEL # Z
0400           ORA #$30           ;PH COUNTER OVERFLOW=$3Z
0410           STA ERROR
0420 Q         BIT PHDIO+1        ;DID PD COUNT OVERFLOW?
0430           BPL FWSTORE        ;NO, OK
0440           TYA
0450           LSR A              ;GET CHANNEL # Z
0460           ORA #$20           ;PD COUNTER OVERFLOW=$2Z
0470           STA ERROR
0480 FWSTORE   LDA PHULT+2        ;READ PH PRB,CLEAR FLAGS
0490           AND #7             ;GET 3 HI BITS OF PH COUNT
0500           PHA                ;SAVE THEM ON STACK
0510           LDA PHULT          ;READ PH PRA,CLEAR COUNTER
0520           CLC
0530           ADC PHBUFF,Y       ;ADD LOW BYTE OF PH COUNT
0540           STA PHBUFF,Y       ;STORE NEW LOW BYTE
0550           PLA                ;RETRIEVE HIGH BITS
0560           ADC PHBUFF+1,Y     ;ADD HIGH BYTE OF PH COUNT
0570           STA PHBUFF+1,Y     ;STORE NEW HIGH BYTE
0580           ADC #7             ;HIGH BYTE +7
0590           CMP MAXCOUNT       ;IS THIS >= MAXCOUNT?
0600           BCC Q              ;NO, OK
0610           STX NO.CYC         ;YES, SIGNAL STOP
0612           TYA
0614           LSR A              ;GET CHANNEL # Z
0616           ORA #$50           ;PH MAXCOUNT=$5Z
0618           STA ERROR
0620 Q         LDA PHDIO+2        ;READ PD PRB,CLEAR FLAGS
0630           AND #7             ;GET 3 HI BITS OF PD COUNT
0640           PHA                ;SAVE THEM ON STACK
0650           LDA PHDIO          ;READ PD PRA,CLEAR COUNTER
0660           CLC
0670           ADC PDBUFF,Y       ;ADD LOW BYTE OF PD COUNT
0680           STA PDBUFF,Y       ;STORE NEW LOW BYTE
0690           PLA                ;RETRIEVE HIGH BITS
0700           ADC PDBUFF+1,Y     ;ADD HIGH BYTE OF PD COUNT
0710           STA PDBUFF+1,Y     ;STORE NEW HIGH BYTE
0720           ADC #7             ;HIGH BYTE +7
0730           CMP MAXCOUNT       ;IS THIS >= MAXCOUNT?
0740           BCC ENDFIL         ;NO, OK
0750           STX NO.CYC         ;YES, SIGNAL STOP
0752           TYA
0754           LSR A              ;GET CHANNEL # Z
0756           ORA #$40           ;PD MAXCOUNT=$4Z
0758           STA ERROR
0760 ENDFIL    INY
0770           INY                ;UPDATE CHANNEL INDEX
0780           CPY #24            ;DONE ALL 12 CHANNELS?
0790           BEQ ENDCYC         ;YES
0795           JMP FILTER?        ;NO, DO NEXT CHANNEL
0800 ENDCYC    CPX NO.CYC         ;DONE REQ'D # OF CYCLES?
0810           BEQ ENDFW          ;YES
0815           JMP CYCLE?         ;NO, DO NEXT CYCLE
```

Linker File

This is the file that links the routines together and provides the assembler with instructions on where to put the output. It also contains extra entry points for most of the routines so that all entry points are together in one place at the start of the machine code.

```
--------------------FILE RAMASS.CNT--------------------
0010           .HJ
0020           .CI                ;RAM CONTROL FILE
0030
0040           ;DATE86-221
0050
0060           .BA $7918
0070           .HC $7918
0080           .OS
0090
0100
0110           JMP PIACONF
0120           JMP OPEN
0130           JMP CLOSE
0140           JMP ADALL
0150           JMP ADUSR
0160           JMP READCL
0170           JMP SETCL
0180           JMP STEPR
0190           JMP ZERON
0200           JMP FWHEEL
0210 .
0220           .FI "PIA.SRC1218"   ;CONFIGURES EACH OF PIAS
0230           .FI "BUD.SRC1218"   ;DEFINES,DISPLAYS BUFFER
0240           .FI "CLK.SRC1211"   ;READS REAL TIME CLOCK
0250           .FI "SCL.SRC1211"   ;SETS CLOCK
0260           .FI "SM.SRC1218A"   ;DRIVES STEPPER MOTORS
0270           .FI "AD.SRC1218"    ;DRIVES A TO D
0280           .FI "FW.SRC1221"    ;READS FILTER WHEEL DATA
0290           .EN
```

The output from the assembler is a block of machine code that occupies just less than a thousand bytes.

The buffer used to transfer information between the BASIC program and the machine code routines is shown in Table B.1. Labels used in the assembly code can be seen to correspond to locations in this buffer. The position of the buffer in the computers memory was chosen so that the BASIC operating system would

Use	Organisation	Memory locations	
Photodiode counts	12× 2 bytes	$0381–$0398	897–920
Photomultiplier counts	12× 2 bytes	$0399–$03b0	921–944
Motor positions	4× 2 bytes	$03b1–$03b8	945–952
A–D values	8× 1 byte	$03b9–$03c0	953–960
Date and time	13× 1 byte	$03c1–$03cd	961–973
Miscellaneous	11× 1 byte	$03ce–$03d8	974–983

Table B.1: The data buffer used to communicate between BASIC and machine code routines. The two columns for memory location give the addresses in hexadecimal and decimal respectively.

not alter it.

B.2 BASIC routines

The BASIC routines were written in a style designed to maximise speed of execution rather than readability. Thus statements are joined in single lines with few embedded spaces and short variable names, as reading any superfluous characters, including comments, slows the program's execution. Two further features that makes BASIC less readable are:

- All variables are global and cannot be passed as parameters to subroutines. This means that the side-effects of each subroutine, that is the variables it changes, are difficult to identify without a careful inspection of the subroutine itself.
- Subroutines are called by line number only and can't be given meaningful names. To partially counter this the first line of each routine is a comment line giving a short description of the task it performs.

The routines are presented here, grouped by function. Calls to the machine code routines are made with the BASIC command SYS(*address*).

The Clock Routines

The BASIC routines define a set of variables for the date and time. This is generally used to represent the time when the next reading will be taken. The data in the buffer, which are the most recently read data from the clock, represent the current time.

```
9000 REM**READ REAL TIME CLOCK**
9010 BU=961:SYS(OC+15)
9030 REMGET RID OF CLOCK DATA BITS
9040 POKEBU+7,(PEEK(BU+7)AND243)
9050 POKEBU+4,(PEEK(BU+4)AND243)
9060 FORA=0TO12:POKEBU+A,(PEEK(BU+A)AND63):NEXTA
9070 RETURN
```

```
9200 REM**ASSIGN DATE AND TIME TO VARIABLES
9210 BU=961:A=10:B=528
9220 IFE<>0THEN9260
9230 SE=A*PEEK(BU+11)+PEEK(BU+12)-B
9240 MI=A*PEEK(BU+9)+PEEK(BU+10)-B
9250 HR=A*PEEK(BU+7)+PEEK(BU+8)-B
9260 DY=A*PEEK(BU+4)+PEEK(BU+5)-B
9270 MO=A*PEEK(BU+2)+PEEK(BU+3)-B
9280 YR=A*PEEK(BU)+PEEK(BU+1)-B-80
9300 A=1:B=.5:C=0
9310 IFMO<3THEN9340
9320 A=3:B=59.5:D=YR/4
9330 C=INT(D-INT(D-.1))
9340 TD=INT((MO-A)*30.6+B)
9350 TD=TD+C+DY
9360 D=INT((YR-1)/4)
9370 TD=YR*365+D+TD-1
9380 LH=HR-1
9390 RETURN

9400 REM**PRINT DATE AND TIME FROM BUFFER**
9430 BU=961:B=PEEK(BU+6)-47
9450 PRINTMID$("SUNMONTUEWEDTHUFRISAT",3*B-2,3);", ";
9460 B=10*PEEK(BU+2)+PEEK(BU+3)-528
9480 PRINTMID$("JANFEBMARAPRMAYJUNJULAUGSEPOCTNOVDEC",3*B-2,3);" ";
9490 PRINTCHR$(PEEK(BU+4));CHR$(PEEK(BU+5));", 19";
9510 PRINTCHR$(PEEK(BU));CHR$(PEEK(BU+1));". ";
9530 PRINTCHR$(PEEK(BU+7));CHR$(PEEK(BU+8));":";
9550 PRINTCHR$(PEEK(BU+9));CHR$(PEEK(BU+10));":";
9570 PRINTCHR$(PEEK(BU+11));CHR$(PEEK(BU+12));"n"
9590 RETURN

9600 REM**COMPARE TIME VARIABLES TO BUFFER**
9610 BU=961:E=0
9620 B=528:A=10
9630 IFYR<>A*PEEK(BU)+PEEK(BU+1)-B-80THENE=-1
9640 IFMO<>A*PEEK(BU+2)+PEEK(BU+3)-BTHENE=-1
9650 IFDY<>A*PEEK(BU+4)+PEEK(BU+5)-BTHENE=-1
9660 DM=A*PEEK(BU+7)+PEEK(BU+8)-B-HR
9670 DM=60*DM+A*PEEK(BU+9)+PEEK(BU+10)-B-MI
9680 DM=DM+(A*PEEK(BU+11)+PEEK(BU+12)-B-SE)/60
9690 RETURN

9800 REM**WAIT UNTIL CLOCK TIME EQUALS VARIABLES**
9810 GOSUB9000:GOSUB9600
9830 IFE<>0THENPRINT"DATE INCORRECT":GOSUB9200:GOSUB9400:STOP
9840 IFDM>0THENPRINT"TIME HAS ALREADY PASSED":PRINT#4,"*";:C=-1:GOSUB9900
9850 IFDM=0THENRETURN
9860 GOSUB9400:GOTO9810
9900 REM***INCREMENT TIME VARIABLES***
9910 MI=INT(MI+1):IFMI>=60THENMI=INT(MI-60):HR=INT(HR+1)
9920 IFSE<>0THENSE=0:GOTO9910
9930 RETURN
```

The A–D and Shutter Routines

Three routines that respectively read the analogue to digital converter's eight channels, assign the three of them currently used to BASIC variables and display the values on the screen, along with calls to the routines to open and close the shutter above the photomultiplier tube.

```
8000 REM**READ ALL CHANNELS OF A/D**
8010 SYS(0C+9)
8200 REM**ASSIGN A/D DATA **
8210 BU=953:A=255:B=.5:C=.1
8220 HT=INT(PEEK(BU)*1100/A+B)
8230 TF=C*INT((PEEK(BU+1)*51/A+B)/C)
```

```
8240 TA=C*INT((PEEK(BU+2)*51/A+B-10)/C)
8250 RETURN
8400 REM**PRINT A/D DATA**
8410 PRINT"TUBE HT= ";HT;"w VOLTS  "
8420 PRINT"TEMP(FILT)= ";TF;"w DEG C  "
8430 PRINT"TEMP(AMB)= ";TA;"w DEG C  "
8440 RETURN
8600 REM**OPEN SHUTTER**
8610 SYS(OC+3):RETURN
8650 REM CLOSE SHUTTER**
8660 SYS(OC+6):RETURN
```

The Filter Reading Routines

Again three routines that obtain, assign, and display the data, which in this case are the counts from the photodetectors for each of the filters.

```
7000 REM**TAKE FILTER READINGS**
7001 PRINT"r  **TAKING FILTER COUNTS**   o"
7020 BU=977:POKEBU,NC:POKE(BU+1),MC
7040 SYS(OC+27):NC=PEEK(977)
7200 REM**ASSIGN FILTER READINGS**
7210 BU=897:B=256:D=0
7220 FORN=OTO1:FORM=OTO11
7230 A=BU+24*N+2*M
7240 C=(PEEK(A)+B*PEEK(A+1))/NC
7245 C(M,N)=C:IFC>DTHEND=C
7250 NEXT:NEXT:RETURN
7400 REM**PRINT FILTER READINGS**
7410 PRINT"FILTER#   DIODE COUNT    TUBE COUNT"
7420 FORM=OTO11
7430 PRINTM;TAB(10);C(M,0);TAB(25);C(M,1)
7440 NEXT:RETURN
```

The Motor Routines

Two routines to handle the motor movements, the main one and a call to zero the motors. The position that the BASIC system wants the motors in is held in the variables ZE and AZ which are the zenith and azimuth in degrees. The azimuth is measured *clockwise* from south, a convenient choice for the southern hemisphere. The offset between this and the azimuth motor's coordinates is stored in the BASIC variable AI as well as in three bytes of the data buffer. When making measurements from a fixed platform where the offset is known the value is initialised by writing the appropriate value to the buffer and calling a routine to set AI from that.

```
6000 REM**MOVE MOTORS TO POSITION GIVEN BY VARIABLES**
6001 PRINT"MOVING MOTORS"
6005 BU=945:C=.0225:D=256:E=16000
6010 A=ZE/C-20:IFA<OTHENA=0
6020 B=INT(A/D):A=A-D*B
6030 POKEBU,A:POKE(BU+1),B
6035 A=AZ/C+AI-20
6036 IFA<OTHENA=A+E
6037 IFA>=ETHENA=A-E
6040 B=INT(A/D):A=A-D*B
6050 POKE(BU+2),A:POKE(BU+3),B
6060 SYS(OC+21)
6070 A=ZE/C+.5:B=INT(A/D):A=A-D*B
6080 POKEBU,A:POKE(BU+1),B
6090 A=AZ/C+AI+.5
6091 IFA<OTHENA=A+E
6092 IFA>=ETHENA=A-E
```

```
 6100 B=INT(A/D):A=A-D*B
 6110 POKE(BU+2),A:POKE(BU+3),B
 6120 SYS(OC+21)
 6199 RETURN
 6200 REM**SET AI TO VALUE HELD IN BUFFER**
 6210 BU=974:D=256
 6220 A=PEEK(BU):IFA>1THENA=-1
 6230 AI=A*(PEEK(BU+1)+D*PEEK(BU+2))
 6240 RETURN
 6400 REM**PRINT BASIC POSITION**
 6410 A=.1:D=.5:B=A*INT(ZE/A+D):C=A*INT(AZ/A+D)
 6420 PRINT"ZENITH ";B;"w DEG, ";TAB(16);"AZIMUTH ";C;"w DEG ":RETURN

 6800 REM**ZERO THE MOTORS**
 6801 PRINT"ZEROING MOTORS"
 6805 ZE=0:AZ=0:AI=AI:SYS(OC+24):RETURN
```

A further routine to allow for manual control of the azimuth motor was written.

```
6600 REM**STEP AZI MOTOR FROM KEYBOARD**
 6605 PRINT"c  rKEYBOARD STEPPER FOR AZIMUTHH MOTORo"
 6610 PRINT"sPRESS r+o OR r-o TO SET STEPPING DIRECTION"
 6615 PRINT"      (POSITIVE IS ANTICLOCKWISE)"
 6620 PRINT"sPRESS rRo TO RETURN TO CALLING ROUTINE"
 6625 PRINT"sPRESSING A NUMBER N (0-9) WILL MOVE THE"
 6630 PRINT"MOTOR BY 2^N STEPS (1STEP=.0225 DEG)s"
 6635 C=.0225:FORN=0TO9:PRINTN;TAB(5);2^N;TAB(10);"STEPS";TAB(18);C*2^N;TAB(23);"DEG":NEXT
 6640 BU=947:D=256:E=0
 6650 A=PEEK(BU)+D*PEEK(BU+1)
 6655 AI=INT(A-AZ/C+.5)
 6660 PRINT"srMOVED SO FARo"
 6665 PRINTAI;"w STEPS (";AI*C;"w DEG)      nnn"
 6670 A=SGN(AI):IFA<0THENA=255
 6675 POKE974,A:A=ABS(AI):B=INT(A/D):A=A-D*B:POKE975,A:POKE976,B
 6690 GETA$
 6700 IF A$="+"THENE=1
 6710 IF A$="-"THENE=-1
 6720 IF A$="R"THENRETURN
 6730 IFA$<"0"OR A$>"9"THEN6690
 6740 A=PEEK(BU)+D*PEEK(BU+1)
 6750 A=A+E*2^VAL(A$)
 6753 IFA<0THENA=0
 6754 IFA>16000THENA=16000
 6760 B=INT(A/D)::A=A-D*B
 6770 POKEBU,A:POKE(BU+1),B
 6780 SYS(OC+21):GOTO6650
```

The Solar Tracking Algorithm

This was based loosely on the FORTRAN program given by Walraven (1978). A small refraction correction, effective only at large zenith angles, according to (Archer, 1980)[3] is included.

```
 5000 REM**CALCULATE ZENITH & AZIMUTH**
 5010 GOSUB9600
 5020 IFE<>0THENGOSUB9200
 5030 IFHR<>LHTHENGOSUB5200
 5040 A=60:B=(MI+SE/A)/A
 5050 RA=CRA+GRA*B:DE=CDE+GDE*B
 5060 UT=HR+B-TZ:TT=TD+UT/24
 5070 A=1.759335+P2*(TT/365.25-YR)+3.694E-7*TT
```

[3]As the photometer's program was calculating positions even for times when the sun was below the horizon the singularity in this empirical correction at 92.7° caused some difficulty. This was done by using Archer's correction for zenith angles $< 91.5°$ and a constant correction for larger angles.

```
5075 IFA>=P2THENA=A-P2
5080 A=A+(UT*15-LO)*RD
5085 IFA>=P2THENA=A-P2
5090 C=RA-A
5095 D=LA*RD
5100 B=SIN(D)*SIN(DE)+COS(D)*COS(DE)*COS(C)
5110 ZE=p/2-ATN(B/SQR(1-B*B))
5120 B=COS(DE)*SIN(C)/SIN(ZE)
5130 AZ=ATN(B/SQR(1-B*B))
5140 AZ=AZ/RD
5150 IFCOS(ZE)>=SIN(DE)/SIN(D)THENAZ=180-AZ
5160 IFAZ<0THENAZ=AZ+360
5162 REM**REFRACTION CORRECTION TO ZE**
5163 IFZE/RD>91.5THENZE=ZE-.019:GOTO5170
5164 B=COS(ZE):A=1/(.955+(20.267*B))-.047121
5166 B=B+.0083*A:ZE=p/2-ATN(B/SQR(1-B*B))
5170 ZE=ZE/RD
5190 RETURN
5200 REM**SET UP LINEAR APPROX'N FOR R.ASC'N & DECL'N**
5210 HR=HR+1:GOSUB5400:GRA=RA:GDE=DE
5220 HR=HR-1:GOSUB5400:CRA=RA:CDE=DE
5224 IFZE<>180THENPRINT#4
5225 PRINT#4,RIGHT$(STR$(HR),2);
5230 GRA=GRA-RA:GDE=GDE-DE:LH=HR:RETURN
5400 REM**CALCULATE R.ASC'N & DECL'N**
5410 UT=HR-TZ
5420 TT=TD+UT/24
5430 A=P2*TT/365.25
5440 B=-0.031271-4.53963E-7*TT+A
5450 C=4.900968+3.67474E-7*TT
5460 C=C+(0.033434-2.3E-9*TT)*SIN(B)
5470 C=C+0.000349*SIN(2*B)+A
5480 D=0.40914-6.2149E-9*TT
5490 RA=ATN(TAN(C)*COS(D))
5500 IFCOS(C)<0THENRA=RA+P2/2
5510 IFRA<0THENRA=RA+P2
5520 B=SIN(C)*SIN(D)
5530 DE=ATN(B/SQR(1-B*B))
5540 RETURN
```

Miscellaneous Routines

Grouped together are the routines that initialise the variables[4], open a disk data file, write a record to that file, display the current data and display error messages. The name of the data file includes the date and hour it is opened to avoid duplicate names. The format of the data written to the disk is a direct copy of the data buffer contents as this gives the most efficient packing on the disk. A checksum is added so that single-bit errors can be detected in the data when it is read back.

```
4000 REM**SET UP VARIABLES**
4005 DIMC(11,1),P(11,1)
4010 A=0:B=0:C=0:D=0:E=0
4020 I=0:J=0:K=0:L=0:M=0:N=0
4030 OC=31000:SYSOC:REM38912,40960
4040 BU=897:NC=1:MC=64:P2=2*p:RD=p/180:LA=-43.51:LO=-172.58:TZ=12:LR=-0:LZ=99
4060 L$="RUTHERFORD BLDG.,U OF C,ILAM"
4065 POKE974,255:POKE975,16:POKE976,10:GOSUB6200:REM AZI SET FOR THIS SITE
4070 DEFFNAM(X)=1/COS(X*RD)
4090 RETURN
4100 REM**OPEN DISK DATA FILE FOR WRITE **
4110 A$="DATA/":BU=960:FORN=1TO9
```

[4] *All* variables in BASIC are global. The ones that are to be used often are declared first to increase the speed with which they are accessed.

```
4120 A$=A$+CHR$(PEEK(BU+N)):NEXTN
4130 PRINT"cssssDATA FILE CALLED r";A$;"o"
4140 DOPEN#8,(A$),W,D1
4150 IFDS=0THENPRINT"ssNOW OPEN FOR WRITE"
4155 PRINT#4,"  START OF FILE  ";A$
4160 IFDS<>0THENPRINT#4,DS$
4170 RETURN
4200 REM**WRITE DATA TO DISK WITH CHECKSUM**
4210 BU=896:B=0:D=256
4215 IFDS<>0THENPRINT#4,DS$
4220 FORN=1TO87:A=PEEK(BU+N):B=B+A:B=B-D*INT(B/D)
4230 PRINT#8,CHR$(A);:NEXTN
4240 LR=HR*60+MI:LZ=ZE
4250 POKE(BU+88),B:PRINT#8,CHR$(B)
4255 IFDS<>0THENPRINTDS$:STOP
4260 RETURN
4300 REM**PRINT BASIC TIME**
4310 PRINT"sss"M$;
4320 PRINTHR;":";MI;":";SE;"ss":RETURN
4600 REM**PRINT ALL RELEVANT DATA**
4610 PRINT"c":GOSUB9400
4620 PRINT"s":GOSUB6400
4630 GOSUB8400
4640 PRINT:GOSUB7400
4650 PRINT:GOSUB4800
4690 RETURN
4700 REM**PRINT BUFFER**
4710 SYS(0C+163):RETURN
4800 REM**PRINT ERROR CODE**
4810 E=PEEK(983):A=EAND240:B=EAND15
4820 IFE=0THENPRINT"OK":RETURN
4830 IFA=0THENGOTO4850
4839 IFA>80ORA<32ORB>11THENPRINT"?????":RETURN
4840 IF(AAND32)=32THENPRINT"rCOUNTER OVERFLOWo ON ":PRINT#4,E
4841 IF(AAND64)=64THENPRINT"MAXIMUM COUNT ON ";
4842 IF(AAND16)=16THENPRINT"TUBE, ";
4843 IF(AAND16)=0THENPRINT"DIODE, ";
4844 PRINT"FILTER#";B:RETURN
4850 IFB>4THENPRINT"?????":RETURN
4851 IFB=1THENPRINT"ZENITH MOTOR AT LIMIT":RETURN
4852 IFB=2THENPRINT"AZIMUTH MOTOR AT LIMIT":PR4,"AZI LIMIT":RETURN
4853 IFB=3THENPRINT"BOTH MOTORS AT LIMIT":RETURN
4854 IFB=4THENPRINT"CLOCK NOT WORKING":RETURN
```

Main Control Loop

A listing of the main control part of the program as used for measurements in Christchurch is reproduced here. As already remarked, it is not very readable. The first line is a call to a machine code routine, necessary because the program memory flags need restoring if the program has been loaded from a bootstrap program. Various messages are printed to the screen to keep the operator informed of what the program is doing. The subroutines that are called by line number can be identified by reference to their listings.

```
1 IFPEEK(634)=169THENSYS634
10 GOSUB3600:MI=MI+1:SE=0:LZ=180:LR=0
15 GOSUB9900:IFHR=24THENGOSUB3800:GOSUB3000:GOSUB3700
20 M$="FINDING POSITION FOR ":GOSUB4300:GOSUB5000:IFZE>90THENZE=180
25 IFZE=180ANDHR>12THENGOSUB3800:GOSUB3000:GOSUB3700:GOTO15
26 IFZE=180THENGOSUB9800:GOTO15
30 IFHR*60+MI-LR>=200RABS(FNAM(ZE)-FNAM(LZ))>=0.1THENGOTO50
40 PRINT"STANDBY.":GOSUB6000:GOSUB9800:PRINT#4,".";:GOTO15
50 GOSUB3200:IFD<20THENPRINT"sDUD READING?,NOT SAVING":PRINT#4,"?";:GOTO15
60 PRINT"sGOOD READING!,SAVING":GOSUB4200:PRINT#4,"!";:GOTO15
199 STOP
2998 GETA$:IFA$<>CHR$(13)THEN2998
2999 STOP
```

```
3000 REM**HOLD WHILE MIDNIGHT PASSES**
3010 PRINT#4,"WAITING FOR MIDNIGHT -- ";
3020 GOSUB9000:GOSUB9200:IFHR>0THEN3020
3030 PRINT#4,"GOT IT":LR=-1:RETURN
3200 REM**TAKE READING AT GIVEN POSITION AND TIME**
3210 NC=30:GOSUB9600:IFE=-1THENSTOP
3220 PRINT"sss":GOSUB6400:GOSUB6000:
3230 M$="TAKING READING AT ":GOSUB4300:GOSUB9800:IFC=-1THEND=0:RETURN
3240 GOSUB7000:GOSUB8000
3250 RETURN
3600 REM**COLD START UP (AZIMUTH SETTING ASSUMED)**
3605 GOSUB4000:GOSUB9000:GOSUB9200:GOSUB8000
3610 PRINT"c":GOSUB5600:PRINT"ss":GOSUB9400:PRINT
3620 OPEN4,4:GOSUB6800:GOSUB5000:IFZE>90THENZE=180
3625 GOSUB6000
3700 REM **WARM START**
3730 GOSUB9000:GOSUB9200
3740 GOSUB4100:GOSUB8600
3750 RETURN
3800 REM**FINISH UP**
3805 PRINT"CLOSING DATA FILE"
3810 DCLOSE:PRINT#4,"END OF FILE"
3830 RETURN
```

Different programs were used for the measurements at other sites. The latitude and longitude were coded into the program in the subroutine that initialised the variables. For the measurements at Lauder a version that allowed positioning of the azimuth motor at the start of each day using the keyboard stepping routine was used as the photometer was operated from a mobile platform that was packed away each day. The program for the Antarctic measurements was considerably modified, as described in Section 4.3.

References

Ångström, A., 1929: *On the atmospheric transmission of sun radiation and on dust in the air.* Geogr. Ann. **H**:2.

Ångström, A., 1932: *The quantitative determining of radiant light by the method of electrical compensation.* Phys. Rev. **1**:365.

Ångström, A., 1970: *Apparent solar constant variations and their relation to variability of atmospheric transmission.* Tellus **22**:205.

Armstrong, R.J., and C.J. Richards, 1981: *The measurement of atmospheric turbidity.* The Meteorological Magazine **110**:303.

Archer, C.B., 1980: *Comments on "Calculating the position of the sun".* Solar Energy **25**:91.

Basher, R.E., 1975: *Stratospheric circulation: a narrowband filter spectrophotometer for total ozone determination.* PhD thesis, University of Canterbury, Christchurch, New Zealand, 201pp.

Basher, R.E., 1977: *The effect of bandwidth on filter instrument total ozone accuracy.* J. Appl. Meteor. **16**:803.

Basher, R.E., 1978: *Total ozone measurement: intercomparison of prototype New Zealand filter instrument and Dobson spectrophotometer.* NASA Tech paper 1277.

Basher, R.E., 1982: *Units for column amounts of ozone and other atmospheric gases.* Quart. J. Roy. Met. Soc. **108**:460.

Basher, R.E., 1982b: *Review of the Dobson spectrophotometer and its accuracy.* WMO Global Ozone Research and Monitoring Project No. 13. 94pp.

Bates, D.R., 1984: *Rayleigh scattering by air.* Planet. Space Sci. **32**:785.

Blifford, I.H., 1966: *Factors affecting the performance of commercial interference filters.* Appl. Opt. **5**:105.

Bowman, K.P., 1987: *Global trends in total ozone.* Science **239**:48.

Brewer, A.W., 1973: *A replacement for the Dobson spectrophotometer?* Pure and Appl. Geophys. **106–108**:919.

Brasseur, G., and A. De Rudder, 1988: *The potential impact on atmospheric ozone and temperature of increasing trace gas concentrations.* J. Geophys. Res. **92**:10903-10920.

Brasseur, G., and S. Solomon, 1986: *Aeronomy of the middle atmosphere.* Atmospheric science library, 2^{nd} ed., Reidel, 452pp.

Brewer, A.W., and J.B. Kerr, 1973: *Total ozone measurements in cloudy weather.* Pure and Appl. Geophys. **106–108**:928.

Carleton, N., ed., 1974: *Astrophysics: Optical and infrared.* Methods of experimental physics. Volume 12A. Academic Press, 587pp.

Cary. *Instructions for Cary recording spectrophotometer Model 14R.* Cary instruments, 2724 South Peck Rd, Monrovia, California 91016.

Chanin M.L., 1983a: *The intercomparison ozone campaign held in France in June 1981: Description of the campaign.* Planet. Space Sci. **31**:707.

Chanin M.L., 1983b: *The intercomparison ozone campaign held in France in June 1981: Concluding remarks.* Planet. Space Sci. **31**:811.

Chapman, S., 1931: *The absorption and dissociative or ionising effect of monochromatic radiations in an atmosphere on a rotating earth.* Proc. Phys. Soc. **43**:483.

Cornu, A., 1879: *Observations de la limite ultraviolette du spectre solaire, à diverses altitudes.* Compt. Read, **89**:808.

Covey, C., S. Schneider and S. Thompson, 1984: *Global atmospheric effects of massive smoke injections from a nuclear war — results from general circulation model simulations.* Nature **308**:21.

Craig, R.A., 1965: *The upper atmosphere: meteorology and physics.* International Geophysical Series, Vol. 8, Academic Press, 509pp.

Crutzen, P.J., and F. Arnold, 1986: *Nitric acid cloud formation in the cold Antarctic stratosphere: A major cause for the springtime "ozone hole".* Nature **324**:651.

De Luisi, J.J., 1975: *Measurements of the extraterrestrial solar radiant flux from 2981 to 4000 Å and its transmission through the atmosphere as it is affected by dust and ozone.* J. Geophys. Res. **80**:345.

Deepack, A., 1986: *Remote sensing of atmospheres and oceans.* Academic Press, 641pp.

Department of Scientific Research, New Zealand, Antarctic Division 1986: *New Zealand Antarctic research program 1986–87.* ISSN-0110-7240-NZ.

Dobson, G.M.B., 1930: *Observations of the amount of ozone in the earth's atmosphere and its relation to other geophysical conditions, PartIV.* Proc. Roy. Soc. London, **A129**:411.

Dobson, G.M.B., 1931: *A photoelectric spectrophotometer for measuring the amount of atmospheric ozone.* Proc. Phys. Soc. London **43**:324.

Dobson, G.M.B., 1957a: *Observers' handbook for the ozone spectrophotometer* Ann. IGY **5**:46.

Dobson, G.M.B., 1957b: *Adjustment and calibration of the ozone spectrophotometer.* Ann. IGY **5**:90.

Elterman, L., 1968: *UV, visible and IR attenuation for altitudes to 50km.* AFCRL-68-0153 Air Force Geophysics Laboratory, 49pp.

Fabry, C., and H. Buisson, 1913: *L'absorption de l'ultraviolet par l'ozone et la limite du spectre solaire.* J. Phys. Radium, Paris **Sèr3,2**:197.

Farman, J.C., and R.A. Hamilton, 1975: *Measurements of atmospheric ozone at the Argentine Islands and Halley Bay 1957–72.* Br. Antarc. Surv. Sci. Rep. No. 90, 40pp.

Farman, J.C., B.G. Gardiner and J.C. Shanklin, 1985: *Large losses of total ozone in Antarctica reveal seasonal ClO_x/NO_x interaction.* Nature **315**:207.

Farmer, C.B., G.C. Toon, P.W. Schaper, J.F. Blavier and L.L. Lowes, 1987: *Stratospheric trace gases in the spring 1986 Antarctic atmosphere.* Nature **329**:126.

Fröhlich, C., and G.E. Shaw, 1980: *New determination of Rayleigh scattering in the terrestrial atmosphere.* Appl. Opt. **19**:1773.

Fowler, A., and Lord Rayleigh, 1917: *Atmospheric bands of atmospheric ozone in the spectra of sun and stars.* Proc. Roy. Soc. **A93**:577.

Furman, Sh.A., and M.D. Levina, 1971: *Effect of moisture on the optical characteristics of narrow band interference filters.* Opt. Spectrosc. **30**:404.

Griggs, M., 1968: *Absorption coefficients of ozone in the ultraviolet and visible regions.* J. Chem. Phys. **49**:857.

Götz, F.W.P., 1931: *Das atmosphärische ozon.* Bietr. geophys. **1**:180.

Hartley, W.N., 1881a: *On the absorption spectrum of ozone.* J. Chem. Soc. **39**:57.

Hartley, W.N., 1881b: *On the absorption of solar rays by atmospheric ozone.* J. Chem. Soc. **39**:111.

Heath, D.F, 1988: *Non-seasonal changes in total column ozone from satellite observations, 1970–86.* Nature **332**:219.

Hofmann, D.J., 1987: *Perturbations to the global atmosphere associated with the El Chichón volcanic eruption of 1982.* Rev. Geophys. **25**:743.

Hofmann, D.J., J.W. Harder, S.R. Rolf and J.M. Rosen, 1987: *Balloon-borne observations of the development and vertical structure of the Antarctic ozone hole in 1986.* Nature **326**:59.

Hoyt, D.V., 1977: *A redetermination of the Rayleigh optical depth and its application to selected solar radiation problems.* J. Appl. Meteor. **16**:432.

Houghton, J.T., 1986: *The physics of atmospheres.* 2nd ed., Cambridge University Press, 271pp.

Huggins, W., 1890: *On a new group of lines in the photographic spectrum of Sirius.* Proc. Roy. Soc. **A48**:216.

International Ozone Commission, IAMAP, 1980: *Proceedings of the Quadrennial Ozone Symposium held in Boulder, Colorado 4–9 August 1980* ed J. London.

International Ozone Commission, IAMAP, 1984: *Atmospheric Ozone, Proceedings the Quadrennial Ozone Symposium held in Halkidiki, Greece, 3–7 Sept 1984.* Reidel, ed. C.S.Zerefos and A.Ghazi.

Junge, C.E., 1963: *Air radiation and chemistry.* International Geophysical Series, Vol. 4, Academic Press, 382pp.

Kasten, F., 1966: *A new table and approximation formula for the relative optical air mass.* Arch. Meteorol. Geophys. Bioklim **B14**:206.

King, L.V., 1923: *On the complex anisotropic molecule in relation to the dispersion and scattering of light.* Proc. Roy. Soc. London **A104**:333.

King, M.D. and D.M. Byrne, 1976: *A method for inferring total ozone content from the spectral variation of total optical depth obtained with a solar radiometer.* J. Atmos. Sci. **33**:2242.

King, M.D., D.M. Byrne, B.M. Herman and J.A. Reagan, 1978: *Aerosol size distributions obtained by inversion of spectral optical depth measurements.* J. Atm. Sci. **35**:2153.

King, M.D., 1982: *Sensitivity of constrained linear inversions to the selection of the Lagrange multiplier.* J. Atm. Sci. **39**:1356.

Klenk, K.F., 1980: *Absorption coefficients of ozone for the backscatter UV experiment.* Appl. Opt. **19**:236.

Krueger, A.J., M.R. Schoeberl and R.S. Stolarski, 1987: *TOMS observations of total ozone in the 1986 antarctic spring.* Geophys. Res. Lett. **14**:527.

Linke, F., 1922: *Transmissions Koeffizient und trübungsfactor.* Beitr. Phys. Atmos **10**:91.

MacKie, R.M., and M.J. Rycroft, 1988: *Health and the ozone layer.* Brit. Med. J. **297**:369.

Mahlman, J.D., and S.B. Fels, 1986: *Antarctic ozone decreases: A dynamical cause?* Geophys. Res Lett. **13**:1316.

Malone, R.C., L.H. Auer, G.A. Glatzmaier, M.C. Wood and O.B. Toon, 1986: *Nuclear winter: Three dimensional simulations including Interactive transport, scavenging and solar heating of smoke.* J. Geophys. Res. **91**:1039.

Matthews, W.A., 1971: *Atmospheric ozone.* PhD thesis, University of Canterbury, Christchurch, New Zealand.

Matthews, W.A., 1972: *Agreement between Dobson spectrophotometer and filter ozonometer measurements of total ozone.* J Appl. Meteor. **11**:239.

Matthews, W.A., R.E. Basher and G.J. Fraser, 1974: *Filter ozone spectrophotometer.* Pure and Appl. Geophys **112**:931.

McCormick, M.P., H.M. Steele, P. Hamill, W.P. Chu and T.J. Swisser, 1982: *Polar stratospheric cloud sightings by SAM II.* J. Atmos. Sci. **39**:1387.

McElroy, M.B., R.J. Salawitch, S.C. Wofsy and J.A. Logan, 1986: *Reductions of Antarctic ozone due to synergistic interactions of chlorine and bromine.* Nature **321**:759.

McKenzie, R.L., 1981: *Practical calibration of interference filters.* Physics and Engineering Laboratory Report No.722, DSIR, New Zealand, 26pp.

McKenzie, R.L., and P.V. Johnson, 1984: *Springtime stratospheric NO_2 in Antarctica.* Geophys. Res. Lett. **11**:73.

Middleton, W.E., 1961: *Pierre Bouger's optical treatise on graduation of light.* University of Toronto press, 241pp.

Mitchell, J.M.Jr., 1982: *El Chichón, weather maker of the century.* Weatherwise **35**:252.

Monin, A.S., 1986: *An introdution to the theory of climate.* Atmospheric science library, Reidel, 261pp.

Mount, G.H., R.W. Sanders, A.L. Schmeltekopf and S. Solomon, 1987: *Visible spectroscopy at McMurdo station, Antarctica 1. Overview and daily variations of NO_2 and O_3, Austral spring, 1986.* J. Geophys. Res. **92**:8329.

Murgatroyd, R.J., 1982: *Recent progess in studies of the stratosphere.* Quart. J. Roy Meteor. Soc. **108**:271.

National Oceanic and Atmospheric Administration, 1988: *An eight-year climatology of meteorological and SBUV ozone data.* NOAA Technical Report NWS 40, 125pp.

National Aeronautics and Space Administration, 1986: *Present state of knowledge of the upper atmosphere: an assessment report.* NASA Reference Publication 1162, 134pp.

National Aeronautics and Space Administration, 1988: *Present state of knowledge of the upper atmosphere 1988: an assessment report.* NASA Reference Publication 1208, 200pp.

National Research Council (U.S.), 1984: *The effects of a major nuclear exchange.* National Acadamy Press, Washington, 193pp.

Neckel, H., and D. Labs, 1981: *Improved data of solar spectral irradiance from 0.33 to 1.25 μ.* Solar Physics **74**:231.

Nicolet, M., R.R. Meier and D.E. Anderson, Jr., 1982: *Radiation field in the troposphere and stratosphere — II. Numerical analysis.* Planet. Space Sci. **30**:935.

Ohman, Y., ed., 1958: *Annals of the International Geophysical Year.* Vol. 5, Part 6, Pergamon, 402pp.

Penndorf, R., 1957: *Tables of the refractive index for standard air and the Rayleigh scattering coefficient for the spectral region between 0.2 and 20.0 μ and their application to atmospheric optics.* J. Opt. Soc. **47**:176.

Philips 1970: *Photomultipliers.* Philips Application Book. Electronic Components and Materials Division, Eindhoven. 150pp.

Pyle, J., 1988: *Reactions on ice crystals.* Nature **334**:297.

Quenzel, H., 1970: *Determination of size distribution of atmospheric aerosol particles from spectral solar radiation measurements.* J. Geophys. Res. **75**:2915.

Rayleigh, Lord (J.W.Strutt), 1899: *On the transmission of light through an atmosphere containing small particles in suspension, and on the origin of the blue of the sky.* Phil. Mag. **47**:375.

Rayleigh, Lord (J.W.Strutt), 1918: *On the scattering of light by a cloud of similar small particles of any shape and oriented at random.* Phil. Mag. **35**:373.

Reinsel, G.C., G.C. Tiao, S.K. Ahn, M. Pugh, S. Basu, J.J. DeLuisi, C.L. Mateer, A.J. Miller, P.S. Connel and D.J. Wuebbles, 1988: *An analysis of the 7-year record of SBUV satellite ozone data: Global profile features and trends in total ozone.* J. Geophys. Res. **93**:1689.

Schneider, S.H., 1987: *Climate modelling.* Scientific American, May 1987, p72.

Schlesinger, M.E., and J.F.B. Mitchell, 1987: *Climate model simulations of the equilibrium climatic response to increased carbon dioxide.* Rev. Geophys. **25**:760.

Schoeberl, M.R., and A.J. Krueger, 1986 *An overview of the Antarctic ozone depletion issue.* Geophys. Res Lett. **13**:1191.

Shaw, G.E., 1973: *Investigations of atmospheric extinction using direct solar radiation measurements with a multi-wavelength radimeter.* J. Appl. Meteor. **12**:374.

Shaw, G.E., 1976: *Error analysis of multi-wavelength sun photometry.* Pageoph **114**:1.

Shaw, G.E., 1983: *Sun Photometry.* Bul. Am. Met. Soc. **64**:4.

Shaw, G.E., J.A. Reagan and B.M. Herman, 1973: *Investigations of atmospheric extinction using direct solar radiation measurements made with a multiple wavelength radiometer.* J. Appl. Meteor. **12**:374.

Simons, J.W., R.J. Paur, H.A. Webster, III and E.J. Bair, 1973: *Ozone ultraviolet. VI. The ultraviolet spectrum.* J. Chem Phys. **59**:1203.

Solomon, P.M., B. Conner, R.L. de Zafra, A. Parrish, J. Barrett and M. Jaramillo, 1987: *High concentrations of chlorine monoxide at low altitudes in the Antarctic spring stratosphere: secular variation.* Nature **328**:411.

Solomon, S., 1988: *The mystery of the Antarctic ozone hole.* Rev. Geophys. **26**:131.

Solomon, S., G.H. Mount, R.W. Sanders and A.L. Schmeltekopf, 1987: *Visible spectroscopy at McMurdo station, Antarctica 2. Observations of OCLO.* J. Geophys. Res. **92**:8329.

Solomon, S., and M.R. Schoeberl, 1988: *Overview of the polar ozone issue.* Geophys. Res. Lett. **15**:845.

Stolarski, R.S., A.J. Krueger, M.R. Schoeberl, R.D. McPeters, P.A. Newman and J.C. Alpert, 1986: *Nimbus 7 satellite measurements of the springtime Antarctic ozone decrease.* Nature **322**:808.

Tanré, D., C. Devaux, M. Herman, R. Santer and J.Y. Gac, 1988: *Radiative properties of desert aerosols by optical ground-based measurements at solar wavelengths.* J. Geophys. Res. **93**:14223.

Thekaekara, M., 1974: *Extraterrestrial solar spectrum 3000–6100Å at 1Å intervals.* Appl Opt. **13**:518.

Thomason, L.W., R.J. Szymber and B.M. Herman, 1982: *An examination of reduction techniques for determining the Linke turbidity Factor.* J. Appl. Meteor. **21**:1524.

Tung, K.K., M.K.W. Ko, J.M. Rodriguez and N.D. Sze, 1986: *Are Antarctic ozone variations a manifestation of dynamics or chemistry?* Nature **322**:808.

Turco, R.P., P. Hamill and O.B. Toon, 1982: *Statospheric Aerosols: Observation and theory.* Rev. Geophys. Space Phys. **20**:233.

Turco, R.P., O.B. Toon, T.P. Ackerman, J.B. Pollack and C. Sagan, 1983: *Global atmospheric consequences of multiple nuclear explosions.* Science **222**:1283.

Twomey, S., 1963: *On the numerical solution of Fredholm integral equations of the first kind by the inversion of the linear system produced by quadrature.* J. Assoc. Comput. Mach. **10**:97.

Twomey, S., 1965: *The application of numerical filtering to the solution of integral equations encountered in indirect sensing measurements.* J. Franklin Inst. **279**:95.

Twomey, S., 1977: *Atmospheric aerosols.* Developments in Atmospheric Science, Vol. 7, Elsevier, 302pp.

Valley, S.L., ed., 1965: *Handbook of geophysics and space environments.* prepared by Air Force Cambridge Research Laborotories, McGraw Hill, New York.

Vigroux, E., 1953: *Contribution a l'étude expérimentale de l'absorption de l'ozone.* Ann. Phys. **8**:709.

Vigroux, E., 1967: *Détermination des coefficients moyens d'absorption de l'ozone en vue des observations concernant l'ozone atmosphérique a l'aide du spectromètre Dobson.* Ann. Phys. **2**:209.

Volz, F.E., 1959: *Photometer mit selen-photoelement zur spektralen messung der sonnenstrahlung und zur bestimmung der wellenlangenabra'ngigkeit der dunsttrubung.* Arch. Meteorol. Geophys. Bioklim **B10**:100.

Volz, F.E., 1968: *Some results of turbidity networks.* Tellus **21**:625.

Volz, F.E., 1974: *Economical multispectral sun photometer for measurement of aerosol extinction from 0.44 μm to 1.6 μm and precipitable water.* Appl. Opt. **13**:1732.

Walraven, R., 1978: *Calculating the position of the sun*[5]. Solar Energy **10**:393.

West, R.C., 1982: *Programming the PET/CBM* Level, London, 504pp.

Wofsy, S.C., M.J. Molina, R.J. Salawitch, L.E. Fox and M.B. McElroy, 1988: *Interactions between HCl, NO_x and H_2O ice in the Antarctic stratosphere: Implications for ozone.* J. Geophys. Res. **93**:2442.

[5]Erratum ibid **22**:195 (1979)

World Meteorological Organisation, 1978: *International operations handbook for measurement of background atmospheric pollution.* Geneva WMO, No. 491.

World Meteorological Organisation, 1982a: *The Stratosphere 1981: theory and measurements.* Geneva, WMO Global Ozone Research and Monitoring Project No. 11.

World Meteorological Organisation, 1982b: *Report on the meeting of experts on sources of error in detection of ozone trends.* Geneva, WMO Global Ozone Research and Monitoring Project No. 12, 48pp.

World Meteorological Organisation, 1986: *Atmospheric ozone 1985: Assessment of our understanding of the processes controlling its present distribution and change.* Geneva, WMO Global Ozone Research and Monitoring Project No. 16, 3 Vols., 1090pp.

Yamamoto, G. and M. Tanaka, 1969: *Determination of aerosol size distribution from spectral attenuation measurements.* Appl. Opt. **8**:447.

Young, A.T., 1980: *Revised depolarisation corrections for atmospheric extinction.* Appl. Opt. **19**:3427.

Young, A.T., 1981a: *On the Rayleigh-scattering optical depth of the atmosphere.* J. Appl. Meteor. **20**:328.

Young, A.T., 1981b: *Rayleigh scattering.* Appl. Opt. **20**:533.

Acknowledgements

I would like to thank all of the many people and organisations that have provided the financial, technical, scientific and moral support for me to complete this project.

Special thanks must go to my supervisor, Dr Fraser, who has never failed to provide the right support and advice throughout the many and varied stages of this project. At times when problems occurred which seemed insoluble, it was his objective view that helped me bring them back down to size. At times when the way forward did not seem clear, it was his guidance that pointed a way. Even being 2×10^4 km away on sabbatical leave did not prevent him from doing this, thanks to electronic mail. While he was away, Dr R. G. T. Bennet provided assistance as acting supervisor. All of my post-graduate colleagues in the atmospheric research group have helped me during my time here but especially so Bryan Lawrence, usually over a shared dose of caffeine, and Bill Brown.

Dr Reid E. Basher of the New Zealand Meteorological Service, who built the last University of Canterbury photometer, provided the design for this instrument and gave me much useful advice during the early stages of the project.

I have worked with nearly all of the technical staff in the Physics Department from both the mechanical and electronic workshops during the course of this project and their cooperation is acknowledged. Without belittling the contribution that others have made, special thanks must go to the late Terry Rowe who built most of the photometer, to Graeme Kershaw who bailed us out of some design problems, to Ross Ritchie and Greg Haslett for designing and building the electronics and to Bruce Bradshaw who built the skylight and accompanied me to the Antarctic to help install it and the photometer. Thanks also to the various people that have provided computer programming assistance.

I would also like to thank those organisations that have provided financial support for this project; the University Grants Committee for a post-graduate scholarship, the Physics Department of the University of Canterbury for logistic, financial and technical support and the New Zealand Meteorological Service for the funding for a large part of the equipment.

The Antarctic Division of the DSIR, both the permanent staff and the Scott Base 1986–87 summer and winter-over crews, helped logistically for the measurements at Arrival Heights and the Physics and Engineering Laboratory, Atmospheric Station provided support and accommodation for the measurements taken at Lauder. The last year of this project was completed without any formal financial support and I am extremely gratefull to those that have helped ease that particular burden, my parents and my enterprising friend Euan Godfrey.

Thanks also to David Fletcher for permission to use the cartoon at the beginning of this document.